Insights into early biogenesis steps of the human small mitochondrial ribosomal subunit

Dissertation

for the award of the degree

"Doctor rerum naturalium" (Dr. rer. Nat)
of the Georg-August-Universität Göttingen

within the doctoral program: Molecular medicine
of the Georg-August University School of Science (GAUSS)

submitted by

Mandy Mong-Quyen Mai

from Lüdenscheid, Germany

Göttingen, 2021

Members of the Thesis Committee

Dr. Ricarda Richter-Dennerlein (Supervisor and First Referee)	University Medical Center Department of Cellular Biochemistry Göttingen, Germany
Prof. Dr. Dörthe M. Katschinski (Second Referee)	University Medical Center Department of Cardiovascular Physiology Göttingen, Germany
Prof. Dr. Markus T. Bohnsack (Third Referee)	University Medical Center Department of Molecular Biology Göttingen, Germany

Members of the Examination Board

Prof. Dr. Bernd Wollnik	University Medical Center Institute of Human Genetics Göttingen, Germany
Prof. Dr. Ralph Kehlenbach	University Medical Center Department of Molecular Biology Göttingen, Germany
Prof. Dr. Michael Thumm	University Medical Center Department of Cellular Biochemistry Göttingen, Germany

Date of oral examination: 20th May 2021

Affidavit

Herewith I declare that my dissertation “Insights into early biogenesis steps of the human small mitochondrial ribosomal subunit” has been independently written by me and with no other sources and aids than quoted.

Mandy Mong-Quyen Mai

Göttingen, March 2021

Table of Contents

List of figures

List of tables

Abbreviations

Table 1: Abbreviations

A	Adenine
Å	Ångström
ADP	Adenosine diphosphate
AF	assembly factor
Ala	Alanine
Aqua dest.	Aqua destillata
ArfB	Alternative ribosome-rescue factor B
Arg	Arginine
A site	Aminoacyl site
Asn	Asparagine
Asp	Aspartic acid
ATP	Adenosine triphosphate
bp	Base pair(s)
BSA	Bovine serum albumin
C	Cytosine
CP	Central protuberance
Cryo-EM	Cryogenic electron microscopy
C-terminus	Carboxyl-terminus
Cys	Cysteine
Del	Deletion
Dig.	Digitonin
DMEM	Dulbecco's modified Eagle's medium
DNA	deoxyribonucleic acid
dNTP	2'-deoxynucleoside-5'-triphosphate
DRP1	Dynamin related protein 1
DTT	Dithiothreitol
Dup	Duplication
E. coli	Escherichia coli
EDTA	Ethylendiamintetraacetic acid
ER	Endoplasmic Reticulum
E site	Exit site
EtOH	Ethanol
FAD	Flavin adenine dinucleotide
FADH2	Reduced flavin adenine dinucleotide
FASTKD4	FAST kinase domain-containing protein 4
FCS	Fetal calf serum
Fe-S	Iron-sulfur
FIS1	Mitochondrial fission protein 1
G	Guanine
gDNA	genomic DNA
GDP	Guanosine diphosphate
Gln	Glutamine
Glu	Glutamic acid
GTP	Guanosine triphosphate
h	Helix

H. sapiens	Homo sapiens
HEK293T	Human embryonic kidney cell line
HEPES	4-(2-hydroxylethyl)-1-piperazinethanesulfonic acid
His	Histidine
HSP	Heavy strand promoter
H strand	Heavy strand
IMM	Inner mitochondrial membrane
IP	Immunoprecipitation
kDa	Kilo-Dalton
Leu	Leucine
LFQ	Label free quantification
LSP	Light strand promoter
L strand	Light strand
LSU	Large subunit
Lys	Lysine
MAM	Mitochondria-associated endoplasmic reticulum membrane
Mba1	Multi-copy bypass of AFG3 protein
Met	Methionine
MetOH	Methanol
MFN	Mitofusin
mRNA	Messenger ribonucleic acid
MRP	Mitoribosomal protein
mt	Mitochondrial
mtDNA	Mitochondrial deoxyribonucleic acid
mtEF-G1	Mitochondrial elongation factor G
mtEF-Tu	Mitochondrial elongation factor Tu
MTERF1	Mitochondrial termination factor 1
MTFMT	Methionyl-tRNA formyltransferase
mtIF2	Mitochondrial initiation factor 2
mtIF3	Mitochondrial initiation factor 3
mtLSU	Mitochondrial large subunit
mtRF1	Mitochondrial peptide chain release factor 1
mtRF1a	Mitochondrial peptide chain release factor 1-like
mtSSU	Mitochondrial small subunit
mt-tRNA	Mitochondrial transfer ribonucleic acid
NCR	Non-coding region
N-terminal	Amino-terminal
OMM	Outer mitochondrial membrane
OPA1	Optic atrophy 1
OXPHOS	Oxidative phosphorylation system
PAGE	Polyacrylamide gel electrophoresis
PBS	Phosphate buffered saline
PCR	polymerase chain reaction
PES	Polypeptide exit site
Phe	Phenylalanine
PK	Proteinase K
PMSF	Phenylmethylsulfonylfluoride
POLRMT	Mitochondrial DNA-directed RNA polymerase
PPR	Pentatricopeptide repeat

Pro	Proline
P site	Peptidyl site
PTC	Peptidyl transferase centre
PVDF	Polyvinylidene fluoride
RNA	ribonucleic acid
ROS	Reactive oxygen species
rpm	Rounds per minute
RRF	Ribosome recycling factor
rRNA	Ribosomal ribonucleic acid
S. cerevisiae	Saccharomyces cerevisiae
SAM	Sorting and assembly machinery
SDS	Sodium dodecyl sulfate
SILAC	Stable isotope labelling by amino acids in cell culture
SSU	small subunit
T	Thymine
T. brucei	Trypanosoma brucei
TAE	Tris/acetate/EDTA buffer
TEFM	Transcription elongation factor
TFAM	Mitochondrial transcription factor A
TFB2M	Mitochondrial transcription factor B2
TIM	Translocase of the inner mitochondrial membrane
TOM	Translocase of the outer mitochondrial membrane
tRNA	Transfer ribonucleic acid
TRNT1	tRNA nucleotidyltransferase 1
U	Uracil
UTR	Untranslated region
v/v	Volume / volume
Val	Valine
VDAC	Voltage-dependent anion-selective channel
WT	Wild type

1. Abstract

The rise of high-resolution cryo-EM structures of the human mitochondrial ribosome increased the understanding of the function and assembly. As the mitochondrial ribosome differs in structure and composition compared to its bacterial counterpart, it is tempting to believe that the assembly pathway of the mitochondrial ribosome also reveals differences to the bacterial system. Although the assembly of the bacterial ribosome has been excessively studied, the human mitochondrial ribosome biogenesis has yet to be solved. Within the last years, an increasing number of human diseases was reported, which were caused by mutations in genes encoding for proteins required by the mitochondrial ribosome. Therefore, it is crucial to understand the complex mechanism by which the mitochondrial ribosome assembly is facilitated.

In this study, the early assembly pathway of the 28S mtSSU was analyzed in more detail by dissecting the role of the early-binding MRPs uS7m, mS27 and mS40. Ablation of uS7m, mS27 or mS40 did not affect their sub-module formation, albeit late-binding MRPs were strongly decreased in the absence of uS7m, mS27 or mS40. Furthermore, loss of either uS7m, mS27 or mS40 influenced the mtLSU assembly and indicates to a potential cross-dependence between the biogenesis of the mtSSU and mtLSU.

In a second part, analysis of uS7m p.Met184Val revealed that the patient mutation leads to a destabilization of uS7m. Although the patient mutation of uS7m retains its ability to be incorporated during mtSSU biogenesis, the destabilizing nature of the mutation led to a strong decrease of the mtSSU assembly efficiency and results into the decline of mitochondrial translation.

During this work, analysis of the mS40 interactome enabled the identification of NT5DC2 as a mitochondrial matrix protein, which is potentially involved in mitochondrial translation. NT5DC2 could be shown to be strongly decreased when mitochondrial ribosome function was disturbed. Furthermore, ablation of NT5DC2 revealed a decrease in mitochondrial translation, underlining a potential involvement of NT5DC2 in mitochondrial gene expression.

The findings of this study allowed the outline of a potential assembly pathway of the early-binding proteins uS7m, mS27 and mS40 and unraveled a potential interdependency during mtSSU and mtLSU biogenesis.

2. Introduction

2.1 Mitochondria

2.1.1 Structure and importance of mitochondria

Mitochondria are eukaryotic organelles that constitute a central hub for regulating cellular activities. The presence of DNA and an active translation machinery within mitochondria is explained in more detail by the endosymbiotic theory (Corliss and Margulis, 1972). The mammalian mitochondrial DNA (mtDNA) of organelles is present in a circular form similar to bacteria (Timmis et al., 2004). Gray et al. made crucial contributions to a detailed analysis of the mtDNA as well as the confirmation that bacteria are the origin of mitochondria (Gray, 1998; 1983). It was shown further from the rRNA evolutionary tree that mitochondria have an α-proteobacterial lineage (Martijn et al., 2018). Interestingly, sequencing analysis of the mtDNA elucidated a 'reductive evolution'. This results in a smaller mtDNA, encoding for less proteins in higher eukaryotes compared to the large ancestral-like mitochondrial genome of protists (Kurland and Andersson, 2000). Thereby most of the genetic information was transferred into the eukaryotic nucleus, while the mtDNA, located in the matrix of the mitochondrion, encodes for less than 1% (Wiedemann and Pfanner, 2017). The structure of the mitochondrion is strongly influenced by the origin of the organelle. Mitochondria possess two membranes, which differ in their protein and lipid composition (Figure 1). The outer mitochondrial membrane (OMM), which is similar to the ancestral bacterial host membrane in its lipid composition, serves as a barrier between the organelle itself and the cytosol. It only allows small ions and metabolites to diffuse into the organelle by making use of voltage-dependent anion-selective channels (VDAC) (Benz, 1994; O'Brien and Brierley, 1965). This permeable nature of the OMM leads to an ionic composition in the mitochondrial intermembrane space (IMS), which is similar to the cytosol.

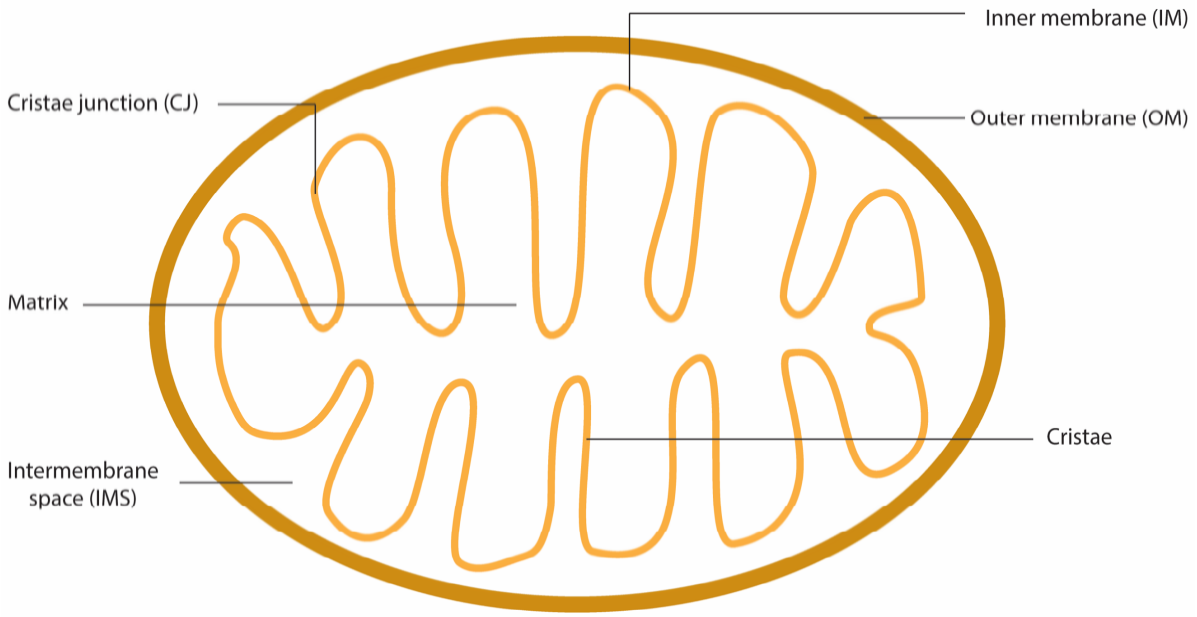

Figure 1: Organization of the mitochondrion.

The inner mitochondrial membrane (IMM) on the other hand retained properties of the eukaryotic membrane (Frey and Mannella, 2000). Invaginations of the IMM into the matrix, leads to the formation of cristae and cristae junctions (CJ). The creation of the cristae is mediated by the multisubunit mitochondrial contact site and cristae organizing system (MICOS) complex and the optic atrophy 1 (OPA1). Opposite of the CJ, dimerization of the ATP-synthase complex (complex V) leads to the formation of the cristae tips (Cogliati et al., 2016; Guarani et al., 2015; Harner et al., 2011; Rabl et al., 2009; Strauss et al., 2008).

The oxidative phosphorylation systems (OXPHOS) is localized in the cristae membrane (Cogliati et al., 2016) and is responsible for the cellular ATP synthesis, one of the most well-known task of mitochondria (Stoldt et al., 2018). Aside from providing the cell with energy in form of ATP, mitochondria are also involved in other important functions: Iron-sulfur (FeS) cluster biogenesis (Pandey et al., 2015), β-oxidation of fatty acids, the tricarboxylic acid (TCA) cycle as well as calcium signaling and apoptosis (Eaton et al., 1996; Rizzuto et al., 2012; Tait and Green, 2012; Van Der Bliek et al., 2017).

2.1.2 The oxidative phosphorylation system

As mentioned above, mitochondria are best known for their role of ATP production, leading to the term 'the powerhouse of the cell'. This is facilitated by aerobic respiration of the eukaryotic cell, which is carried out by the OXPHOS machinery in the IMM. The OXPHOS machinery consists of five complexes, that are mostly of a dual genetic origin: NADH:ubiquinone oxidoreductase (complex I), succinate dehydrogenase (complex II), ubiquinol-cytochrome *c* reductase (complex III) and cytochrome *c* oxidase (complex IV) and the ATP synthase (complex V) (Figure 2).

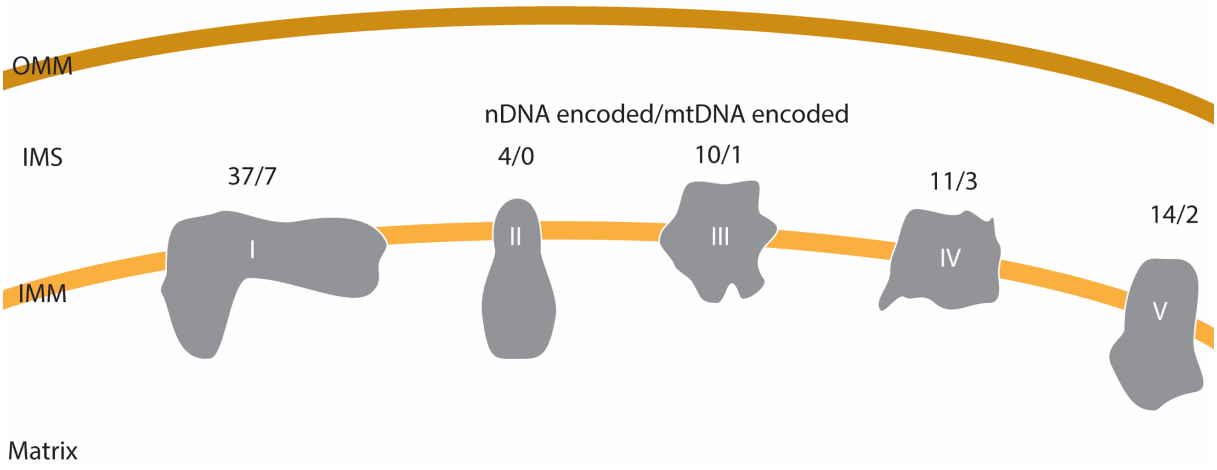

Figure 2: Subunit components of the oxidative phosphorylation system (OXPHOS) are of dual genetic origin aside from complex II. Most of the proteins are translated in the cytosol (nDNA) and imported into the mitochondria. Core proteins of the OXPHOS complexes I, III, IV and V are mitochondrial encoded (mtDNA). (Balsa et al., 2012; Bezawork-Geleta et al., 2017; Fernandez-Vizarra, 2015; He et al., 2018; Zong et al., 2018).

Within the glycolysis, TCA cycle and β-oxidation, NADH and $FADH_2$ are generated and subsequently oxidized by the OXPHOS complexes I and II in the IMM. Electrons from these reducing equivalents are then transferred trough the complexes I-IV and are required for the reduction of molecular oxygen to water by complex IV. The energy generated by this transfer is used to move protons from the matrix to the IMS to generate an electrochemical gradient. This created membrane potential is then employed for the ATP production catalyzed by complex V (Belevich and Verkhovsky, 2008; Koopman et al., 2013; Saraste, 1999).

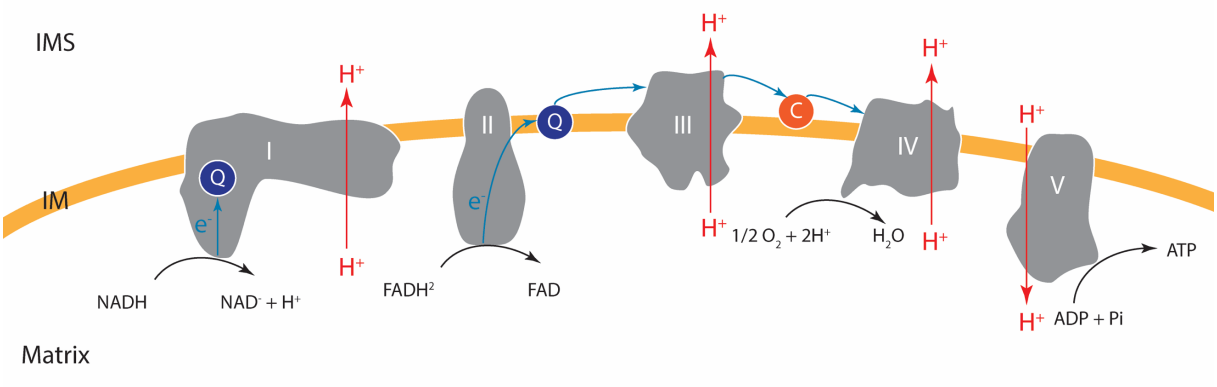

Figure 3: Oxidative phosphorylation machinery (OXPHOS). The respiratory chain complexes (complex I, II, III and IV) transfer electrons from reducing equivalents (NADH and $FADH_2$) to oxygen with the help of ubiquinone (Q, blue circle) and cytochrome c (C, red circle). As a result, oxygen is reduced to water by complex IV. The transportation of electrons through complexes I, III and IV generates a proton gradient. This gradient is then used by complex V to generate ATP.

The largest complex within the OXPHOS system is the NADH:ubiquinone oxidoreductase (complex I), which oxidizes NADH. Complex I consist of 45 subunits, whereby 37 are encoded in the nucleus and 7 are encoded by the mitochondrial genome (Balsa et al., 2012; Sharma et al., 2009; Signes and Fernandez-Vizarra, 2018). The succinate dehydrogenase (complex II), the second and smallest complex of the OXPHOS system, consists of 4 nuclear-encoded proteins and oxidize $FADH_2$ (Bezawork-Geleta et al., 2017; Signes and Fernandez-Vizarra, 2018). While both complexes can subsequently transfer two electrons to ubiquinone, only complex I can transport protons across the IMM into the IMS (Cecchini, 2003; Fiedorczuk et al., 2016). The reduced ubiquinol is oxidized by the third complex, ubiquinol-cytochrome *c* reductase (complex III), which transfers electrons from the ubiquinol to the electron carrier, cytochrome *c*. Complex III consists of 10 nuclear-encoded proteins and one mitochondrial-encoded protein. The reduced cytochrome *c* transfers then electrons to the cytochrome *c* oxidase (complex IV), which uses the electrons to reduce molecular oxygen to water while transferring a proton across the IMM (Saraste, 1999; Signes and Fernandez-Vizarra, 2018). Complex IV is the last complex belonging to the electron transport chain and consists of 11 nuclear-encoded and 3 mitochondrial-encoded subunits (Balsa et al., 2012; Cogliati et al., 2016; Saraste, 1999; Signes and Fernandez-Vizarra, 2018). The 4 complexes together with the ATP synthase (complex V) form the so called OXPHOS system. Complex V is a 16-subunit large complex which

uses the proton gradient generated by complex I, III and IV to synthesize ATP (Figure 3) (He et al., 2018; Signes and Fernandez-Vizarra, 2018).

2.1.3 Import of the nuclear-encoded proteins into mitochondria

Only 1% the mitochondrial proteome is encoded by the mtDNA. Most of the mitochondrial proteins are nuclear-encoded and need to be imported from the cytosol into the mitochondria by specialized translocases (Meisinger et al., 2008; Wiedemann and Pfanner, 2017).

One of the import pathways, which most of the mitochondrial proteins follow is the presequence pathway: In order to target proteins to the mitochondria, precursor proteins (pre-proteins) need to contain a specific signal, a cleavable N-terminal positively charged presequence. Presequence containing proteins are translocated through the OMM by the translocase of the outer membrane (TOM) and inserted through the IMM or directed to the mitochondrial matrix via the translocase of the inner membrane (TIM23). Translocation of proteins into the matrix requires energy in form of the membrane potential and the presequence translocase-associated motor (PAM). Once in the matrix, the mitochondrial presequence peptidase cleaves the presequence from the precursor protein (Callegari et al., 2020; Chacinska et al., 2005; Kang et al., 2017; Wiedemann and Pfanner, 2017). Also, all the factors required for mitochondrial gene expression are translated in the cytosol and need to be imported into the mitochondrial matrix.

2.2 Mitochondrial gene expression

2.2.1 The mitochondrial genome

As mentioned above, only a portion of the mitochondrial proteins are encoded by the mtDNA. The mtDNA is exclusively maternally inherited, making it highly susceptible in accumulating harmful mutations over time. The mtDNA co-evolved with their eukaryotic host cells, whereby the co-evolutional events occurred independently within the lineages, leading to a high diversity between different species (Burger et al., 2003). These co-evolutionary events led to a decrease in size of the mtDNA (Burger et al., 2003).

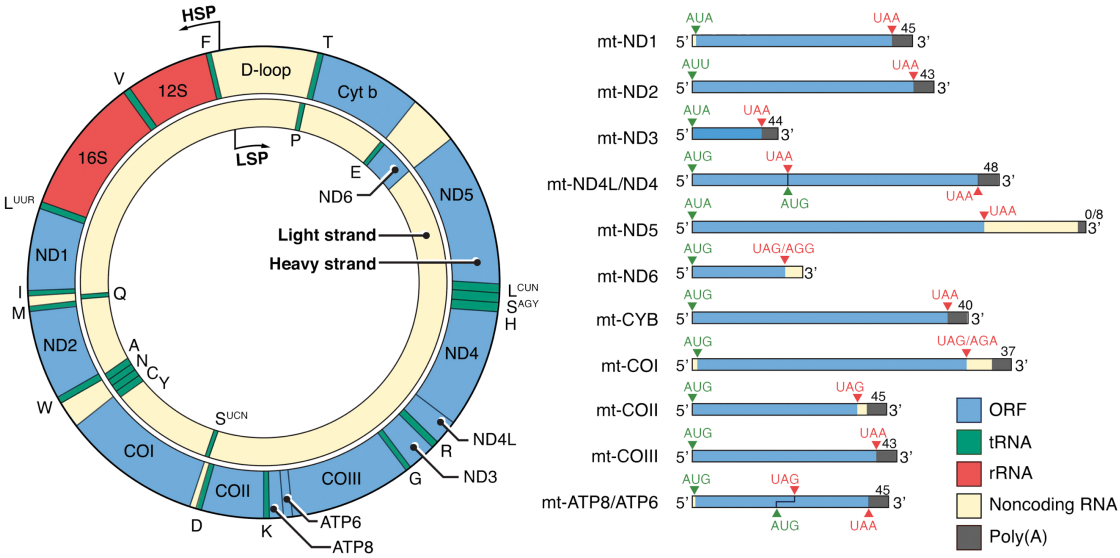

Figure 4: Organization of the mitochondrial genome and its transcripts. The mtDNA consists of an H- and L-Strand. The mtDNA encodes for 11 mRNAs of the OXPHOS core proteins (blue), 2 mt-rRNA cores of the mitochondrial ribosome (red) and 22 tRNAs (green). The non-coding regions are represented in beige. Only ND5, ND6, CO1 and CO2, contain a short 3' untranslated region (UTR). Aside from ND5 and ND6, a polyA tail is present in all transcripts. Furthermore a 5' UTR is not present in mitochondrial encoded transcripts. Picture adapted from (Hällberg and Larsson, 2014).

The human mtDNA is a double-stranded, circular molecule, consisting of 16 569 bp. It consists of 37 genes encoding for two mitochondrial rRNAs (mt-rRNA) (12S and 16S mt-rRNA), 22 mitochondrial tRNAs (mt-tRNA) and 13 proteins, that are core subunits of the OXPHOS complexes I, III, IV and V (Anderson et al., 1981). The two mtDNA strands, labelled historically as the light (L) and heavy (H) strand differ in their base composition (Berk and Clayton, 1974). The heavy strand is rich in guanines, therefore possessing a higher molecular mass. Interestingly, most of the genetic information is stored in the heavy strand, although both strands encode functional elements (Figure 4). The light strand encoded for the replication primer of the heavy strand, 7 mt-tRNAs, and ND6, a complex I subunit (Battey and Clayton, 1978). The origin of the heavy strand, the heavy strand promotor (HSP) and the light strand promotor (LSP) are localized in the non-coding region of the mtDNA called D-loop (Gustafsson et al., 2016).

The mitochondrial DNA is, similar to bacterial DNA packed into small structures, namely nucleoids (Dame et al., 2012). In mammals, the mtDNA molecule of approximately 5 μm lengths is densely packed into nucleoids of roughly 100 nm (Kukat and Larsson, 2013; Nass, 1966). The maintenance of the mtDNA nucleoid structure is

done by the mitochondrial transcription factor A (TFAM). TFAM belongs to the high mobility group (HMG)-box family and has the ability to bind DNA (Malarkey and Churchill, 2012). Additionally TFAM is able to pack mtDNA into compact nucleoids through a cooperative binding mode, whereby the condensation of the mtDNA molecule is increased upon enriched TFAM protein-DNA interaction (Bogenhagen, 2012).

2.2.2 Mitochondrial transcription

Nucleoids not only contain components important for mtDNA packing but also for maintenance and transcription. Transcription of mtDNA takes place in the matrix (Pearce et al., 2017; Satoh and Kuroiwa, 1991). Initiation of transcription in human mitochondria is driven by POLRMT, a DNA dependent RNA polymerase. POLRMT resembles structurally the RNA polymerases in T7 bacteriophages (Ringel et al., 2011; Tiranti et al., 1997). In fact, two pentatricopeptide repeat (PPR) domains similar to the T7 bacteriophages can be found at the N-terminal domain of POLRMT (Ringel et al., 2011). These PPR domains are found in proteins associated with RNA and are required for the protein-RNA interaction (Barkan et al., 2012). In contrast to bacteriophage polymerases, where promotor regions are recognized without additional proteins, the initiation of transcription in mammals requires the already mentioned TFAM and the mitochondrial transcription factor B2 (TFB2M). TFB2M is a ribosomal methyltransferase but also functions as a protein which denatures DNA during initiation of transcription (Falkenberg et al., 2002). To initiate transcription TFAM binds to the mtDNA at the promotor region of the H and L strands (HSP and LSP) and recruits POLRMT to the promotor with its N-terminal extension. TFB2M modifies the structure of POLRMT and induce thereby an opening in the promotor sequence. For the elongation step, POLRMT requires the transcription elongation factor (TEFM), which promotes POLRMT in its interaction with the DNA-RNA template (Posse et al., 2015). TEFM furthermore assists POLRMT in bypassing highly structured RNA that stimulates transcription post oxidative lesion, which are able to lead to premature termination of transcription (Agaronyan et al., 2015).

The mitochondrial termination factor 1 (MTERF1) has been identified as a factor involved in the termination of the LSP transcription at the 3'-end of the mt-rRNA coding

sequence. This factor prevents the replication fork from progressing into the mt-rRNA genes while these mt-rRNAs are being transcribed. MTERF1 serves also to avoid transcription of the antisense sequence of the mt-rRNA (Hillen et al., 2018; Shi et al., 2016; Terzioglu et al., 2013). Further members of the MTERF family (MTERF 2-4) are also associated to other processes, like the mitochondrial ribosome assembly through formation of the MTERF4-NSUN4 heterodimer (Metodiev et al., 2014).

2.2.3 Mitochondrial RNA processing

Once the H and L strand are transcribed into large polycistronic and intron free mt-RNA molecules, these mt-RNAs need to be further processed to release their functional elements. The mt-rRNA as well as most of the protein coding sequences are flanked by mt-tRNA. To release the functional elements from the polycistronic transcript, the mt-tRNAs are processed by the endonuclease RNase P and RNase Z at the 5'- and 3'-end. This process is also known as the widely accepted "tRNA punctuation model" (Ojala et al., 1981). Processing of the polycistronic transcripts takes place in mitochondrial RNA granules (MRG), that contain mt-RNA processing and modification enzymes including RNase P and RNase Z (Holzmann et al., 2008; Jourdain et al., 2013). After the 5' and 3' end processing, tRNAs undergo extensive post-transcriptional maturation, such as the 3'-terminal CCA addition catalyzed by TRNT1 (Hou, 2010; Reinhard et al., 2017). The G-rich sequence factor 1 protein (GRSF1) is able to bind RNA and was suggested to play a role in the processing of classical and tRNA-less RNA precursors. While not experimentally determined, it is assumed that GRSF1 might be involved in the mtSSU assembly as loss of GRSF1 leads to an abnormal cleavage of primary tRNA transcripts. This results further into a reduction of mitochondrial encoded proteins and mitochondrial ribosome assembly (Antonicka et al., 2013; Jourdain et al., 2013).

As a consequence of the mt-tRNA processing, the mitochondrial mRNA (mt-mRNA) is released, with the exceptions of *ND5/Cyt b* and *ATP6/COX3*, which are not flanked by mt-tRNAs (Figure 4). The mechanism underlying the processing of these mt-mRNAs remains enigmatic (Barchiesi et al., 2015). Various Fas-activated serine/threonine kinases (FASTK) have been reported to be required for mt-RNA stability as well as for processing of precursors like *ND5/CYTB*. However, their endonucleolytic activity has

yet to be shown (Boehm et al., 2017). In contrast to the cytosolic mRNAs, mammalian mt-mRNAs lack significant 5' and 3' untranslated regions (UTR) (Temperley et al., 2010). They also do not present a Shine-Dalgarno Sequence or a 7-methylguanosine cap at the 5'-end. The latter is essential in eukaryotes for translation initiation, whereby in mitochondria translation initiation and regulation remains to be further elucidated (Cowling, 2009; Hällberg and Larsson, 2014; Montoya et al., 1981). Most of the mitochondrial mt-mRNAs contain a short polyA tail of 45 – 50 nt length at the 3'-end and in some cases, polyadenylation is required for some transcripts to complete the STOP codon UAA. The exception is *ND5* and *ND6*, which can be immediately translated upon release from the polycistronic transcript (Ojala et al., 1981; Temperley et al., 2010).

2.2.4 Mitochondrial translation

Mitochondrial translation is similar to the bacterial and the cytosolic eukaryotic translation. It can be summarized in a four-step process: i) Translation initiation, where the ribosome assembles around the mt-mRNA and positions itself at the start codon; ii) elongation, where through addition of amino acids the polypeptide is formed; iii) termination, where the polypeptide chain is released from the ribosome and iv) ribosome recycling, where the ribosome is dissociated into subunits and can re-initiate a new round of translation (Figure 5). Translation in mitochondria is dependent on nuclear-encoded translation factors, which have homologues in bacteria (Christian and Spremulli, 2012). In bacteria, translation initiation is aided through three initiation factors, IF 1 – 3. Each of them binds to a specific site of the bacterial 30S small subunit and assists in the formation of the 30S initiation complex (30SIC) (Gualerzi and Pon, 2015). During the transition from 30S to 30SIC the three IFs disassociate from the 30S. The 3'-end of the 16S rRNAs, component of the 30S, interacts with the highly conserved Shine-Dalgarno sequence of the mRNA. This enables the 30S to recognize the start codon for translation initiation (Gualerzi and Pon, 2015). In contrast to bacteria, mammalian mt-mRNAs lack 5'- UTR and therefore a Shine-Dalgarno sequence is not present in the mt-mRNA. Accordingly, the complementary anti-Shine-Dalgarno sequence in the mammalian mt-rRNA (12S mt-rRNA) of the small ribosome subunit (SSU) is also missing (Jones et al., 2008). In mammals, the start codon is located within three nucleotides of the 5'-end (Jones et al., 2008; Koc and Spremulli,

2002) and only IF2 and IF3 homologues were indentified in mitochondria (mtIF2, mtIF3), while an IF1 homologue has yet to be identified (Koc and Spremulli, 2002). It has been shown that mtIF2, having a 37 amino acid insertion, is able to functionally replace IF1 in *E. coli* (Gaur et al., 2008).

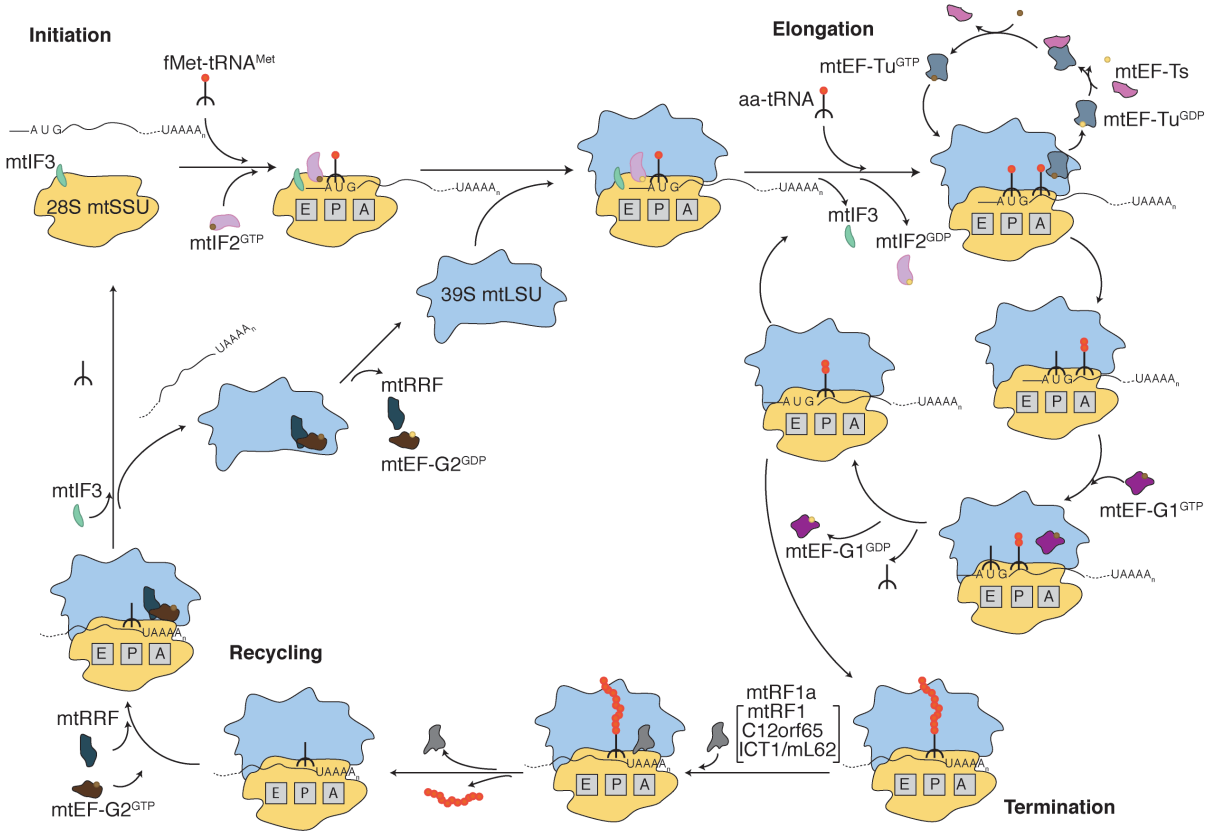

Figure 5: Mitochondrial translation cycle. Picture adapted from (Smits et al., 2010) and the representation of the initiation steps are adapted from (Koripella et al., 2020b; Kummer et al., 2018)

In the first step of translation initiation in mammalian mitochondria, mtIF3 is recruited to the 28S mitochondrial small subunit (mtSSU) and prevents premature 55S monosome formation in the absence of mt-mRNA (Amunts et al., 2015; Greber et al., 2015). In the presence of mt-mRNA, GTP-bound mtIF2 ($mtIF2^{GTP}$) recognizes and assists in the placement of the formylated Met-$tRNA^{Met}$ ($fMet\text{-}tRNA^{Met}$) into the P site (binding site of the peptidyl tRNA) of the mtSSU. During translation initiation, mitochondrial ribosomal proteins (MRPs) of the mtSSU also participate in the mt-mRNA docking. mS39, a mitochondrial ribosomal specific PPR protein, binds to the mt-mRNA at the mitochondrial ribosomal mRNA entry channel (Amunts et al., 2015; Greber et al., 2015; Kummer et al., 2018). Furthermore uS5m, another MRP of the mtSSU, aids to place the mt-mRNA to the A site and P site. A positively charged

mitochondrial specific extension of uS5m enables its interaction with the mt-mRNA, which is recognized at the A site. Then, uS5m guides then the mt-mRNA towards the P site, where codon-anticodon interaction stabilizes the mt-mRNA in the frame (Figure 5) (Kummer et al., 2018). This stabilization is supported through the specific recognition of fMet-tRNA^{Met} by mtIF2^{GTP}. In mitochondria only one type of tRNA^{Met} is used during translation initiation and elongation, albeit fMet-tRNA^{Met} is used during translation initiation. The formyl group on the tRNA^{Met} methionine is therefore the sole determinant that allows mtIF2 to distinguish between initiation and elongation (Kummer et al., 2018). After assembling the initiation complex, the 39S mitochondrial ribosomal large subunit (mtLSU) joins (Kummer et al., 2018). The interaction between the mtSSU and the mtLSU is completed upon hydrolysis of GTP to GDP by mtIF2 and release of mtIF2 and mtIF3 (Christian and Spremulli, 2010; 2012; Kummer et al., 2018).

Recent studies by Khawaja et al. (2020) suggest a mechanism of mitochondrial translation initiation, which is distinct to the one described in bacteria. The MRP mS37 is proposed to stabilize the mtSSU in the presence of mtIF3. This mitochondrial pre-initiation complex (mtPIC-1) inhibits the binding of fMet-tRNA^{Met} to the mtSSU. Afterwards, the accommodation of mtIF2^{GTP} results in the second mitochondrial pre-initiation complex (mtPIC-2). The formation of mtPIC-2 allows the recruitment of the mtLSU and release of mtIF3, which is replaced by fMet-tRNA^{Met}. The association of the mt-mRNA was described as the last step during the assembly of the translation initiation complex (Khawaja et al., 2020). Which pathway is more likely is still under debate.

Recent Cryo-EM studies by Koripella et al. (2020) and Kummer et al. (2018) showed a conformational change of the MRP mL45 between the initiation and elongation stage. The ribosomal exit tunnel, is blocked by the N-terminal tail of mL45 during the elongation stage. Therefore the N-terminal extension of mL45 has to be removed to allow elongation (Koripella et al., 2020b; Kummer et al., 2018). This conformational change is suggested to be required in mediating membrane anchoring of the 55S ribosome to the IMM (Koripella et al., 2020b).

The elongation process is mediated by the mitochondrial elongation factors mtEF-Tu, mtEF-Ts and mtEF-G1(Hammarsund et al., 2001; Ling et al., 1997). It starts with the

recruitment of mtEF-Tu^{GTP} coupled with an aminoacyl-tRNA (aa-tRNA) to enter the A site of the 55S monosome. Upon base pairing of the introduced aminoacyl-tRNA with the mt-mRNA at the codon-anticodon site, GTP is hydrolyzed to catalyze peptide bond formation. The mtEF-Tu^{GDP} complex is released from the ribosome and mtEF-Tu^{GDP} is re-charged with GTP by the help of mtEF-Ts for a new elongation cycle (Figure 5) (Cai et al., 2000). The GTPase mtEF-G1 catalyzes the translocation of the peptidyl-tRNAs from the A to the P site accompanied with the coordinated movement of the deacylated mt-tRNA from the P site to the exit (E) site (Figure 5) (Agirrezabala and Frank, 2009; Schwartzbach and Spremulli, 1989).

During translation termination, class I release factors recognize sequence specific the STOP codon in the A site and facilitate the hydrolysis of the ester bond between the peptidyl mt-tRNA and the nascent peptide chain. While bacteria utilize the classical stop codons UAA, UAG and UGA, mitochondria only make use of UAA and UAG codons (Figure 4) (Korkmaz et al., 2014; Richter et al., 2010a). UGA has been reassigned as tryptophan. The codons AGA and AGG do not encode for arginine and have been suggested to be stop codons for the mitochondrial transcripts *MTCO1* and *MTND6* (Anderson et al., 1981). However, a -1 frameshift by the mitochondrial ribosome will result in UAG STOP codon in the A site of these transcripts, which can be recognized by a canonical release factor (Temperley et al., 2010). Four translation termination factors have been identified in mammalian mitochondria: mitochondrial release factors 1 and 1a (mtRF1, mtRF1a), immature colon carcinoma transcript-1 (ICT1) and C12orf65. The mitochondrial release factor mtRF1a is also able to recognize the STOP codons UAA and UAG (Richter et al., 2010b; Soleimanpour-Lichaei et al., 2007). A recent study provided evidence, that C12orf65 plays a role in the mitochondrial ribosome-associated quality control (mtRQC) pathway and acts as a release factor on stalled and split mtLSU mt-tRNA-nascent chains (Figure 5) (Desai et al., 2020). The release factor ICT1, a bacterial ArfB homolog, is able to facilitate peptide release in a codon-independent manner, suggesting that it might be involved in rescuing stalled ribosomes (Richter et al., 2010b). Interestingly, ICT1 (mL62) has also been recruited to the mitochondrial ribosome and is a structural component of the central protuberance (Brown et al., 2014; Richter et al., 2010b).

After the release of the emerging peptide chain, the ribosome is recycled by mtRRF and mtEF-G2. By occupying the A site of the mitochondrial ribosome, mtRRF and EF-G2 promote the disassociation of the 55S monosome and the release of the deacylated mt-tRNA as well as the mt-mRNA. The free mtSSU associates with mtIF3 again and the subunits are available for a new translation cycle (Figure 5) (Christian and Spremulli, 2012; Koripella et al., 2020a)

2.3 The mitochondrial ribosome

2.3.1 Structure

The structure of the mammalian mitochondrial ribosome differs significantly from the bacterial ancestor (Figure 6).

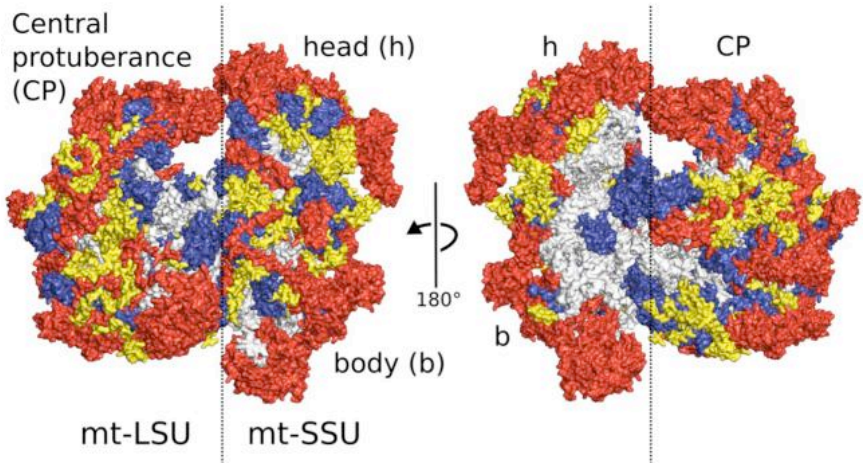

Figure 6: Overview of the human 55S mitochondrial ribosome Conserved proteins of the bacterial and human mitochondrial ribosome are depicted in blue. The human homologues of the bacterial ribosomal proteins that contain mitochondrial specific extensions are shown in yellow. Mitochondrial ribosome specific proteins are shown in red and the mt-rRNA in grey. Picture adapted from (Amunts et al., 2015)

A reduction of the mitochondrial mt-rRNA is strongly noticeable in the length of the mammalian mt-rRNA (12S: 954 nt, 16S: 1559 nt) (Anderson et al., 1981) compared to the length of the bacterial (16S: 1542 nt, 23S: 2904 nt, 5S: 120 nt) (Schaechter and Group, 2001) or yeast (15S: 1649 nt, 21S: 3296 nt) (Amunts et al., 2014; Desai et al., 2017) mitochondrial rRNA. Contrary to the decline of mitochondrial mt-rRNA, the number of MRPs expanded from 54 in bacteria to 82 in mammalian and yeast mitochondria (Table 2) (Greber and Ban, 2016). Cryogenic electron microscopy (Cryo-EM) analysis provided structural insights into the different organization between

mitochondrial ribosomes in yeast and mammals compared to the bacterial ribosome (Amunts et al., 2015; Brown et al., 2014; Desai et al., 2017; Greber et al., 2015; 2014; Sharma et al., 2003).

Table 2: Overview of the composition of different ribosomes. Table adapted from (Greber and Ban, 2016).

	Bacteria (E. coli)	Eukaryotic cytosol	Mammalian mitochondria	Yeast mitochondria
Ribosome	70S	80S	55S	74S
Molecular weight	2.3 MDa	3.3 – 4.3 MDa	2.7 MDa	3 – 3.3 MDa
rRNA cores	3	4	2 + 1 tRNA	2
No. of proteins	54	79 – 80	82	82
Large subunit	50S	60S	39S	54S
rRNAs	23S/5S	26S-28S/5.8S/5S	16S + mt-tRNA$^{Phe/Val}$	21S
No. of proteins	33	46 – 47	52	46
Small subunit	30S	40S	28S	37S
rRNAs	16S	18S	12S	15S
No. of proteins	21	33	30	36

The most noteworthy difference of the mitochondrial ribosome, compared to its bacterial ancestor, is the loss of the 5S rRNA (Nierlich, 1982). The 5S rRNA is a conserved structure in all domains of life. It serves as a structural scaffold and forms the central protuberance (CP) with ribosomal proteins in the large subunit (Korepanov et al., 2012). The CP is located in the large subunit contacts the small subunit, serving as a physical bridge between the two subunits as well as movement coordination during translation (Ben-Shem et al., 2011). Although the 5S rRNA is missing in mitochondria, a structural mt-tRNA, mt-tRNA^{Val} in human and mt-tRNA^{Phe} in porcine, were positioned similar to the 5S rRNA in bacteria (Brown et al., 2014; Greber et al., 2014). Furthermore, both mt-tRNAs flanked the 12S mt-rRNA of the mtSSU and are able to interact with MRPs in the CP, especially with the MRP uL18m. Remarkably, uL18m, homologue to the bacterial uL18, shares a preserved interaction with the 5S rRNA (Greber and Ban, 2016). Interestingly, in yeast, instead of replacing the 5S rRNA by a structural mt-tRNA similar to mammalian, an expansion of an already existing mt-rRNA serves as a replacement (Amunts et al., 2014).

Another distinct structural adaption is the mammalian polypeptide exit tunnel, the path nascent chains are passing to be released from the ribosome. The mitochondrial

ribosome evolved, contrary to eukaryotic cytosolic or bacterial ribosomes, to adjust to the synthesis of membrane proteins (Brown et al., 2014). The evolution of the peptide exit tunnel was alleviated through the exchange of former bacterial rRNA structures with MRPs, adding to the ability to establish new characteristics to the exit tunnel surface. In fact, all protein residues facing the surface of the exit tunnel have a hydrophobic nature like the wall of the polypeptide exit tunnel. This suggest that i) the exit tunnel mimics the hydrophobic environment of the membrane and ii) that the increased hydrophobic interaction serves to slow down the rate of elongation. This enables transmembrane domains to fold and the assembly of the OXPHOS complex to proceed within an increased time span (Brown et al., 2014).

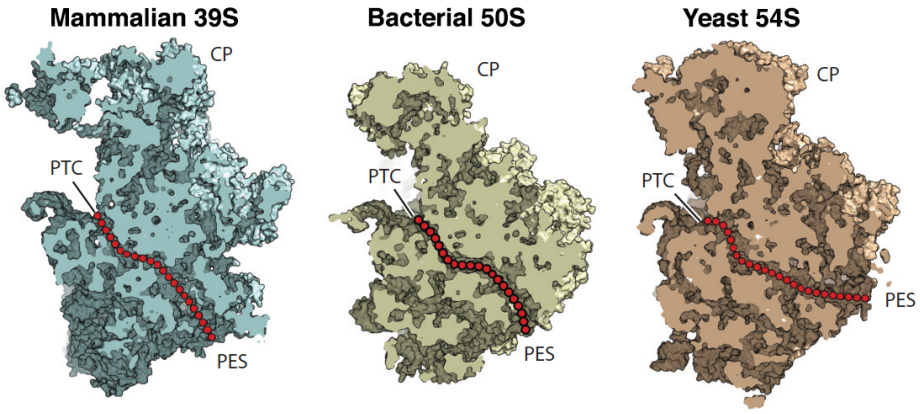

Figure 7: Comparison of the polypeptide tunnel path of bacterial, mammalian and yeast mitochondrial ribosomes. The polypeptide exit site (PES) in mammalian mitochondria resembles the bacterial one, while the yeast PES was re-localized. Further abbreviations used: CP = central protuberance, PTC = peptidyl transferase center. Picture adapted from (Greber and Ban, 2016).

Interestingly, the exit tunnel of the human mitochondrial ribosome still shows resemblance to its bacterial ancestor, while the exit tunnel of the yeast mitochondrial ribosome was re-localized 3.5 nm away from the bacterial counterpart (Figure 7) (Amunts et al., 2014; Brown et al., 2014). Loss of the helix 24 of the 18S rRNA created the path into the solvent for the nascent chain. Furthermore, extension of the mitochondrial ribosomal protein uL23m blocked the conserved path in the ribosome. These two major structural changes led to the re-localization of the mitochondrial exit tunnel (Amunts et al., 2014).

Another structural difference of the mitochondrial ribosome lies at the end of the exit tunnel. The mammalian mL45 has C-terminal helices which extend into the inner

mitochondrial membrane (Greber et al., 2014). mL45 mediates the membrane association of the mitochondrial ribosome and assists in the membrane insertion of mitochondrial polypeptides (Englmeier et al., 2017; Greber et al., 2014). The mL45 yeast homolog, Mba1, emphasize the crucial trait of membrane association of mitochondrial ribosomes. Mba1 is occasionally associated with the mitochondrial ribosome and mediates the membrane association of translational active mitochondrial ribosomes. Furthermore, Mba1 acts as a shuttling factor of polypeptide nascent chains from the mitochondrial ribosome to OXPHOS assembly intermediates (Amunts et al., 2014; Lorenzi et al., 2016; Ott et al., 2006; Preuss et al., 2001).

Although the evolutional changes led to several adaptions of the mitochondrial ribosome, only few mitochondrial specific elements in the mt-rRNA catalytic core of the ribosome are still conserved among species. Variations within the A, P and E sites are present and affect the mitochondrial translation. The conventional four-armed, cloverleaf secondary structure of the tRNAs shows in many human mt-tRNAs either the absence or a reduction of the D- or T-loop, resulting in a loss of the tRNA elbow (Brown et al., 2014). Furthermore, uL25 as well as part of the rRNA helix H38, which are responsible to fixate the tRNA elbow to the A site in bacteria, are missing in mitochondria. Similar deletions were observed in the P site. uL5 and the helix H84 are lost, although they are required to stabilize the tRNA elbow in bacteria (Brown et al., 2014). It was instead suggested that the P site finger compensates the loss of the ribosome-tRNA interaction in the mitochondrial P site. It was proposed that the P site finger is formed by mL48 and mL40 (Greber et al., 2015) . This new structural element originates from the CP and reaches between the A and P site mt-tRNAs where it contacts both (Greber et al., 2014). Interestingly, the E site is mostly unmodified when compared to its bacterial predecessor. The CCA sequence binding pocket is fully conserved in mitochondrial as well as bacterial ribosomes. Another highly conserved element is the decoding site. It is localized in the mtSSU and displays similar interactions within codon-anticodon helixes, which emphasizes the highly conserved mechanism of protein translation in mitochondria and bacteria (Greber et al., 2015; Koch et al., 2015).

2.3.2 Assembly of the bacterial ribosome

The bacterial ribosome consists of the 30S small subunit (SSU) and the 50S large subunit (LSU) which are composed of three rRNAs (16S, 23S and 5S) and 54 proteins (Greber and Ban, 2016). The assembly of the ribosome is an energetically costly and rapid process which happens independently for both subunits (Chen et al., 2012; Lindahl, 1975). Earliest studies revealed *in vitro* a cooperative nature of the 30S and 50S ribosomal subunit assembly (Herold and Nierhaus, 1987; Mizushima and Nomura, 1970; Traub and Nomura, 1968). The Nomura assembly map shows the complete assembly of the 30S and the Nierhaus assembly map the complete assembly of the 50S subunit *in vitro* (Figure 8). Albeit both assembly maps showed protein binding dependencies in a hierarchical order, the assembly *in vitro* was reconstituted in the absence of assembly factors and represents thermodynamic information of the 30S assembly rather than the kinetic of protein binding. The Nomura assembly map served as the basis for further studies of the 30S assembly (Lindahl, 1975; Sykes and Williamson, 2009; Williamson, 2003). *In vivo*, the different intermediates are distinguished by the subunits as well as their sedimentation coefficient (Lindahl, 1973; Nierhaus et al., 1973).

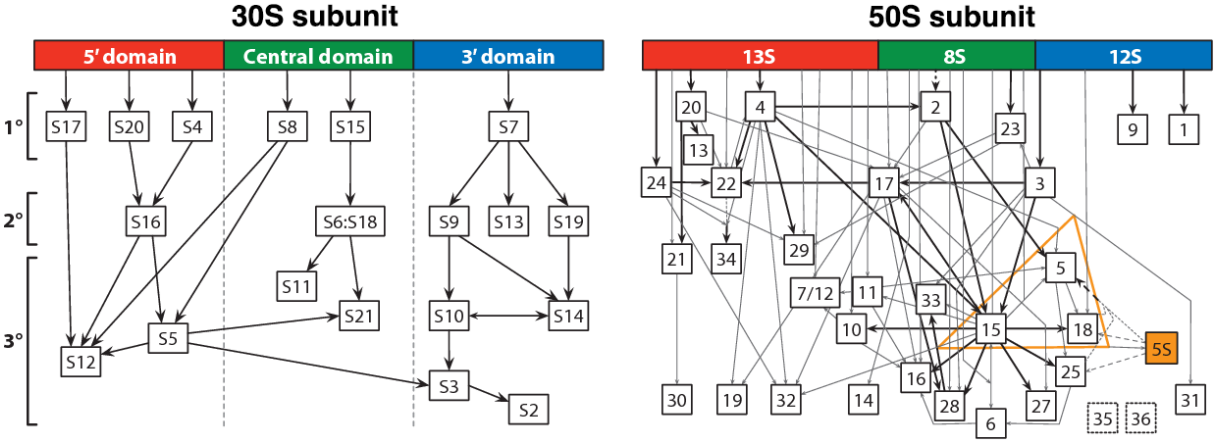

Figure 8: Assembly maps according to Nomura and Nierhaus. The Nomura assembly maps describes thermodynamically the binding of ribosomal proteins of the small subunit to assembly the 30S subunit (left). A clear hierarchy of which are primary (1°), secondary (2°) or tertiary (3°) binding proteins is depicted. Furthermore, there is a clear division into 5' (red), central (green) and 3' (blue) domain, which describes where ribosomal proteins of the SSU bind to the 16S rRNA. Similarly, the assembly of the 50S large subunit is described thermodynamically by the Nierhaus assembly map (right). Integration of the 5S rRNA (orange) is depended on the ribosomal proteins L5, L15 and L18. Furthermore, the Nierhaus assembly map provides a similar division of the 23S rRNA to the domains shown in the Nomura assembly map. Figure adapted from (Shajani et al., 2011)

The 16S, 23S as well as 5S rRNA are transcribed into one long transcript and further processed by up to five nucleases. After maturation, the 16S and 23S rRNAs undergo modifications such as pseudouridylation and methylation (Decatur and Fournier, 2002).

It has been suggested that the assembly of the 30S and 50S subunit follows several assembly pathways (Williamson, 2005). The ribosomal proteins S4 and S7 are assembly initiator proteins and initiate the 30S subunit biogenesis (Nowotny and Nierhaus, 1988). Thereby it was suggested that S4 and S7 initiate their own assembly domain, whereby the S4 assembly domain is compromise of the SSU proteins S4, S20, S16, S15, S6 and S18, while the S7 assembly domain consists of S7, S9, S19 and S3. At a later stage it was proposed that the two domains are interconnected by the ribosomal proteins S8 and S5 (Nowotny and Nierhaus, 1988). During SSU assembly, S7 binds to the 3'-end of the 16S rRNA and initiates its folding, which enables the binding of other ribosomal proteins to form the head of the 30S subunit (Robert and Brakier-Gingras, 2001). Interesstingly, in *E. coli* the expression of ribosomal proteins is regulated by primary binding proteins, which are able to apply a feedback control (Zengel and Lindahl, 1994).

2.3.3 Assembly factors of the bacterial ribosome

Proteins that assist the ribosome assembly are RNA-modifying enzymes, RNA helicases, GTPases and chaperones. In *E. coli* four DEAD-box proteins, proteins with the amino acid sequence Asp-Glu-Ala-Asp or D-E-A-D, have been described to play a role in the ribosome biogenesis: DbpA, CsdA, SrmB and RhlE (Charollais, 2004; Iost and Jain, 2019; Jain, 2008; Trubetskoy et al., 2009). All four were reported to play a role at different stages of the 50S subunit assembly, specifically SrmB and CsdA become important factors at cold temperatures (Charollais, 2004; Iost and Jain, 2019; Iost et al., 2013; Trubetskoy et al., 2009).

GTPases are universally conserved in eukaryotes and bacteria and represent a major class of assembly factors (Britton, 2009; Karbstein, 2007). To date, seven GTPases have been found to be involved in the ribosome biogenesis in *E. coli*. Four proteins, RbgA, ObgE, YsxC and YphC, are involved in the 50S biogenesis while Era, RsgA and

YqeH are implicated in the 30S assembly (Britton, 2009). As an example of this class of proteins, RbgA, ObgE and Era will be further described.

The conserved ribosome biogenesis GTPase A (RbgA), has an essential function in the assembly of the 50S LSU. RbgA acts as a mediator between the transition of a 45S LSU intermediate to the 50S LSU by protecting nucleotides near the A and P site of the 23S rRNA. Then, RbgA recruits either directly or through other ribosomal proteins the ribosomal proteins L17, L27 and L36 to complete the assembly of the 50S LSU (Uicker et al., 2006). The Obg protein in *E. coli* (ObgE) is an essential GTPase, which is widely conserved from bacteria to eukaryotes. While ObgE plays a direct role in chromosome segregation, it also is suggested to be involved in the formation of the 70S monosome by having quality control function of the late stage of assembly of the 50S LSU (Feng et al., 2014; Kobayashi et al., 2001). Depletion of *E. coli* ras (Era) leads to the loss of the 70S monosome and accumulation of the respective subunits. It was shown that Era binds to the anti-Shine-Dalgarno sequence. Thereby Era inhibits the binding of mRNAs with the Shine-Dalgarno sequence and the assembly of the ribosomal protein bS1 to mature SSU. It was suggested that the presence of Era precedes the final maturation steps of the 16S rRNA, indicating that Era stabilizes the 16S rRNA during the last maturation steps (Sharma et al., 2005; Tu et al., 2009).

There are currently two protein machines and one cold shock protein known to be involved in the ribosome biogenesis: DnaK-DnaJ-GrpE, GroEL-GroES and ribosome-binding factor A (RbfA) (Hage et al., 2001; Jones et al., 1996; Shajani et al., 2011; Xia et al., 2003). Briefly, the exact mechanism by which the heat shock protein 70 chaperone machine DnaK-DnaJ-GrpE and the GroEL-GroES heat shock proteins facilitate the ribosome assembly remains to be elusive. It is known that at high temperatures both chaperone machines support the assembly of the 30S with the latter 50S subunit (Hage et al., 2001; Maki et al., 2002; Refaii and Alix, 2009). RbfA is a cold shock protein and has been proposed to aids the processing of 17S to 16S rRNA. Additionally, it was also suggested to be involved in the 16S rRNA maturation by binding to the 5' terminal helix region of the 16S rRNA (Dammel and Noller, 1995; Jones et al., 1996; Xia et al., 2003). Furthermore, a recent study suggested that binding of RbfA to pre-30S subunits serves as a quality control point in ribosome biogenesis and translation. RbfA, together with the translation initiation factor 3 (IF3) are proposed

to form a barrier between ribosome biogenesis and translation. IF3 is able to release RbfA from mature 30S but not from pre-30S subunits. Pre-30S subunits with associated RbfA are therefore unable to prematurely enter the translation cycle (Sharma and Woodson, 2019).

The ribosomal maturation factors RimM, RimP and RimJ assist in the 30S maturation by accelerating the binding rates between the 16S rRNA and ribosomal proteins as shown in *in vitro* studies (Bunner et al., 2010; Williamson, 2003)**.** Moreover, KsgA modifies in the 16S rRNA adenosines A1518 and 1519 of the 3' terminal helix. A model was proposed, where methylation of KsgA promotes the 30S assembly. This indicates that KsgA is a potential regulator of the ribosome biogenesis by limiting the maturation of the immature 30S (Connolly et al., 2008; Formenoy et al., 1994).

2.3.4 Assembly of the mammalian mitochondrial ribosome

As mentioned above, the mitochondrial ribosome differs in structure and composition compared to its bacterial counterpart (Greber and Ban, 2016). In addition, mitochondrial ribosomes are of dual genetic origin. While the mt-rRNA is encoded by the mtDNA, MRPs are solely nuclear-encoded proteins, which needs to be imported into the mitochondria (Anderson et al., 1981). A kinetic model for the mitochondrial ribosome assembly suggests early-, intermediate- and late-binding MRPs (Figure 9) (Bogenhagen et al., 2018). The exact timeline in which different MRPs or assembly intermediates form and interact with the mt-rRNA cores of the mitochondrial subunits is not fully determined. It was suggested that small sets of proteins might form sub-modules (Bogenhagen et al., 2018).

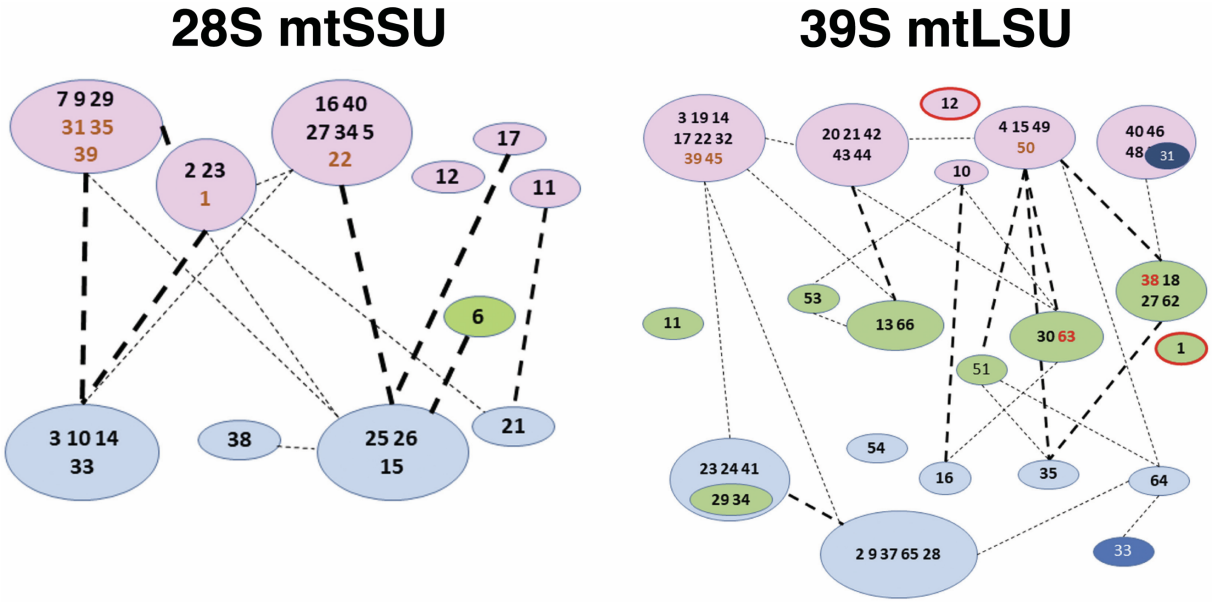

Figure 9: Assembly kinetic of the mammalian mitochondrial ribosome. Early (magenta) intermediate (green) and late (blue) binding mitochondrial ribosomal proteins are shown respectively for the mtSSU (left) and mtLSU (right). Proteins lacking RNA contacts are depicted in boldface brown color. Interactions between the assembly intermediates are depicted in dashed lines, whereby the interactions are strong (heavy dashed lines) or light (lighter dashed lines). bL31m (dark blue) appeared early in the analysis but joins the assembly at a later stage. uL1m and bL12m (outlined in red) were included in the assembly kinetic but could not be identified in the cryoEM structure. Figure adapted from (Bogenhagen et al., 2018).

Furthermore, a variability in the kinetics of MRPs interaction with intact mitochondrial ribosome was present. Therefore, Bogenhagen et al. (2018) suggested that newly imported MRPs might form new mitochondrial ribosomes with disassembled ones (Figure 9). The process of mitochondrial ribosome assembly in human cells was proposed to take place within 2 – 3 h while the assembly of bacterial ribosomes is completed within 2 min (Gelfand and Attardi, 1981). The rate limiting step of the assembly is dictated by two factors: i) the accessibility of the MRPs at different assembly stages and ii) the coordination of the assembly of MRPs with the synthesis and processing of the mt-rRNAs (Bogenhagen et al., 2018; Gelfand and Attardi, 1981). While RNA-protein interactions play a major role during bacterial ribosome assembly, it is proposed that protein-protein interactions are more relevant for human mitochondrial ribosome biogenesis (Greber and Ban, 2016). as the protein content substantially increased while the RNA was reduced during evolution. Out of 82 MRPs, 36 are unique for mitochondria and have no bacterial homologues (Amunts et al., 2015; Suzuki et al., 2001). The remaining MRPs contain N- and C-terminal extensions. Recent studies provided evidence that the mitochondrial ribosome assembly takes

place in a co-transcriptional manner (Rackham et al., 2016). It was proposed that the assembly occurs in nucleoids and RNA granules, which serve as temporal space to regulate mitochondrial gene expression, RNA processing, maturation as well as the mitochondrial ribosome assembly and translation initiation (Antonicka and Shoubridge, 2015; Bogenhagen et al., 2014; Jourdain et al., 2016; Tu and Barrientos, 2015).

2.3.5 Assembly factors of the mitochondrial ribosome

To date, few assembly factors are known to play a role in the mtSSU assembly. The mitochondrial transcription factor B1 (TFB1M), which is homolog to the bacterial methyltransferase KsgA, methylates two adenines (A936 and A937) at the 3'-end of the 12S mt-rRNA. Loss of TFB1M in mouse models results in embryonic lethality (Metodiev et al., 2009). NOP2/Sun RNA Methyltransferase 4 (NSUN4), a m^5C methyltransferase that belongs to the same family as bacterial RsmB, methylates C841 in the 12S mt-rRNA (Metodiev et al., 2009). Similar to TFB1M, homozygous deletion of NSUN4 leads to embryonic lethality. Conditional inactivation of NSUN4 in mice hearts leads to OXPHOS deficiency resulting from impaired mitochondrial ribosome assembly (Metodiev et al., 2014). Recently, a member of the mammalian methyltransferase-like family (METTL15) was identified to methylate the cytosine residue C839 in the 12S mt-rRNA (Chen et al., 2019; Haute et al., 2019). Furthermore, the tRNA methyltransferase 2 homolog B (TRMT2B) was reported to methylate the 12S rRNA at U429 (Powell and Minczuk, 2020). Both, METTL15 and TRMT2B share homologies to *E. coli* methyltransferases (RsmH and TrmA) that methylate the 16S rRNA of the bacterial SSU (Powell and Minczuk, 2020; Wei et al., 2012). While deletion of METTL15 in HeLa cells results in a decrease of mitochondrial encoded proteins (Haute et al., 2019), knockout of TRMT2B in HeLa cells neither disrupts the mitochondrial ribosome stability nor impacts the mitochondrial translation significantly (Powell and Minczuk, 2020).

The Era-like 1 (ERAL1) protein, the mammalian homolog of the bacterial Era GTPase, is a mitochondrial RNA chaperone, which protects the 12S mt-rRNA from degradation during the assembly of the mtSSU (Dennerlein et al., 2010). Depletion of ERAL1 in HEK293T and HeLa cells leads to cell-cycle arrest and increases the population of apoptotic cells due to a decrease of mitochondrial translation caused by a reduction of

12S mt-rRNA (Dennerlein et al., 2010; Uchiumi et al., 2010). Additionally, the human ribosome-binding factor A (mtRBFA), the human ortholog of bacterial Rbfa, was shown to bind to the same helix of the 12S mt-rRNA as ERAL1 (Rozanska et al., 2017). It is thereby suggested, that ERAL1 chaperones the 12S mt-rRNA during the mtSSU biogenesis before mtRBFA binds to the adenines A936 and A937 of the 12S mt-rRNA, potentially at a late stage of mtSSU biogenesis (Rozanska et al., 2017). There mtRBFA is most likely needed as a quality control mechanism that facilitate the final maturation steps of the 12S mt-rRNA at A936 and A937 for their methylation (Rozanska et al., 2017). The mitochondrial ribosome-associated GTPase 3, MTG3 (C4orf14, NOA1), a homolog of bacterial YqeH, shows a GTP dependent interaction with the 28S mtSSU that further facilitates the biogenesis (He et al., 2012). Inactivation of MTG3 in mice led to a decreased viability in the embryos mid-gestation. Ablation of MTG3 in HEK293T cells and MEFs resulted in a decrease in mitochondrial translation (He et al., 2012; Kolanczyk et al., 2011). Recent studies showed furthermore, that the human homologue of the bacterial endoribonuclease YBEY (C21orf57) mediates the 28S mtSSU assembly by recruiting the MRP uS11m. YBEY deficiency in HEK293T and Hap1 cells revealed defects in mitochondrial ribosome assembly leading to growth deficiency (D'Souza et al., 2019; Ghosal et al., 2017; Summer et al., 2020). A recent study furthermore showed that two isoforms of regulator of chromosome condensation (RCC1)-like (RCC1L) are able to interact with the mtSSU and mtLSU during the biogenesis (Reyes et al., 2020). Thereby the isoform $RCC1L^{V1}$ was suggested to target GTPBP10, while $RCC1L^{V3}$ potentially targets ERAL1 and MTG3. Reyes et al. (2020) suggests that $RCC1L^{V1}$ and $RCC1L^{V3}$ might acts as a GDP/GTP exchange factor (GEF) for the GTPases ERAL1, MTG3 and GTPBP10.

Contrary to the mtSSU subunit assembly factors, a larger subset of proteins is known to facilitate the biogenesis of the mtLSU. The tRNA methyltransferase 61B (TRMT61B), mitochondrial methyltransferases 1 – 3 (MRM1 – 3) and RNA pseudouridine synthase D4 (RPUSD4) have been identified to modify the 16S mt-rRNA at the residues A947, G1145, U1369, G1370 and U1397 respectively (Antonicka et al., 2017; Bar-Yaacov et al., 2016; Lee and Bogenhagen, 2014; Rorbach et al., 2014). While it is still unclear how loss of TRMT61B impacts the mtLSU biogenesis, analysis of MRM 1 – 3 depletions showed more diverse results (Bar-Yaacov et al.,

2016). siRNA mediated silencing of MRM1 shows no significant effect, while depletion of MRM2 and MRM3 leads to a disrupted mtLSU assembly (Lee and Bogenhagen, 2014; Rorbach et al., 2014). Similarly, loss of RPUSD4 leads to an impaired mtLSU assembly due to degradation of the 16S mt-rRNA, resulting in respiratory deficiencies in 143B cells (Zaganelli et al., 2017). The RNA-binding proteins mitochondrial transcription termination factor (MTERF3), FAS-activated serine/threonine kinase 2 (FASTKD2), the putative RNA helicases DEAD-box helicase 28 (DDX28) and DEAH-box helicase DHX30 assist in the assembly of the mtLSU (Antonicka and Shoubridge, 2015; Popow et al., 2015; Tu and Barrientos, 2015; Wredenberg et al., 2013). While the role of DHX30 remains to be determined, knockout and knockdown analysis of either MTERF3, FASTKD2 or DDX28 revealed an impaired mtLSU assembly. Knockout of MTERF3 in mouse models is embryonic lethal (Antonicka and Shoubridge, 2015; Park et al., 2007; Tu and Barrientos, 2015; Wredenberg et al., 2013).

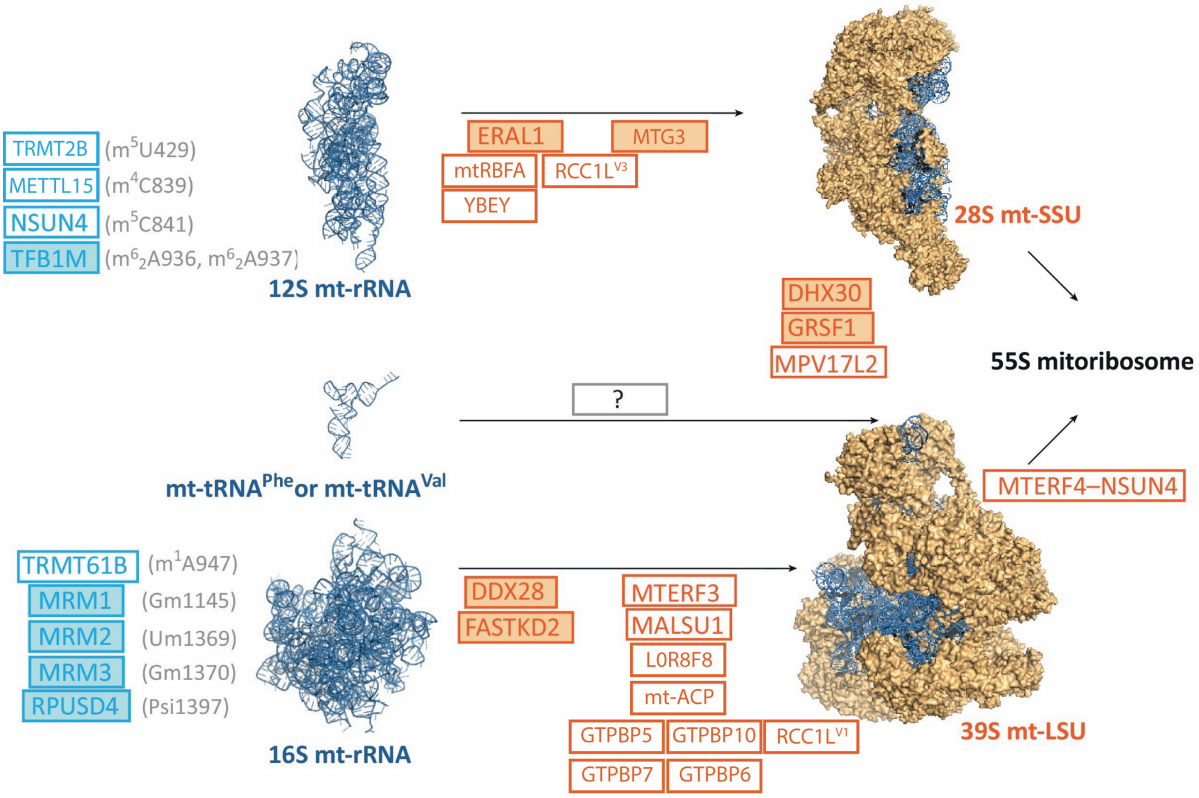

Figure 10: Summary of currently known and predicted assembly factors during mitochondrial ribosome biogenesis. There are four known nucleotides, which are modified in the 12S mt-rRNA and five of 16S mt-rRNA. The enzymes facilitating the modification for the 12S mt-rRNA are TRMT2B, METTL15, NSUN4 and TFB1M, while TRMT61B, MRM1 – 3 and RPUSD4 are the enzymes modifying the 16S mt-rRNA at the indicated positions (blue). Factors required for the assembly of the mtSSU, mtLSU and 55S mitochondrial ribosome are

depicted in orange. Solid colors indicate that these proteins are localized to the mitochondrial RNA granules. Figure adapted from (Pearce et al., 2017).

Mitochondrial assembly of ribosomal large subunit protein 1 (MALSU1/C7orf30) belongs to the ribosome silencing factor family (RsfS). The bacterial counterpart interacts with the ribosomal protein uL14 to form a RsfS-LSU complex (Li et al., 2015). In mitochondria, MALSU1 stabilizes the assembly of the mtLSU at late stages of biogenesis through the conserved interaction with uL14m (Fung et al., 2013; Rorbach et al., 2012). MALSU1 forms a module together with L0R8F8 and mitochondrial acyl carrier protein (mt-ACP), preventing premature subunit joining (Brown et al., 2017). Loss of MALSU1 leads to an instable assembly of the mtLSU and as a consequence interferes with 55S ribosome formation and therefore negatively affects OXPHOS assembly (Fung et al., 2013; Rorbach et al., 2012). Additionally, MPV17-like protein 2 (MPV17L2) was suggested to play a role in the later stages during ribosome biogenesis associating with the mtLSU and the 55S monosome in cooperation with MALSU1. Depletion of MPV17L2 leads inhibition of mtSSU uncoupling from the nucleoid (Dalla Rosa et al., 2014).

Recent studies revealed several conserved GTPases to be involved in late stages of mtLSU biogenesis: GTPBP5 (MTG2), GTPBP6, GTPBP7 (MTG1) and GTPBP10. The human Obg protein GTPBP5 interacts with the 16S mt-rRNA and facilitates 2'-*O*-methylation of G1145 and U1369 catalyzed by MRM1 and MRM2. Subsequently bL36m is recruited to the mtLSU (Cipullo et al., 2020; Maiti et al., 2020; Rorbach et al., 2014). Similar to GTPBP5, GTPBP10 is a human homologue of bacterial ObgE. GTPBP10 plays a role at late stages of the mtLSU maturation upstream of GTPBP5, but its molecular function needs to be further elucidated (Lavdovskaia et al., 2018; Maiti et al., 2018). GTPBP7 is the human homologue of bacterial RbgA and interacts with the MRPs uL19m and mS27 suggesting that GTPBP7 might be involved in forming the mB6 intersubunit bridge (Kim and Barrientos, 2018). Interestingly, in the absence of GTPBP6 an accumulation of the late-stage mtLSU biogenesis factors MALSU1, GTPBP5, GTPBP7, GTPBP10, NSUN4 and MTERF4 were observed, indicating that the mtLSU biogenesis is stalled in the absence of GTPBP6 at a late biogenesis step (Lavdovskaia et al., 2020). In GTPBP5-deficient cells a similar accumulation of late mtLSU assembly factors was observed (Maiti et al., 2020). There, MALSU1, GTPBP7, NSUN4 and MTERF4 showed elevated levels (Maiti et al., 2020).

The mitochondrial transcription termination factor 4 (MTERF4) belongs to the MTERF family, consisting of four proteins which are believed to have regulatory roles in transcription termination and mitochondrial protein synthesis (Chen et al., 2005; Roberti et al., 2006). MTERF4 has been reported to bind to the 16S mt-rRNA (Cámara et al., 2011; Spåhr et al., 2012). Interestingly, NSUN4 and MTERF4 form a heterodimeric complex and have a preference to bind double-stranded RNA fragments, thereby promoting the assembly of the 55S monosome. Loss of MTERF4 leads to an impaired mitochondrial ribosome assembly, resulting in a reduction in mitochondrial translation (Cámara et al., 2011; Metodiev et al., 2014; Spåhr et al., 2012).

2.3.6 The mitochondrial ribosome in human diseases

Mitochondrial diseases affect 1 in 5 000 of the population (Boczonadi and Horvath, 2014). Mutations in genes encoding for proteins involved in the energy production facilitated by mitochondria lead to OXPHOS disorders associated with neurodegenerative diseases, heart failures and muscle weakness (Koopman et al., 2013). Thereby mutations can occur in the mtDNA in genes coding for the OXPHOS core subunits, the mt-rRNA and mt-tRNA or in the nuclear-encoded genes that code for the structural OXPHOS subunits, assembly factors or MRPs (Koopman et al., 2013). In recent years, more mitochondrial diseases were reported, which were caused by mutations occurring in genes encoding for mitochondrial ribosomal proteins (Bogenhagen et al., 2018). Bogenhagen et al. (2018) suggested that these mutations affect proteins present in the early stages of mitochondrial ribosomal assembly. These mutations are associated with hereditary diseases, representing a diverse range of phenotypical, often multisystemic, presentation in the patients (DiMauro et al., 2013; Ferrari et al., 2020; Vafai and Mootha, 2012). On the molecular level, the mutations lead to an instability of the protein and affect negatively the mitochondrial ribosomal subunit assembly (Carroll et al., 2013; Emdadul Haque et al., 2008). This often results in OXPHOS deficiency in a tissue dependent manner, leading to severe phenotypes, e.g. lactic acidosis, Leigh syndrome, neuronal disorders or cardiac dysfunction which can lead to a low viability in early life (Baertling et al., 2015; Lake et al., 2017; Serre et al., 2013). As two examples, mutations in the MRPs uS7m and mS22 will be described in more detail. Menezees et al. reported in 2015 about siblings diagnosed with

hypoglycemia, lactic acidosis and congenital sensorineural deafness at birth. The clinical progression of the disease became more severe over time, leading to the death of patient 1 (P1) as a teenager. Patient 2 (P2) on the other hand was, last reviewed, generally well. Whole exome sequencing revealed a c.550A>G (p.Met184Val) mutation in the *MRPS7* gene. Both patients were homozygous for the c.550A>G mutation (Menezes et al., 2015). Analysis of P1 fibroblasts showed highly reduced levels of uS7m as well as reduced levels of complex I, III and IV. Furthermore, mRNA analysis showed that *MRPS7* mRNA levels were reduced, implying a mRNA instability of *MRPS7* induced by the mutation. This results in an instable mtSSU while mtLSU assembly was unaffected (Menezes et al., 2015).

The mS22 mutations reported by Saada et al. and Baertling et al., c.509G>A (p.Arg170His) and c.1032_1035dup (p.Leu346Asnfs*21) respectively, are associated with severe clinical phenotypes for which reason the patients died shortly after birth. On the contrary, the mS22 mutations reported by Smits et al. and Chen et al., c.644T>C (p.Leu215Pro), c.404G>A (p.Arg135Gln) and c.605G>A (p.Arg202His) respectively showed a milder disease progress in the patients. Interestingly, analysis of the OXPHOS complexes in all four studies revealed a decrease in complex I, III and IV except for the mutations reported by Chen et al. (c.404G>A and c.605G>A) (Baertling et al., 2015; Saada et al., 2007; Smits et al., 2011). The mutations c.404G>A and c.605G>A led to primary ovarian insufficiencies with no further effects on the OXPHOS activity or mt-rRNA levels (Chen et al., 2018). As mS22 was suggested to be an early-assembling MRP of the mtSSU (Bogenhagen et al., 2018), the severity of the different mutations might be a result of the disruption of the mtSSU biogenesis at early stages. As Chen et al. (2018) reported two mutations with a less severe phenotype, this might indicate that the mutation does not affect the mitochondrial translation directly.

The following table summarizes the known MRP mutations associated with diseases.

Table 3: Summary of presently known mutations of mitochondrial ribosomal proteins and assembly factors. Mutations and most represented phenotypes in patients.

MRP		Mutation	Phenotype	Reference
mtLSU	uL3m	c.950C>G (p.Pro317Arg)	Hypertrophic cardiomyopathy, hepatic dysfunctions	(Galmiche et al., 2011)
	bL12m	c.542C>T (p.Ala181Val)	Prenatal hypotrophy, growth retardation, neurological deterioration	(Serre et al., 2013)
	uL24m	c.272T>C (p.Leu91Pro)	Movement disorder, cerebellar atrophy, choreoathetosis of limbs and face, mental retardation	(Di Nottia et al., 2020)
	mL44	c.467T>G (p.Leu156Arg); c.233G>A (p.Arg78Gln); c.467T>G, p.(Leu156Arg)	Cardiomyopathy, hepatic steatosis, hemiplegic migraine, Leigh-like lesions in the brain, pigmentary retinopathy	(Carroll et al., 2013; Distelmaier et al., 2015)
mtSSU	bS1m	c.356A>G, p.(Lys119Arg); c.214_395del, p.(Gly72Glufs*16)	Growth retardation, sensineural deafness, facial dysmorphism, hepatomegaly	(Pulman et al., 2019)
	uS2m	c.328C>T (p.Arg110Cys); c.340G>A (p.Asp114Asn); c.413G>A (p.Arg138His)	Sensorineural deafness, hypoglycemia	(Gardeitchik et al., 2018)
	uS7m	c.550A>G, (p.Met184Val)	Bilateral sensorineural deafness, hypoglycemia, lactic acidosis	(Menezes et al., 2015)
	uS14m	c.322C>T (p.Arg108Cys)	Wolf-Parkinson White syndrome, muscle hypotonia, dysmorphism	(Jackson et al., 2019)
	bS16m	c.331C>T (p.Arg111*)	Agenesis of corpus callosum, hypotonia, lactic acidosis	(Miller et al., 2004)
	mS22	c.339+5G>A; c.509G>A (p.Arg170His);	Dysmorphic features, agenesis of corpus callosum, delayed	(Baertling et al., 2015; Chen et al., 2018; Kılıç et al.,

		c.404G>A (p.Arg135Gln); c.605G>A (p.Arg202His); c.644T>C (p.Leu215Pro); c.1032_1035dup (p.Leu346Asnfs*21)	puperty, primary ovarian insufficiency, Cornelia de-Lange like features, Leigh-like syndrome, muscle hypotonia, lactic acidemia, Wolf-Parkinson-White syndrome, Mosaic Down syndrome	2017; Saada et al., 2007; Smits et al., 2011)
	mS23	c.119C>G (p.Pro40Arg)	Hepatic disease	(Kohda et al., 2016)
	mS25	c.215C>T (p.Pro72Leu)	Encephalomyopathy, psychomotor delay, partial agenesis of corpus callosum	(Bugiardini et al., 2019)
	mS34	c.321+1G>T (p.Val100_Gln107del); c.322-10G>A (p.Asn108Leufs*12, Asn108Glyfs*50); c.37G>A (p.Glu13Lys); c.94C>T (p.Gln32∗)	Leigh/-like syndrome, microcephaly, hypotonia	(Lake et al., 2017)
	mS39	c.415-2A>G (p.Cys139Glufs*71); c.1747-1748insCT (p.PheSerfs*3)	Leigh syndrome	(Borna et al., 2019)

2.4 Aims

The mitochondrial ribosome differs in structure and composition compared to its bacterial counterpart. While the bacterial ribosome assembly has been extensively studied, little is known about human mitochondrial ribosome biogenesis. It is tempting to believe that the assembly pathway of the mitochondrial ribosome also evolved to adjust to the structural changes. First kinetic studies done by Bogenhagen et al. (2018) suggest a potential assembly pathway of the mitochondrial ribosome. It is thereby important to point out that this study does not provide detailed insights into the mitochondrial ribosome biogenesis, as it also contains inconsistencies in their data acquisition.

Additionally, a study provided by Zeng et al. (2018) revealed insights into the mitochondrial ribosome biogenesis in yeast, where MRPs assemble in sub-modules upon further integration into the respective subunits. Thereby, the studies of Zeng et al. (2018) and Bogenhagen et al. (2018) agree that the biogenesis of the mitochondrial ribosome is potentially facilitated by the assembly of MRPs into sub-modules before they further form the mitochondrial ribosome. With the rise of human diseases caused by mutations in mitochondria, especially in genes encoding for MRPs of the mtSSU, understanding the mitochondrial ribosome biogenesis becomes more relevant. A mutation in the gene encoding for uS7m (uS7m p.Met184Val) was reported by Menezes et al. (2015) to cause congenital sensorineural deafness in humans. uS7m was described by Bogenhagen et al. (2018) alongside mS40 and mS27 as early appearing MRPs in the mtSSU assembly, albeit in distinct sub-modules. Furthermore, Davies et al. (2012) identified mS27 as a PPR protein, enabling it to interact with RNA. According to Bogenhagen et al. (2018), mS27 assembles early and is part of the same sub-module as mS40. Interestingly, mS27 is stable even in cells lacking mtDNA, which is in contrast to other MRPs (Kim and Barrientos, 2018), possibly indicating a secondary function of mS27 besides being a structural component of the mitochondrial ribosome.

To further assess the composition and to illustrate a more detailed understanding in early stages of mtSSU biogenesis, the sub-modules containing uS7m, mS40 and mS27 were investigated in detail. Therefore, the aim of this thesis is to provide further

insights into the assembly pathway of the human 28S mtSSU by addressing the following questions:

i) How does loss of uS7m, mS27 or mS40 affect the assembly of the mtSSU?
ii) Do defects in early mtSSU assembly affect the biogenesis of the mtLSU?
iii) Do distinct mtSSU sub-modules depend on each other?
iv) In which chronological order assemble MRPs in their sub-modules?
v) How does the patient mutation of uS7m affect mtSSU assembly?
vi) Which auxiliary factors assist mtSSU assembly during early stages?

The results obtained in this study will contribute to a more detailed understanding of the assembly of early sub-modules during mtSSU biogenesis. Furthermore, this study provides the possibility to identify novel factors that potentially play a role in mitochondrial biogenesis, leading to further insights into the mtSSU assembly.

3. Materials and Methodes

3.1 Materials

3.1.1 Chemicals

Table 4: List of used chemicals in this study.

Chemical	Manufacturer
[^{32}P]-γ-ATP	Hartmann Analytic
[^{35}S]-L-methionine	Hartmann Analytic
2-Propanol	Roth
Acetic acid	Roth
Acetone	Roth
Acrylamide (2xcrystallized)	Roth
Acrylamide/bisacrylamide (37.5:1) solution	Roth
Agarose NEEO ultra-quality	Roth
Ammonium acetate	Roth
Ammonium chloride (NH_4Cl)	MERCK
Ammonium hydroxide solution	Sigma-Aldrich
Ammonium persulfate (APS)	Roth
Ampicillin	AppliChem GmbH
Anti-FLAG M2 Affinity Gel	Sigma-Aldrich
Bacto™ Agar	BD
Bacto™ Peptone	BD
Bacto™ Tryptone	BD
Bacto™ Yeast Extract	BD
Bis-acrylamide (2X)	SERVA
Blasticidine S HCl	ThermoFisher Scientific
BPB (Bromophenol blue)	MERCK
BSA (Bovine Serum Albumin)	Sigma Life Science
Calcium chloride dihydrate	Roth
Chloroform	Roth
CNBr activated Sepharose 4B	GE Healthcare
cOmplete™ Protease inhibitor cocktail tablets	Roche
Coomassie Brilliant Blue R-250	Serva
DMEM, high glucose, no glutamine, no methionine, no cystine	Gibco
Developing solution Developer G153	Agfa
di-Potassium hydrogen phosphate	Roth
di-Sodium hydrogen phosphate (Na_2HPO_4)	AppliChem GmbH
Digitonin	Calbiochem
DMSO (dimethyl sulphoxide)	MERCK
DNA Gel Loading Dye (6x)	Thermo Scientific
DNase I	Thermo Scientific
dNTP Mix	Thermo Scientific
DTT (1.4-Dithiothreitol)	Roth
EDTA (Ethylendiamine tetraacetic acid)	Roth
Emetine	Invitrogen
Ethanol	Roth

Ethidium Bromide (0.025%)	Roth
FCS (fetal calf serum)	Biochrom
Fixing solution Rapid Fixer G354	Agfa
FLAG-peptide	Sigma-Aldrich
Formaldehyde	Sigma-Aldrich
GeneJuice® Transfection Reagent	Novagen
GeneRuler DNA Ladder Mix	Thermo Scientific
Glycerol	Sigma-Aldrich
Glycine	Roth
HEPES (4-(2-hydroxyethyl)-1-piperazineethanesulfonic acid)	Roth
Hydrochloric acid 37% w/v	Roth
Hydrogen peroxide	Sigma-Aldrich
Hygromycine B	Life Technologies
L-Glutamine 200mM (100X)	gibco
Lipofectamine 3000	Invitrogen
Lipofectamine RNAiMAX	Invitrogen
Magnesium chloride heptahydrate	MERCK
Manganese (II) chloride tetrahydrate	Roth
Methanol	Roth
Methylene blue (MB)	Merck
MOPS (Morpholinopropanesulfonic acid)	Roth
Morpholinopropanesulfonic acid (MOPS)	Roth
NaH_2PO_4	Roth
NP-40 (Nonidet P40, 4-Nonylphenyl-polyethylene glycol)	Sigma Life Science
Nupage 20x running buffer	Invitrogen
NuPage LDS Sample buffer 4x	Invitrogen
Opti-MEM™	Gibco
Penicillin Streptomycin	Gibco
Phenol	Roth
Phosphatase alkaline	Roche
Pierce™ ECL Western Blotting Substrate	Life Technologies
Plasmocin™	invivogen
PMSF (Phenylmethyl sulphonyl fluoride)	Roth
Ponceau S (C.I. 27195)	Roth
Potassium chloride	Roth
Potassium dihydrogen phosphate	Roth
Potassium hydroxide	Roth
Precision Plus Protein™ All Blue Prestained Standards (10-250kD)	Bio-Rad
Profilactic Plasmocin™	invivogen
Protein-A sepharose	GE healthcare
Proteinase K	Roth
RiboLock RNase Inhibitor	Thermo Scientific
Roti-Quant® Reagent	Roth
SDS (sodium dodecyl sulfate)	Roth
Silver nitrate ($AgNO_3$)	Roth
Sodium acetate (NaOAc)	Roth
Sodium azide (NaN^3)	Sigma-Aldrich

Sodium carbonate (Na_2Co_3)	MERCK
Sodium chloride (NaCl)	Roth
Sodium citrate	Roth
Sodium dihydrogen phosphate (NaH_2PO_4)	Roth
Sodium hydrogen carbonate ($NaHCO_3$)	MERCK
Sodium hydroxide (NaOH)	AppliChem GmbH
Sodium pyruvate solution	Sigma Life Science
Sodium Thiosulfate ($Na_2S_2O_3$)	Sigma Chemical Co.
Sucrose, D(+)	Roth
TCA (Trichloroacetic acid)	Roth
TEMED (Tetramethylethylendiamine)	Roth
Tetracycline	Roth
Trehalose	Roth
tri-Sodium Citrate Dihydrate	Roth
Tricine	Roth
TRIS (Tris(hydroxymethyl)aminomethane)	Roth
Tris(2-carboxyethyl)-phosphine hydrochloride (TCEP)	Sigma-Aldrich
Triton X-100	Roth
TRIzol™ Reagent	Ambion
Tween-20	Roth
Uridine	Sigma-Aldrich
Xylene cyanol	Roth

3.1.2 Kits and Disposables

In Table 5 is a list of all disposables and kits used in this study

Table 5: Used disposables and kits.

Item	**Manufacturer**
Blotting paper	Heinemann Labortechnik
Bottle Top Filter 500 ml, 45 mm neck	Corning
Cell culture flask Nunc™ EasYFlask™ Nunclon™ Delta Surface 25cm², 75cm²	Thermo Scientific
Cellstar® Cell Culture Dishes, PS, 145/20 mm	Greiner Bio-One
Cellstar® Cell Culture Plate 6, 12, 24, 96 Well	Greiner Bio-One
Cellstar® Tubes 50 ml, 15 ml	Greiner Bio-One
CryoPure Tube 1.6 ml	Sartstedt
Disposable hypodermic needle Sterican® 21G x 3 1/8“/ ∅ 0.80 x 80 mm, 14G x 3 1/8”/ ∅ 2.10 x 80 mm	B. Braun
DreamTaq™ Hot Start DNA Polymerase	Thermo scientific
Econo-Pac® Disposable Chromatography Columns, 10 ml	Bio-Rad
Fast digestion enzymes	Thermo Fisher
First Strand cDNA Synthesis Kit	Thermo Scientific

Graduated filter tips 1000 µl, 300 µl, 20 µl, 10 µl	Greiner Bio-One
Immobilon®-P membrane, PVDF, 0.45 µm	Merck Millipore
KOD Hot Start DNA Polymerase	Novagen
MColorpHast™ pH indicator stripes pH 5.0-10.0	Merck Millipore
Micro tube 1.5 ml protein Low binding	Sarstedt
Micro tubes 2.0 ml, 1.5 ml	Sarstedt
Multiply®- Pro cup 0.2 ml	Sarstedt
Nitrocellulose membrane Amersham™ Protran™ 0.2µm NC	GE Healthcare Life Science
NuPAGE™ 4-12% Bis-Tris Midi Gel	Invitrogen
Open-top centrifuge tubes polyallomer (13x51 mm)	Seton
Open-top centrifuge tubes polyallomer (25x89 mm)	Seton
Open-top polyclear™ centrifuge tubes (14x89 mm)	Seton
Pipette tips 1000 µl, 200 µl, 10 µl	Sarstedt
T4 Polynucleotide Kinase	Thermo Scientific
QuickExtract™ DNA Extraction Solution	Lucigen
Rapid DNA Ligation Kit	Thermo Scientific
Reaction tubes 0.6 ml	Biozym
SafeSeal tube 5 ml	Sarstedt
Spin columns Mobicol “classic”	MoBiTec
Super RX-N Fuji Medical X-ray film	Fujifilm
Syringe Omnifix® Luer Lock Solo, 10 ml	B. Braun
TOPO TA Cloning® Kit for Sequencing	Invitrogen
Wizard® *Plus* SV Minipreps DNA Purification System	Promega
Wizard® SV Gel and PCR Clean-Up System	Promega

3.1.3 Instruments and equipment

Instruments and equipment used in this work are stated in Table 6.

Table 6: Instruments and equipment:

Instrument/Equipment	Model	Manufacturer/Supplier
Centrifuge	5418	Eppendorf
	5427R	Eppendorf
	5804R	Eppendorf
	Optima L-90K Ultracentrifuge	Beckman Coulter
	Optima L-80 Ultracentrifuge	Beckman Coulter
Electrophoresis	Blotting chamber PerfectBlue™ “Semi-Dry” Electro Blotter Sedec™ M	peqlab
	Power Supply EV3020, EV2650	Consort
	Wide Mini-Sub® Cell GT	Bio-Rad
	PowerPac HC™ Power Supply	Bio-Rad

Miscellaneous	GeneTouch Thermal Cycler	BIOER
	Gradient Station™	Biocomp
	Homogenisator Potter-Elvehjem with PTFE pistil 15ml	Sartorius
	Homogenisator Potter-Elvehjem with PTFE pistil 2ml	Omnilab
	Homogenisator Potter-Elvehjem with PTFE pistil 5ml	Omnilab
	Incubator Heraeus® Hera cell 150	Thermo Scientific
	Light microscope	Zeiss
	Pipettes	Gilson
	Sterile Hood Heraeus® Hera safe	Thermo Scientific
	Thermomixer comfort	Eppendorf
	Vortex-Genie 2	Scientific Industries
	Storage Phosphor screen	GE Healthcare
	Synergy H1 microplate reader	BioTek
	Nanodrop™ One^{C} Microvolume UV-Vis Spectrophotometer	Thermo Scientific
	Homogenisator machine homogen^{plus}	schuett-biotec.de
	Rocking table RS-RR10	PHOENIX instrument
	Fisherbrand™ Glass Funnel Filter with Sintered Glass Disc	Fisherbrand™
	Accu-jet® pro	Brand
	X-ray cassette 24x30	rego X-ray GmbH
	Magnetic stirrer MR3001	HEIDOLPH
Rotors	SW 41 Ti	Beckman Coulter
Scanner	Developing machine Curix 60	AGFA
	Typhoon FLA 9500 Phoshpoimager	GE Healthcare

3.1.4 Cells and microorganisms

Human cell lines used in this study are listed in Table 7 and in

Table 8 is the list of bacterial cell lines used in this work.

Table 7: Cell lines used in this study.

Cell line	**Source**
Flp-In™ T-REx™ 293 (HEK293T WT)	ThermoFisher Scientific, R78007
Flp-In™ T-REx™ 293 uS7m$^{-/-}$	This study
Flp-In™ T-REx™ 293 uS7m$^{-/-}$ + uS7m^{FLAG} (uS7m Rescue)	This study

Flp-In™ T-REx™ 293 uS7m$^{-/-}$ + uS7m^{WT} (uS7m Rescue)	This study
Flp-In™ T-REx™ 293 mS27$^{-/-}$	generated by Elena Lavdovskaia
Flp-In™ T-REx™ 293 mS27$^{-/-}$ +mS27^{FLAG} (mS27 Rescue cl. 1)	This study
Flp-In™ T-REx™ 293 mS27$^{-/-}$ +mS27^{FLAG} (mS27 Rescue cl. 2)	This study
Flp-In™ T-REx™ 293 mS40$^{-/-}$	generated by Elena Lavdovskaia
Flp-In™ T-REx™ 293 mS40$^{-/-}$ +mS40^{FLAG} (mS40 Rescue)	This study
Flp-In™ T-REx™ 293 NT5DC2$^{-/-}$	generated by Emely Steube
Flp-In™ T-REx™ 293 POLDIP2$^{-/-}$ clone B8II	generated by Emely Steube
Flp-In™ T-REx™ 293 POLDIP2$^{-/-}$ clone H8II	generated by Emely Steube
Flp-In™ T-REx™ 293 bS16m^{FLAG}	This study
Flp-In™ T-REx™ 293 mS22^{FLAG}	generated by Ricarda Richter-Dennerlein
Flp-In™ T-REx™ 293 mS27^{FLAG}	generated by Ricarda Richter-Dennerlein
Flp-In™ T-REx™ 293 mS40^{FLAG}	generated by Ricarda Richter-Dennerlein

Table 8: Bacterial cell lines used in this work.

Bacterial cell line	Source
E. coli TOP10 One Shot® Chemicallly Competent Cells	Invitrogen
E. coli XL1-Blue	Stratagene

3.1.5 Antibodies

A list of primary antibodies used in this work is shown in Table 9. Secondary antibodies coupled with HRP (goat-anti-rabbit and goat-anti-mouse) were purchased from Dianova GmbH (Hamburg, Germany).

Table 9: List of primary antibodies used in this work.

Protein	Antibody	Dilution	Company
uL1m	Anti-MRPL1 rabbit polyclonal	1:10 000	Gift from Peter Rehling
bL12m	Anti-MRPL12 rabbit polyclonal	1:5 000	ProteinTech (14795-1-AP)
uL13m	Anti-MRPL13 rabbit polyclonal	1:5 000	ProteinTech (16241-1-AP)

uL23m	Anti-MRPL23 rabbit polyclonal	1:10 000	Gift from Peter Rehling
bL32m	Anti-MRPL32 rabbit polyclonal	1:5 000	Gift from Peter Rehling
uS7m	Anti-MRPS7 rabbit polyclonal	1:5 000	Sigma-Aldrich (HPA023007)
uS14m	Anti-MRPS14 rabbit polyclonal	1:5 000	ProteinTech (16301-1-AP)
uS15m	Anti-MRPS15 rabbit polyclonal	1:5 000	ProteinTech (17006-1-AP)
bS16m	Anti-MRPS16 rabbit polyclonal	1:5 000	ProteinTech (16735-1-AP)
mS22	Anti-MRPS22 rabbit polyclonal	1:5 000	ProteinTech (10984-1-AP)
mS25	Anti-MRPS25 rabbit polyclonal	1:5 000	ProteinTech (15277-1-AP)
mS27	Anti-MRPS27 rabbit polyclonal	1:10 000	ProteinTech (17280-1AP)
mS29	Anti-DAP3 rabbit polyclonal	1:5 000	ProteinTech (10276-1-AP)
mS35	Anti-MRPS35 rabbit polyclonal	1:10 000	ProteinTech (16457-1-AP)
mS40	Anti-MRPS18b rabbit polyclonal	1:5 000	ProteinTech (16139-1-AP)
ERAL1	Anti-ERAL1 rabbit polyclonal	1:5 000	Gift from Peter Rehling
GTPBP10	Anti-GTPBP10 rabbit polyclonal	1:1 000	novusbio (NBP1-85055)
MALSU1	Anti-MALSU1 rabbit polyclonal	1:5 000	ProteinTech (22838-1-AP)
NSUN4	Anti-NSUN4 rabbit polyclonal	1:5 000	ProteinTech (16320-1-AP)
NT5DC2	Anti-NT5DC2 rabbit polyclonal	1:5 000	abcam (ab173963)
POLDIP2	Anti-POLDIP2 rabbit polyclonal	1:5 000	ProteinTech (15080-1-AP)
TFB1M	Anti-TFB1M rabbit polyclonal	1:5 000	ProteinTech (16604-1-AP)
VWA8	Anti-VWA8 rabbit polyclonal	1:10 000	home-made
VWA8	Anti-VWA8 rabbit polyclonal	1:5 000	abcam (ab184725)
COX1	Anti-COX1 rabbit polyclonal	1:10 000	Gift from Peter Rehling
COX2	Anti-COX2 mouse monoclonal	1:5 000	abcam (ab110258)
FLAG	Anti-FLAG mouse monoclonal	1:1 000	Sigma-Aldrich (F1804)
Calnexin	Anti-Calnexin mouse monoclonal	1:200 000	ProteinTech (66903-1-Ig)
SDHA	Anti-SDHA mouse monoclonal	1:20 000	ThermoFisher (459200)
MFN2	Anti-MFN2 rabbit polyclonal	1:1 000	ProteinTech (12186-1-AP)

TIM23	Anti-TIM23 rabbit polyclonal	1:1 000	Gift from Peter Rehling
TOM70	Anti-TOM70 rabbit polyclonal	1:1 000	Gift from Peter Rehling

3.1.6 Plasmids and oligonucleotides

Oligonucleotides were purchased from Microsynth SEQLAB (Göttingen, Germany) and are listed in Table 10.

Table 10: Oligonucleotides used in this study.

Primer	**Sequence (5' – 3')**
forward primer to amplify bS16m	CTCCTTGATATCCCACCATGGTCCACCTCAC TACTCTCCTC
reverse primer to amplify bS16m	CCTTCTCTCGAGCTACTTATCGTCGTCATCC TTGTAATCTGTTTCTGTAGCCTCTGTATCTGT AGC
Guide sequence 1_2 for CRISPR/Cas9 targeting uS7m	CACCGTCGGGCAACCTTCACTGCGG
Complement to guide sequence 1_2 for CRISPR/Cas9 targeting uS7m	AAACCCGCAGTGAAGGTTGCCCGA C
Forward primer to amplify region of uS7m$^{-/-}$	CTGAGAGGAGTGAGTGCCG
Reverse primer to amplify region of uS7m$^{-/-}$	TGAATCCAGATACTCCGGCC
forward primer to amplify region of uS7m	CTTTCTGATATCCTACCACCAGCGGTAGTGG G
reverse primer to amplify region of uS7m	CTTCTTAAAGCTTCCACCATGGCTGCCCCCG CAGTG
forward primer to amplify region of uS7m$^{-/-}$	CTGAGAGGAGTGAGTGCCGTC
revers primer to amplify region of uS7m $^{-/-}$	GGCCAGTACTTTGTTTCCTCC
forward primer to amplify region of mS40 $^{-/-}$	AATTCCTGTCCTGGGCGTACG
reverse primer to amplify region of mS40 $^{-/-}$	GAGTTCAGGTTCCCCTCCAG
forward primer to amplify region of mS27$^{-/-}$	ATGGCTGCCTCCATAGTGCG
revers primer to amplify region of mS27$^{-/-}$	CAGGTATCTTTTACCTGCAGGAG

Guide sequence for E27 for CRISPR/Cas9 targeting VWA8 Exon 27	CAGGACCTTGCCTTACCTTCTTAGTTTC
Complement to guide sequence E27 for CRISPR/Cas9 targeting VWA8 Exon 27	GGCAGCAGGAACAGAAGTTGAGGG
Guide sequence for E1 for CRISPR/Cas9 targeting VWA8 Exon 1	CTGTCCCCTTCTCCGCGCTG
Complement to guide sequence for E1 for CRISPR/Cas9 targeting VWA8 Exon 1	CTGGATTTGACCTTGCTCTCTGAGCCTC
Northern blot probe MTRNR1 (12S mt-rRNA) (Lavdovskaia et al., 2020)	TCGATTACAGAACAGGCTCCTCTAG
Northern blot probe MTRNR2 (16S mt-rRNA) (Lavdovskaia et al., 2018)	GTTTGGCTAAGGTTGTCTGGTAGTA
Northern blot probe MTCO1 (Lavdovskaia et al., 2018)	GTCAGTTGCCAAAGCCTCCGATTATG
Northern blot probe MTCO2 (Lavdovskaia et al., 2020)	GACGTCCGGGAATTGCATCTGTTTT
Northern blot probe 18S-rRNA (Larburu et al., 2016)	TTTACTTCCTCTAGATAGTCAAGTTCGACC

Plasmids used in this study were either bought from Fisher Scientific GmbH (Schwerte, Germany) or isolated from *E. coli* (XL1-blue). A list of the used plasmids in this study is shown in Table 11

Table 11: Plasmids used in this study.

Plasmid	Function	Source
pOG44	expression of Flp recombinase	Invitrogen
pcDNA5/FRT/TO	insertion of tetracycline inducible constructs into FRT sites in Flp-In™ host cell line	Invitrogen
pCR™4-TOPO®	for rapid cloning of Taq-polymerase generated PCR products for sequencing	Invitrogen
pcDNA5-bS16m-FLAG clone 1	tetracycline inducible expression of FLAG-tagged variant of bS16m protein	This study
pcDNA5-mS27-FLAG clone 3	tetracycline inducible expression of FLAG-tagged variant of mS27 protein	This study
pX330	Expression vector for CRISPR/Cas9 mediates gene editing	Kind gift of Abishek Aich (Peter Rehling Lab, Göttingen)

pX330-uS7m-guide1_2 clone 2	Guide plasmid for generation of CRISPR/Cas9 mediates uS7m$^{-/-}$	This study

3.1.7 Software

Software used in this work is listed in Table 12.

Table 12: Used Software.

Software	Producer
Adobe® Illustrator® CS6	Adobe Systems, San Jose, CA, USA
Adobe® Photoshop® CS6	Adobe Systems, San Jose, CA, USA
Gen5™2.04	BioTek Instruments Inc., Winooski, VT, USA
Genious® 11.1.4	Biomatters Ltd., Auckland, New Zealand
ImageQuant TL	GE Healthcare BioSciences AB, Uppsala, Sweden
Microsoft® Office	Microsoft Corporation, Redmond, WA, USA
Papers	Mekentosj, Aalsmeer, Netherlands
R studio 1.2.5033	RStudio, Inc., Boston, MA, USA

3.2 Methods

3.2.1 Cell culture

3.2.1.1 Cell culture maintenance

Human embryonic kidney cells (HEK293-Flp-In T-Rex; HEK293T) were cultivated in Dulbecco's Modified Eagle medium (DMEM), supplemented accordingly, under a 5 % CO_2 humidified atmosphere at 37 °C. To passage them, the medium was removed and PBS/EDTA was used to detach the cells. Cells were centrifuged for 5 minutes at 350 xg at room temperature. The supernatant was discarded and the cell pellet was resuspended in fresh DMEM. Afterwards an appropriate volume of the cell suspension was added to the cell culture flasks for further cultivation or transferred to larger cell culture dishes for expansion.

DMEM: 10% (v/v) FBS, 2 mM L-Glutamine, 1 mM Sodium pyruvate, 50 μg/mL uridine, 100 units/mL Penicillin, 100 μg/mL Streptomycin, sterile filtrated

PBS/EDTA: 0.14 M NaCl, 2.7 mM KCl, 0.01 M Na_2HPO_4, 1.8 mM KH_2PO_4, pH 7.4, add EDTA to a final conc. of 1000 μM

3.2.1.2 Cryo-conservation

To cryo-conserve cells, they were harvested from a 90% confluent 75 cm^2 cell culture flask. The supernatant was discarded and the cell pellet was resuspended in cold freezing media, transferred to freezing vials and stored at -80 °C. For long term storage cryo-vials were transferred to liquid nitrogen.

To take cell lines in culture, cells were quickly thawed in 37 °C water bath and suspension was added dropwise into pre-warmed DMEM. Cells were centrifuged for 5 min at 350 xg and the supernatant was removed. The cells were then resuspended gently in DMEM and transferred into a 75 cm^2 flask.

Freezing medium: DMEM (Dulbecco's modified Eagle's medium), 18 % (v/v) FBS, 9 % (v/v) DMSO, sterile filtrated

3.2.1.3 Mycoplasma testing

To systematically test the cells for the presence of Mycoplasma the MycoplasmaCheck sample preparation protocol from Eurofins genomic was used. Briefly, the cells were maintained in the same media without changing or adding fresh media for three days before testing. The cell confluence on the day of testing was 80 – 90 %. Media (500 µL) from cultured cells was collected into a 1.5 mL reaction tube and boiled for 10 min at 95 °C. After centrifuging the samples at 10 000 xg for 5 seconds, 100 – 200 µL of the supernatant was transferred into a new 1.5 mL reaction tube. Mycoplasma testing was performed by Eurofins.

3.2.1.4 Generating knockout cell lines using the CRISPR/Cas9 technology

HEK293T cells lacking either the MRPs uS7m, mS27 or mS40 or the proteins NT5DC2, POLDIP2, VWA8^{A} or VWA8^{B} were generated using the CRISPR/Cas9 technology developed by Ran et al., 2013. For uS7m the protocol described in Richter-Dennerlein et al., 2016 was followed. Briefly, 100 µM of each oligonucleotide (Table 10) corresponding to guide RNA sequence were mixed with 1x ligase buffer (Rapid DNA Ligation Kit, Thermo Scientific) in ddH_2O in an end volume of 50 µL. Oligonucleotides were annealed at 95 °C for 5 minutes and the temperature decreased by 5 °C/min until 20 °C were reached. The pX330 vector was digested with restriction enzyme BbsI (Thermo Scientific) at 37 °C for 30 min and purified using the Wizard® SV Gel and PCR Clean-up System (Promega). 2 µL of the annealed oligonucleotides were ligated with 50 ng digested pX330 vector and XL1-Blue *E. coli* competent cells were transformed with ligation mix. Plasmid were isolated and sequenced from individual colonies. The day before the transfection, HEK293T WT cells were seeded into a well of a 6-well plate. In 100 µL OptiMEM 5 µL of the transfection reagent GeneJuice (Novagen) was mixed and incubated at room temperature for 5 minutes prior adding 2 µg of pX330-uS7m-CRISPR/Cas and 400 ng of pEGFP-N1 and further incubation at room temperature for 20 min. The media was removed from the cells, the transfection mix was diluted with 600 µL DMEM with suplements and dropwise added. After 2 – 3 hours of incubation at 37 °C, 2 mL of complete growth media was added to the transfected cells. After three days cells were collected for cell sorting (see 2.2.1.6).

For the other mentioned MRPs and proteins, except uS7m, the iDT Protocol (https://eu.idtdna.com/) was applied. In brief, the guide RNA duplex [1 μM] was mixed by annealing an equimolar concentration of Alt-R CRISPR-Cas9 crRNA and Alt-R CRISPR-Cas9 tracrRNA in an end volume of 100 μL at 95 °C for 5 min and cooled slowly in the absence of light until room temperature was reached. The guide RNA duplex was either stored at -20 °C or directly used for ribonucleoprotein (RNP) complex formation. To produce RNP sufficient for the transfection of cells per well in a 96 well plate, 1.5 μL of guide RNA duplex [1 μM] and an equal amount of Alt-R *S.p.* Cas9 enzyme [1 μM] were mixed in Opti-MEM™ (Gibco) in an end volume of 25 μL and incubated at room temperature for 5 minutes. To form the transfection complex, the RNP complex was mixed with 1.2 μL of the Lipofectamine RNAiMax transfection reagent (Invitrogen) as well as 23.8 μL Opti-MEM™ (Gibco), resulting in a total volume of 50 μL. The transfection complex was incubated for 20 minutes at room temperature. During the incubation time, HEK293T wild type cells were counted and diluted to an end concentration of 400 000 cells/mL in complete growth media. After completing the incubation time, the transfection complex was transferred into a well of a 96-well plate and 100 μL of the cell suspension was added, resulting in 40 000 cells/well and a final concentration of 10 nM RNP complex. The cells were incubated 24 h at 37 °C in a standard incubator before cell sorting. For cell sorting, the cells were harvested with PBS/1% FBS and washed once. The cells were afterwards resuspended in DMEM containing 100 U/mL P/S (Gibco) and 5μg/mL Plasmocine prophylactic (Invivogen) and kept at 37°C until cell sorting. Cell sorting was performed by Sabrina Becker, University Medical Center Göttingen Cell Sorting Facility. Single cells, which were either GFP (480 nm) or ATTO-550 (554 nm) positive were sorted by a FACS Vantage SE into a 96-well plate. After 2-3 weeks, individual clones were visible and expanded. Clones were tested for protein ablation by western blotting and genomic DNA was analyzed by PCR followed by sequencing.

3.2.1.5 Stable transfection of HEK293T cells

Stable HEK293T cell lines were generated according to Mick et al., 2012. The day prior to transfection, the cells were seeded into a 6-well plate and cultivated until 50% confluency. Either GeneJuice (Novagen) or Lipofectamine 3000 (Invitrogen) were used as transfection reagents according to the manufacturer's instructions.

Briefly, 3 µL of GeneJuice transfection reagent was added to 100 µL of Opti-MEM™ (Gibco) and incubated at room temperature for 5 minutes. Afterwards 0.9 µg of pOG44 and 0.1 mg of pcDNA5 containing the gene of interest were added, briefly mixed and incubated for additional 15 minutes. To use Lipofectamine 3000 as transfection reagent, 2.25 µg pOG44, 0.25 µg pcDNA5 containing the gene of interest and 5 µL P3000 reagent were mixed in 125 µL Opti-MEM™ (Gibco). In another reaction tube 5 µL Lipofectamine™ 3000 was added in 125 µL Opti-MEM™ (Gibco) and briefly mixed. Both reactions were incubated at room temperature for 15 minutes and afterwards combined.

The media was removed from the wells, and 2 mL of DMEM was added. Transfection mix was added dropwise to the cells. After 4 – 5 hours the media was changed. Two days after transfection the cells were selected using either Hygromycin [100 µg/mL or 50 µg/mL] or a combination of Hygromycin [100 µg/mL] and Blasticidin [5 µg/mL]. Single clones were selected, expanded, induced with [100 ng/mL or 250 ng/mL] tetracycline and screened for protein expression by immunoblotting.

3.2.2 Molecular biology techniques

3.2.2.1 Polymerase chain reaction (PCR)

The KOD Hot Start DNA Polymerase kit (Novagen) was used to amplify DNA fragments following manufactures instructions.

The reaction mix contained:

1x	KOD reaction buffer
0.2 mM	dNTPs
1.5 mM	$MgSO_4$
0.3µM	Forward primer
0.3µM	Reverse primer
0.02 U/µL	KOD DNA polymerase

To this mix, cDNA or 100 ng plasmid DNA were added as a template as well as ddH_2O to an end volume of 50 µL. The PCR conditions used are shown in Table 13

Table 13: PCR temperature conditions. The annealing temperature varied dependend on the used primers.

Temperature [°C]	Time [min]	Cycles
95	02:00	1
95	00:20	
55-60	00:10	35
70	00:20/kb	
4	∞	

3.2.2.2 Agarose gel electrophoresis

To confirm the presence of a specific product, its correct size after PCR amplification and to verify restriction enzyme digestion of plasmids, an agarose gel electrophoresis was carried out. Depending on the product size, a 1 or 1.5 % agarose gel in TAE buffer was prepared by gentle heating and mixing. The gel solution was cooled down to approximately 50 °C prior to ethidium bromide addition [1 μg/mL], poured and left to solidify. DNA was supplied with DNA Gel Loading Dye (6x) (Thermo Scientific) prior to loading onto the gel along with 1μL GeneRuler DNA Ladder (Thermo Scientific). Subsequently, DNA was visualized by UV-light.

TAE-Buffer: 40 mM Tris/acetate pH 8.0, 2 mM EDTA

3.2.2.3 DNA purification

To purify DNA after PCR or restriction digestion, the Wizard® SV Gel and PCR Clean-up System (Promega) or the NucleoSpin® Gel and PCR Clean-up System (Macherey-Nagel) were used, following the manufactures instructions. Briefly, using the Wizard® SV Gel and PCR Clean-up System, an equal volume of membrane binding solution was added to the DNA soluation, carefully mixed and transferred to the provided column. In case of gel extraction, an equal volume of membrane binding solution to gel weight ratio was added and heated at 65 °C until dissolved. The resulting sample was then transferred to the provided column. The columns were centrifuged at 16 000 xg for 1 minute and washed twice with the provided wash solution. To allow the remaining ethanol to evaporate, the empty column was centrifuged once more. The column was then transferred into an RNase free reaction tube. To elute, 50 μL nuclease free water was added and incubated for 1 minute at room temperature and the purified DNA collected by centrifugation at 16 000 xg for 1 minute.

To purify DNA using the NucleoSpin® Gel and PCR Cleanup System, one volume of DNA solution was mixed with two volumes of NTI Buffer and transferred into the provided column. In case of required gel extraction, DNA was excised from the gel and per 100 mg gel 200 μL NTI Buffer was added and heated at 50 °C. If the gel was dissolved, samples were transferred into the provided column. The columns were centrifuged at 11 000 xg for 30 seconds and washed twice with 700 μL NT3 Buffer. To remove residual ethanol, the columns were centrifuged for 1 minute at 11 000 xg and afterwards incubated for 2 – 5 minutes at 70 °C. To elute the sample, 15 μL of pre-heated NE Buffer (50°C) was added to the column and incubated for 5 minutes at room temperature. The purified DNA was collected by transferring the column in an RNase free reaction tube and quantified using Nanodrop^{TM} One^{C} Microvolume UV-Vis Spectrophotometer.

3.2.2.4 Cloning procedure

Purified PCR products and plasmids were digested using FastDigest restriction enzymes (Thermo Scientific) following manufactures instructions. DNA (2-4μg) were digested with 20U enzyme in 1x fast digest buffer. The reaction was incubated at 37 °C for 30-60 minutes at 450 rpm. The digested plasmid was furthermore dephosphorylated using 2 Units of alkaline phosphatase in 1x phosphatase buffer (Roche) at 37 °C for 60 minutes. Prior to ligation, DNA was purified (see 3.2.2.3). The digested PCR amplicon and plasmid DNA (50 ng) were ligated in a molecular ratio 6:1 using the Rapid DNA Ligation Kit (Thermo Scientific). The reaction was performed in 1x ligation buffer containing 5 Units T4 DNA ligase 30 minutes at 22 °C at 450 rpm shaking. Subsequently, XL1 Blue *E. coli* competent cells were transformed with the ligation mix (see 3.2.2.6).

3.2.2.5 Mutagenesis

To introduce DNA mutations into purified plasmids, partially overlapping primers harboring the desired mutations were designed following the protocol designed by Zheng et al. (2004). In brief, the PCR was performed using the KOD Hot Start DNA Polymerase kit as in section 3.2.2.1 with 100 ng plasmid. The PCR conditions used are shown in Table 14.

Table 14: PCR conditions.

Temperature [°C]	Time [min]	Cycles
95	02:00	1
95	00:20	
53	00:10	20
70	03:55	
4	∞	

To the cooled PCR product, 10 Units of Dpn1 (Thermo Scientific) was added to the whole reaction to digest the parental DNA for 1 hour at 37 °C at 500 rpm. After digestion, 5 μL of the plasmid was used for transformation, followed by plasmid isolation (see 3.2.2.7). To assess the successful mutagenesis, isolated plasmids were sequenced.

3.2.2.6 *E. coli* transformation

Competent XL1 Blue *E. coli* cells were thawed on ice and carefully mixed with 4 μL ligation reaction. After incubation of 30 minutes on ice, cells were heat shocked for 1 minute at 42 °C and transferred on ice for 2 minutes. LB medium (900μL) was added to the mixture and bacteria were incubated for 1 hour at 37 °C while shaking. The transformed cells were centrifuged at 8 000 xg for 1 minute and the supernatant discarded. Cells were resuspended in 100 μL LB medium and plated on a LB agar plate containing 100 μg/mL Ampicilin and incubated over night at 37 °C. Single colonies where picked and transferred in a reaction tube containing 5 mL LB media with 0.1 mg/mL Ampicillin and incubated over night at 37 °C at 200 rpm.

LB-medium: 1 % (w/v) tryptone, 0.5 % (w/v) NaCl, 1 % (w/v) yeast extract

LB agar plate: 1 % (w/v) tryptone, 0.5 % (w/v) NaCl, 1 % (w/v) yeast extract, 1.5% agar, 100 μg/mL Ampicilin

3.2.2.7 Isolation of plasmid DNA

To isolate plasmid DNA from *E. coli*, the Wizard® SV Plus Minipreps DNA purification System by Promega was used following the instructions provided by the manufacturer were followed. Bacteria of an overnight liquid culture (3 mL) were collected by centrifugation at 11 000 xg for 30 seconds at room temperature and resuspended in

250 µL of cell resuspension solution. Cell lysis solution (250µL) was added and the samples inverted for four times. Alkaline protease solution (10 µL) was added, the samples were again inverted for four times and incubated for 5 minutes at room temperature. Subsequently the reaction was neutralized using 350 µL of provided solution, mixed and immediately centrifuged at top speed for 10 minutes. The cleared lysate was transferred into a provided spin column and centrifuged at top speed for 1 minute. The columns were washed twice with the provided solution. To elute the DNA, 50 µL ddH_2O was added onto the filter followed by 1 minute of incubation. The column was finally centrifuged at top speed for 1 minute and the DNA concentration was measured using Nanodrop™ One^C Microvolume UV-Vis Spectrophotometer.

3.2.2.8 Isolation of human genomic DNA

HEK293T from a single well of a 96-well plate were harvested. The cell pellet was resuspended in 50 µL of extraction reagent (QuickExtract™ DNA Extraction Solution) and vortexed for 15 seconds. The extract was incubated at 65 °C for 6 minutes, vortexed for 15 second, incubated at 98 °C for 2 minutes and either stored at -80 °C or directly used for PCR.

3.2.2.9 Sequencing

DNA samples were analyzed by sanger sequencing using the service provided by Microsynth SEQLAB (Göttingen, Germany). Samples were provided with a concentration of 100 ng/µL in a total volume of 12 µL per sequencing reaction. If non-standard sequencing primers were required, DNA was mixed with 2 µM of respective oligonucleotide. Results of the sequencing reactions were analysed with the web-based nucleotide BLAST tool from NCBI (https://blast.ncbi.nlm.nih.gov/Blast.cgi) or the software Geneious.

3.2.2.10 TOPO® Sequencing

To sequence heterozygous HEK293T knockout cell lines, TOPO® sequencing was applied using the linearized pCR™4-TOPO® plasmid included in the TOPO TA Cloning® Kit for Sequencing (Invitrogen). The pCR™4-TOPO® plasmid has a covalently bound Topoisomerase I and 3' thymidine overhangs. The sequence which

should be analysed, was amplified by PCR using DreamTaq™ Hot Start DNA Polymerase according to the manufacturer's instructions to obtain a deoxyadenosine at the 3' end. To set up the of the TOPO® cloning reaction was done according to the manufacturers protocol. Briefly, 4 µl of the PCR product was mixed with 1 µl of TOPO® vector and 1 µl salt solution. The reaction was incubation for 5 minutes at room temperature and afterwards cooled down on ice to stop the reaction. For the transformation, 2 µl of the reaction were added into a One Shot® chemically competent *E. coli* (TOP10) vial and incubated on ice for 10 min. Afterwards, heat-shock was performed for 30 s at 42°C and placed on ice. 250 µl pre-warmed S.O.C. medium was added shaken at 200 rpm for 1h at 37°C. 50 µl and 100µL of the cells were plated each on a prewarmed LB-plate containing 100 µg/ml ampicillin and incubated overnight at 37°C. 20 colonies were picked and further processed as described in 3.2.2.7. Each colony contained only one variant of the heterozygous sequence of HEK293T knockout cells, which was sequenced and analyzed as described in 3.2.2.9

3.2.2.11 RNA isolation

To isolate RNA from whole cells, cells where seeded into wells of 6-well plates and cultivated until 80-90% confluency was achieved. The resulting cell pellet of one well was carefully resuspended in 500 µL Trizol (Invitrogen) and incubated at room temperature for 5 minutes. Next, 100 µL Chloroform was added and samples were shaken 15 seconds, incubated at room temperature for 3 minutes and centrifuged for 10 minutes at 12 000 xg at 4 °C. The aqueous phase was transferred to a new reaction tube and RNA was precipitated by the addition of 250 µL isopropanol. Samples were inverted four times, incubated for 10 minutes at room temperature and centrifuged for 10 minutes at 12 000 xg at 4 °C. The supernatant was discarded and the samples were washed twice with 75 % and 100 % ethanol. The supernatant was removed and precipitated RNA was dissolved in 20 µL RNase free water containing 20 Units RNase inhibitor RiboLock (Life Technologies) over night at 4 °C. The RNA concentration was measured using a Nanodrop™ One^{C} Microvolume UV-Vis Spectrophotometer. RNA was stored at -80 °C until further application.

3.2.2.12 Northern blot

To determine mitochondrial RNA steady state levels, RNA samples were analysed by northern blotting as described by Chrzanowska-Lightowlers et al. (1994). Briefly, RNA samples were separated unter denaturing conditions using a 1.2 % agarose gel containing 1x MOPS and 0.91 % formaldehyde. The RNA samples were prepared in a reaction volume of 16 μL containing 2 μg RNA, 1x MOPS, 13.78 % formaldehyde and 4.81 % formamide. Samples were incubated for 15 minutes at 55 °C and subsequently transferred on ice prior to loading on the 1.2 % agarose gel and run at 100 V for 4 – 5 hours. Next, the gel was washed twice in ddH_2O and transferred onto a nylon membrane (Amersham™ Hybond N, GE Healthcare Life Science) over night using 10X SSPE buffer.

Next day the membrane was washed with ddH_2O and dried prior to cross-linking the RNA to the membrane using the auto setting of the UV Stratalinker® 2400 twice. The membrane was either stored at room temperature or directly stained with methylene blue for 5 minutes followed by a washing step with ddH_2O for 5 min.

To detect RNA molecules of interest sequence specific radiolabeled probes were prepared by mixing 1 μM oligonucleotides (Table 10), 1x PNK buffer A (Thermo Scientific), 10 Units PNK (Thermo Scientific) and 1 μCi [γ^{32}P]-ATP (Hartmann Analytic) in a total volume of 20 μL. The probe was incubated for 40 minutes at 37°C. The membrane was prehybridized in 20-50 mL SES1 buffer for at least 30 minutes prior probe addition. The membrane was incubated overnight at 37 °C while rotating. On the following day the membrane was washed twice with 6x SSC buffer and 2x SSC/0.1 % SDS buffer for 30 minutes at 37 °C while shaking. Afterwards the membrane was dried, covered with clear foil and exposed to a phosphor screen (GE Healthcare Life science) for 2 – 6 h or overnight. Digital autoradiography was performed on Typhoon FLA 9500 Phosphoimager followed by quantification according to 3.2.3.11).

10x MOPS: 0.4 M Morpholinopropanesulfonic acid (MOPS), 0.1 M NaOAc, 10 mM EDTA, pH 7.2

10x RNA loading buffer: 50 % (v/v) glycerol, 1 mM EDTA, 0.25 % (w/v) bromophenol blue, 0.25 % (w/v) xylene cyanol, sterile filtrated

20x SSC: 3 M NaCl, 300 mM sodium citrate pH 7.0

20x SSPE: 3 M NaCl, 0.2 M NaH_2PO_4, 20 mM EDTA, pH 7.4

SES1: 250 mM NaPi pH 7.4, 7% (w/v) SDS, 1 mM EDTA pH 8.0

Sequence of Probes:

MTRNR1 (12S mt-rRNA)	5'-TCGATTACAGAACAGGCTCCTCTAG-3'
MTRNR2 (16S mt-rRNA)	5'-GTTTGGCTAAGGTTGTCTGGTAGTA-3'
MTCO1	5'-GTCAGTTGCCAAAGCCTCCGATTATG-3'
MTCO2	5'-GACGTCCGGGAATTGCATCTGTTTT-3'
18S-rRNA	5'-TTTACTTCCTCTAGATAGTCAAGTTCGACC-3'

3.2.3 Protein analysis

3.2.3.1 Preparation of human cell lysates

Cells were harvested with PBS/EDTA and pelleted at 2000 xg for 5 minutes. The pellet was resuspended in 100 – 200 µL NP-40 lysate buffer and vortexed for 30 seconds at room temperature prior centrifugation at 4 °C for 3 minutes at 2000 xg. The supernatant was collected, the protein concentration determined (see 3.2.3.2) and samples were either subjected to western blot analysis or stored at -80 °C

NP-40 lysis buffer: 50 mM Tris/HCl pH 7.4, 130 mM NaCl, 2 mM $MgCl_2$, 1 % NP-40 (v/v), 1 mM PMSF, 1x PI-Mix

3.2.3.2 Determination of protein concentration

To determine the protein concentration, the instruction described by Marion McKinley Bradford (1976) was followed. Briefly, 2 µL cell lysates was mixed with 800 µL ddH_2O and 200 µL Roti®-Quant reagent (Roth). Standart curve solutions were made by diluting BSA-stock [1mg/mL] 200 µL Roti®-Quant reagent (Roth) and adding ddH_2O to a final volume of 1 mL to achieve the final concentrations of 0, 2, 5, 10, 15 and 20

µg/mL. In a 96-well plate, 2x 200 µL/well of standart curve solutions and samples were added and measured using the Synergy H1 microplate reader (BioTek) and quantified with the Gen5™ software (BioTek).

3.2.3.3 SDS Polyacrylamide gel electrophoresis

3.2.3.3.1 Tris-glycine SDS-PAGE

The SDS polyacrylamide gel electrophoresis (SDS-PAGE) was used to separate proteins under denaturing conditions according to their molecular weight. The casting and running system from BioRad were used. 12.5% polyacrylamide gels were prepared according to Table 15.

Table 15: Preparation of 12.5% Polyacralamide gel.

	12.5 % resolving gel	**5% stacking gel**
30% acrylamide solution (Roth)	6.1 mL	1.66 mL
dH_2O	5.56 mL	7.1 mL
1.87 M Tris/HCl, pH 8.8	3.1 mL	--
0.8 M Tris/HCl, pH 6.8	--	1 mL
10 % SDS	150 µL	100 µL
TEMED	15 µL	20 µL
10% APS	150 µL	100 µL

Volumes are sufficient for 4 gels.

The samples were supplied with SDS sample buffer and incubated for 15 minutes at 37 °C under mild shaking or samples were boiled for 5 minutes at 95 °C. Electrophoretic separation was performed at 30 mA per gel in SDS running buffer in MINI-Protean II (BioRad) systems. As a marker, Precision Plus Protein™ All Blue Prestained Standards (10-250kD) from BioRad was used.

4x SDS sample buffer	10 % (v/v) Glycerol, 2 % (w/v) SDS, 0.01 % (w/v) Bromophenol blue, 63 mM Tris/HCl, pH 6.8, 5 mM DTT
SDS running buffer	25 mM Tris, 192 mM glycine, 0.1% (w/v) SDS

3.2.3.3.2 Tris-tricine SDS-PAGE

For a better separation of proteins particulary of low molecular weight, tris-tricine gradient polyacrylamide gels (Schägger, 2006) were prepared using a gradient mixer with a connected peristaltic pump. Resolving gels with 10% and 18% polyacrylamide concentration were prepared according to Table 16. For polymerization, 10% APS and TEMED were used.

Table 16: Preparation of Tris-tricine 10-18 % gel.

	10% separating gel	**18% separating gel**	**4% Stacking**
Acrylamide/bis-acrylamide solution	1.65 ml	2.97 ml	0.5 ml
3x gel buffer	2.67 ml	2.67 ml	2 ml
50% Glycerol	--	2 ml	--
dH_2O	3.68 ml	0.36 ml	3.5 ml
TEMED	3 µl	3 µl	6 µl
10% APS	40 µl	40 µl	60 µl

Volume is sufficient for 1 gel.

Samples containing 1x SDS loading buffer were incubated for 15 minutes at 37°C alongside 5 µL Precision Plus Protein™ All Blue Prestained Standards (10-250kD) (BioRad) prior to loading and electrophoretic separation at 25 mA per gel for 16 hours using custom made midi gel system.

Anode buffer: 0.2 M Tris, pH 8.9

Cathode buffer: 0.1 M Tricine, 0.1% (w/v) SDS, 0.1M Tris, pH 8.25

3x Gel buffer: 1 M Tris, 0.1 % (w/v) SDS, pH 8.45

3.2.3.4 Silver staining of polyacrylamide gels

Proteins were visualized after SDS-PAGE by silver staining. First, the gel was incubated in fixating solution while shaking for 1 hour followed by two washing steps in 50 % ethanol for 20 minutes and another washing for 20 minutes in 30 % ethanol. After fixation, the gel was impregnated 60 seconds with 0.8 mM Na-Thiosulfate followed by three washing steps with ddH_2O for 20 seconds. The gel was stained with 2 g/l $AgNO_3$ in 0.026 % formaldehyde for 20 minutes and washed with ddH_2O. The gel

was developed until the protein bands were visible in 100 mL developing solution. The reaction was stopped by adding 2 mL of 100 % acetic acid followed by incubation in fixating solution for 15 minutes. The stained gel was stored until scanning in 5 % acetic acid solution.

Fixating solution: 50 % Methanol, 12 % Acetic acid

Staining solution: 2 g/l $AgNO_3$, 0.026 % Formaldehyde

Developing solution: 60 g/L Na_2CO_3, 0.0185% Formaldehyde, 16μM $Na_2S_2O_3$

3.2.3.5 Western Blot

To analyse protein samples by immunodetection separated proteins were transferred on a PVDF membrane (GE Healthcare life science and Merck) or nitrocellulose membrane (GE Healthcare life science) performing semi-dry blotting in PEQLAB chambers. PVDF membranes were activated in methanol and nitrocellulose membranes in ddH_2O followed by equilibration in transfer buffer. The membrane was assembled with the gel and whatman blotting papers soaked in blotting buffer. The transfer was performed for 2 hours at 25 V and 250 mA. After transfer, the blotting chambers were disassembled and the PVDF or nitrocellulose membranes stained with Coomassie Brilliant Blue or Ponceau S, respectively. The membranes were dried until further application.

Transfer buffer: 20 mM Tris, 0.02 % (w/v) SDS, 150 mM Glycine, 20 % (v/v) Ethanol

Coomassie staining solution: 0.25 % (w/v) Coomassie Brilliant Blue R-250, 10 % (v/v) Acetic acid, 40 % (v/v) Ethanol

Destainer: 40% Ethanol (v/v), 10% Acetic acid (v/v)

Ponceau S staining solution: 0.1% (w/v) Ponceau, 5% w/v TCA

3.2.3.6 Immunodetection of proteins

Dried PVDF and nitrocellulose membranes were reactivated and destained with Methanol or ddH_2O, respectively, followed by incubation in TBS-T containing 5 % milk

powder for at least 1 hour at room temperature while shaking. Primary antibodies (Table 9) diluted in TBS-T containing 5 % milk powder and 0.2 % sodium azid were applied and incubated at 4 °C overnight under mild shaking or rotation. Membranes were washed once in ddH_2O and then three times with TBS-T for 10 minutes. The corresponding HRP conjugated secondary antibody (Table 9) was applied for at least 90 minutes at room temperature followed by three washing steps with TBS-T. Signals were visualized by using the Pierce® ECL Western Blotting Detection Reagent (Thermo Scientific) and X-ray films.

TBS-T: 20 mM Tris/HCl (pH 7.5), 125 mM NaCl, 0.1 % (v/v) Tween20

3.2.3.7 Isolation of mitochondria from cultured human cells

Mitochondria were isolated as described previously (Mick et al. 2012) with modifications. Cells were resuspended in cold THE buffer containing 0.1 % BSA (Sigma) and 1 mM PMSF (Roth) and incubated for 15 minutes on ice. Cells were transferred into a cooled homogenizer with PTFE-pestle (schuett-biotec.de). The homogenizer was installed into the schuett homgen^{plus} (schuett-biotec.de) and the pestle passed through the solution 20 times at 800 U/min. Debris and unopened cells were removed by centrifuging at 400 xg at 4 °C for 10 minutes and the supernatant was saved. The pellet was resuspended and the procedure was repeated twice. The supernatants were pooled and centrifuged at 11 000 xg for 10 minutes at 4 °C. Finally, mitochondria were resuspended in THE buffer and subjected to further experiments or shock frozen in liquid nitrogen and stored at -80 °C.

THE buffer: 300 mM Trehalose, 10 mM KCl, 10 mM HEPES/KOH pH 7.4

3.2.3.8 Preparation of mitoplasts

To remove cytosolic contamination, crude mitochondria were subjected to further treatments to obtain mitoplasts (see 3.2.3.5). Mitochondria were resuspended in THE buffer in a final concentration of 4 mg/mL. To remove the outer mitochondrial membrane, mitochondria were permeabilized with 0.1 % digitonin (Calbiochem) for 30 minutes on ice prior proteinase K (Roth) addition at a working concentration of 5 mg/mL for 15 minutes. The activity of proteinase K was stopped by adding 2 mM PMSF (Roth) to the sample followed by an incubation on ice for 10 minutes. The

samples were washed twice with THE buffer containing 0.1 % BSA (Sigma) and 1 mM PMSF followed by two washing steps with THE buffer without BSA and PMSF. The pelleted mitoplasts were resuspended in THE buffer and subjected to further experiments.

3.2.3.9 Mitochondrial protein localization assay

30 μg mitochondria were resuspended in 30 μL swelling or THE buffer respectively to get a final concentration of 1 μg/μL. Samples were treated with 0.17 or 0.33 μg/μL proteinase K (Roth) for 15 minutes on ice followed by inactivation with 3.33 μM PMSF (Roth) and incubation for 10 minutes on ice. Samples were then centrifuged at 16 000 xg for 5 minutes at 4°C and the supernatant discarded. As a control, samples in swelling buffer were subjected to sonication three times for 20 seconds and treated with 0.33 μg/μL proteinase K for 15 minutes followed by inactivation with 3.33 μM PMSF. All samples supplemented with SDS sample buffer were boiled at 95°C for 5 minutes and analysed by SDS-PAGE and immunoblotting as described in 3.2.3.3 and 3.2.3.4.

THE buffer: 300 mM Trehalose, 10 mM KCl, 10 mM HEPES/KOH pH 7.4

Swelling buffer: 10 mM HEPES pH 7.4, 1 mM EDTA

3.2.3.10 Co-Immunoprecipitation

Mitocondria isolated from HEK293T cells inducibly expressing a C-terminal FLAG tagged MRP or assembly factor were lysed in solubilization buffer with a detergent to protein ration of 5:1 and protease inhibitor cocktail (Roche) for 30 minutes at 4°C with occasionally mixing. The lysates were cleared by centrifugation at 16 000 xg at 4 °C for 10 minutes and the supernatant diluted with an equal volume of dilution buffer to obtain a detergent to protein ration of 1:1. The sample was subjected to equilibrated anti-FLAG M2 Affinity Gel (Sigma) (30 μL beads suspenseion), with a final protein concentration of 1 μg protein/μL. After incubation for 1 hour at 4 °C on rotating wheel, beads were washed in wash buffer and protease inhibitor cocktail ten times by centrifugation at 5 000 xg for 30 seconds. Proteins were eluted in 100 μL washing buffer containing 0.2 μg/μL FLAG peptide at 4 °C while shaking at 1 000 rpm for 30 minutes. Samples were either taken up in SDS sample buffer (with 50 mM DTT final

concentration) and analyzed by SDS-PAGE and immunoblotting (see 3.2.3.4) or used for sucrose density gradient ultracentrifugation (see 3.2.3.9).

Solubilization buffer:	20 mM HEPES/KOH pH 7.4, 150 mM KCl, 10 % Glycerol, 10 mM $MgCl_2$, 1 % Digitonin, 1 mM PMSF
Dilution buffer:	20 mM HEPES/KOH pH 7.4, 150 mM KCl, 10 % Glycerol, 10 mM $MgCl_2$, 1 mM PMSF
Wash buffer:	20 mM HEPES/KOH pH 7.45, 150 mM KCl, 10 % Glycerol, 10 mM $MgCl_2$, 0.2 % Digitonin, 1 mM PMSF

3.2.3.11 Sucrose density gradient ultracentrifugation

To analyze the distribution of MRPs as well as assembly factors in their presence or absence in assembly complexes, sucrose density gradient ultracentrifugation was performed. The protocol was followed as previously described in Lavdovskaia et al. (2018). To prepare the sucrose gradient, the half position of an 14x89 mm tube (SETON) was marked using the SW41 marker block provided with the Gradient Station™ (BioComp). 5% sucrose gradient buffer was filled to the half-line prior to sublayering with 30% sucrose gradient buffer using a syringe with a needle. The tube was closed with a rubber-lid provided with the Gradient Station™ followed by linear gradient preparation using the “Rotor: SW41, caps: short, 5-30% sucrose 1 step gradient” settings of the Gradient Station™ (BioComp). The gradient was left for 30-60 minutes prior to use at 4°C for stabilization. Mitoplasts (500 μg) were lysed in lysis buffer for 30 minutes on ice and centrifugated at 16 000 xg for 15 minutes at 4 °C. Cleared supernatants (300 μL) or isolated complexes from co-immunoprecipitations (300 μL) were separated by linear 5 – 30 % sucrose gradients at 79 000 xg for 15 hours at 4 °C using the SW41 Ti rotor (Beckman Coulter). Fractions (1-16) were collected using the BioComp fractionator and precipitated with ethanol by adding 2.5 volumes of ice cold 100 % ethanol and 1/3 volume of NaAc pH 6.5 to the sample. Samples were incubated at -20 °C for at least 1 hour, thawed on ice and centrifuged at top speed for 15 minutes at 4 °C. The supernatant was discarded and the samples washed twice with 80 % ethanol and centrifuged at top speed for 2 minutes at 4 °C.

The resulting precipitates were subjected to SDS-PAGE and immunoblotting (see 3.2.3.3 and 3.2.3.4).

Mitoplasts Lysis buffer: 100 mM KCl, 20 mM $MgCl_2$, 20 mM HEPES/KOH pH 7.5, 1 % (w/v) Digitonin, 0.08 U/μL RiboLock RNase Inhibitor, cOmplete^{TM} Protease inhibitor cocktail tablet 1/50 ml

30 % Sucrose Gradient buffer: 30 % (w/v) Sucrose, 100 mM KCl, 20 mM $MgCl_2$, 20 mM HEPES/KOH pH 7.4, cOmpleteTM Protease inhibitor cocktail tablet 1/50 mL

5 % Sucrose Gradient buffer: 5 % (w/v) Sucrose, 100 mM KCl, 20 mM $MgCl_2$, 20 mM HEPES/KOH pH 7.4, cOmpleteTM Protease inhibitor cocktail tablet 1/50 mL

3.2.3.12 [^{35}S]methionine *de novo* synthesis of mitochondrial encoded proteins

[^{35}S]methionine labelling of mitochondrial encoded proteins was performed according to the protocol described by Chomyn (1996). HEK293T cells were cultivated in 25 cm^2 flasks until 80-90% confluence was obtained. The media was discarded and cells were incubated in 2 mL methione/cysteine free media (Gibco) lacking FCS for 10 minutes at 37 °C. This step was repeated prior to addition of 1.5 mL methione/cysteine free media containing 10% dialysed FCS (Biochrom) supplemented with 100 μg/mL emetine dihydrochloride hydrate to inhibit cytosolic translation. After 10 minutes incubation, mitochondrial-encoded proteins were labelled with 200 μCi/mL [^{35}S]methionine for one hour at 37 °C. Cells were harvested at 5 000 xg for 2 minutes with PBS/EDTA and washed twice with PBS. Cells were lysed with NP-40 lysis buffer as described in 3.2.3.1 and the protein concentration determined (see 3.2.3.2). Samples (25 μg and 50 μg) were prepared for SDS-PAGE and immunoblotting (see 3.2.3.3 and 3.2.3.4). Radiolabeled membranes were exposed on storage phosphor screen (GE Healthcare Life Science) and digitalized on Typhoon FLA 9500 Phosphoimager.

3.2.3.13 Quantification

Quantification of western blots, Northern blots and radiolabeled membranes was performed by using the software ImageQuant TL (GE Healthcare Life Science). Bands were manually detected and the background subtracted with the rolling background subtraction tool provided by the software.

3.2.3.14 Statistical analyses

Northern blots were quantified as described in 3.2.3.13. Protein and RNA steady state levels are presented as percentages relative to the wild type control and the error bars indicate the SEM of the mean of $n \geq 3$ experiments.

Western blots were quantified as described in 3.2.3.13 and protein levels of gradients are presented as relative values in a heatmap using the R studio software using a modified code provided by Nicolas Lemus (Research group Bohnsack).

```
library(gplots)
library(RColorBrewer)
setwd("~/Documents/RStudio/Heatmap_Data")
Data <- read.table("Heatmap_Data_WT_VS_KO.txt",header = T,fill=TRUE)
Color <- data.frame(Data[,1:2])
Data[is.na(Data)] <- 0
Color$Protein <- as.character(Color$Protein)
Color[seq(1,92,by=4),3] <- rep("#52d084",23)
Color[seq(2,92,by=4),3] <- rep("#e3c34a",23)
Color[seq(3,92,by=4),3] <- rep("#52bbd0",23)
Color[seq(4,92,by=4),3] <- rep("#d0525f",23)
Color[seq(2,92,by=4),2] <- rep(" ",23)
my_palette <- colorRampPalette(c("#bdbdbd", "#FFFFF", "#3182bd"))(5)

mat <- log((as.matrix(Data[,3:18]))+1)

png("~/Documents/RStudio/Playground/heatmaps_Data_WT_VS_KO.png",
    width = 10*600,                         # 10 x 600 pixels
    height = 10*600,
    res = 600,                              # 600 pixels per inch
    pointsize = 10                          # smaller font size
   )
heatmap.2(mat, main="Comparison HEK293T WT and KO cells", trace="none",
          margins = c(10,12),
          cexRow = 1.5,
          Rowv = F,
          Colv = F,
          labRow = Color$Protein,
          #scale = "row",
          RowSideColors =Color$V3,
          col=my_palette,
          cexCol = 1.5,
          rowsep = c(seq(0,92,by = 4)),
          colsep = c(seq(0,18,by = 1)),
          sepwidth = c(0,0.0001),
          sepcolor = "white"
          )
legend("left",                              # location of the legend on the heatmap plot
       legend = c("WT", "uS7m Mutant",
                  "ms27 -/-", "mS40 -/-"), # category labels
       col = c("#52d084", "#e3c34a",
               "#52bbd0", "#d0525f"),       # color key
       lty= 1,                              # line style
       lwd = 10                             # line width
      )
dev.off()
```

4. Results

4.1 Effect on the mtSSU assembly in the absence of specific MRPs

With the rise of diseases resulting from mutations occurring in genes encoding for MRPs, it became more apparent that the analysis of the mitochondrial ribosome assembly is crucial for their understanding.

Indeed, Bogenhagen et al. (2018) showed that uS7m, mS27 and mS40 act early in the mtSSU assembly, albeit in distinct sub-modules. Additionally, the mutation c.550 A>G (p.Met184Val) occurring in uS7m (Menezes et al., 2015) leads to human diseases with varying phenotypical presentations and clinical prevalence, although the mutation was present in two individual patients. To understand how the loss of uS7m, mS27 and mS40 affects their sub-modules and therefore the mtSSU assembly and whether the mtLSU biogenesis is affected by the ablation of these MRPs, knockout cell lines were generated using the CRISPR/Cas9 technology.

4.1.1 Generation of CRISPR/Cas9 mediates knockouts

CRISPR/Cas9 mediated knockout of uS7m, mS27 and mS40 was performed in HEK293T cells. To identify potential cell lines deficient for uS7m, mS27 or mS40, cell lysates were analyzed by western blotting. Out of the five screened uS7m$^{-/-}$ clones, only clone 6 shows the absence of the uS7m protein and a substantial reduction of COX2 (Figure 11A). Screening of three mS27$^{-/-}$ clones shows that only in clone 4 mS27 is absent. Furthermore, COX2 analysis reveals a decrease to non-detectable levels, resulting in mS27$^{-/-}$ clone 4 being used for further characterizations (Figure 11B).

Two potential mS40$^{-/-}$ clones were obtained, clone 12 being the most promising one, as COX2 is reduced to a non-detectable level, while clone 1 reveals a reduction in COX2 of approximately 90%. Therefore, for further characterization of the effect of mS40 loss, mS40$^{-/-}$ clone 12 was used (Figure 11C).

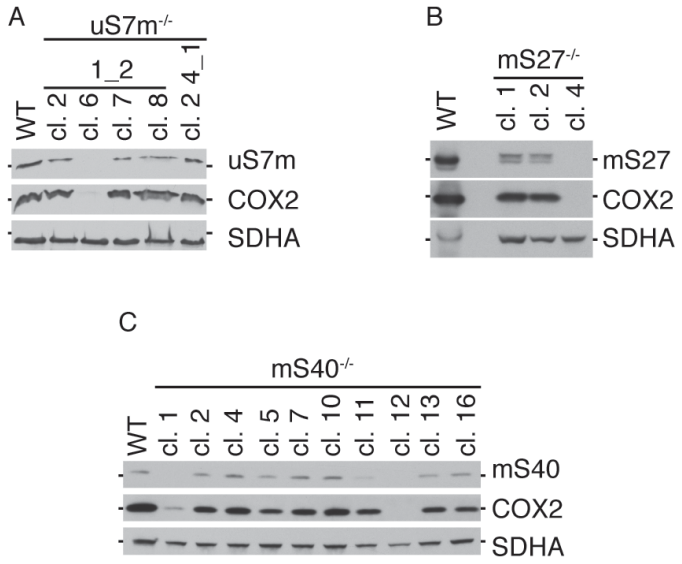

Figure 11: Analysis of different CRISPR/Cas9 generated knockout clones for further characterizations. Cell lysates of different A) uS7m$^{-/-}$, B) mS27$^{-/-}$and C) mS40$^{-/-}$ clones were separated via SDS-PAGE and analyzed by western blot. COX2 detection was used to determine the knockout effect. Lysates of HEK293T WT served as control. SDHA was used as a loading control.

To determine the mutation in uS7m$^{-/-}$ clone 6, mS27$^{-/-}$ clone 4 and mS40$^{-/-}$ clone 12, TOPO sequence analysis was performed as described in chapter 3.2.2.9.

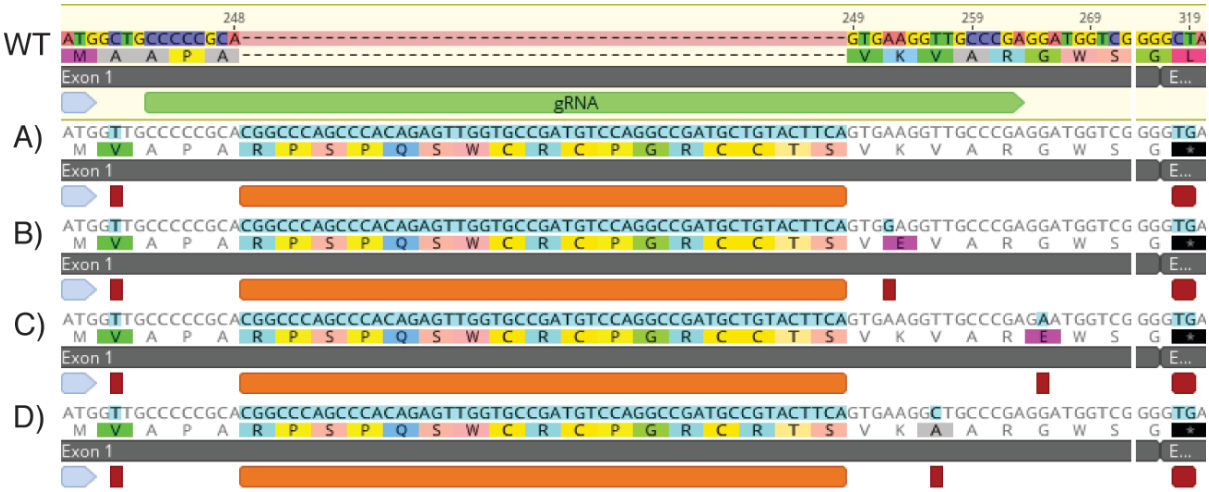

Figure 12: Sequence analysis of 20 uS7m clones by TOPO® sequencing. The uS7m coding sequence consists of 728 base pairs (bp). The start codon ATG is indicated by a light blue arrow and exons in grey. Substitutions are indicated in red and insertions in orange. Wild type (WT) sequence of uS7m and the different mutated sequences are indicated below. The uS7m c.238 C>T; 318_319 CT>TG and the 51bp insertion between c.248_249 was present in all clones. Point mutations in the individual alleles revealed their differences. A) Mutation in allele 1: No further mutations detected except uS7m c.238 C>T; 318_319 CT>TG and the 51bp insertion at c.248_249 in 17 tested clones. B) Mutation in allele 2: Similar to allele 1 but with the addition of uS7m c.252 A>G present in one clone. C) Mutation in allele 3: Similar to allele 1 but with the addition of uS7m c.265 G>A present in one clone. D) Mutation in allele 4: Similar to allele 1 but with the addition of uS7m c.256 T>C present in one clone.

Out of 20 TOPO clones tested, four different versions of *MRPS7* have been identified which might indicate the presence of four alleles in HEK293T cells. As the mutational variants shown in Figure 1B, C and D are present in only 1 clone, it possibly represents a technical issue with the *Taq* polymerase for TOPO cloning, as there is no proof-reading activity available. In all alleles, the mutation c.238 C>T is present in the second codon. BLAST analysis revealed that this substitution is most likely a natural variant (GenBank: AF077042.1). Furthermore, in all alleles, a 51 base pair (bp) insertion is present. The mutations c.318 C>T and 319T>G in exon 2 are present in all tested clones and lead to a premature stop codon (Figure 12).

Figure 13: Sequencing analysis of 18 mS27 clones by TOPO® sequencing. The mS27 coding sequence consists of 1286 bp. The start codon ATG is indicated by a light blue arrow and exons in grey. Substitutions are indicated in red, deletions in turquoise and insertions in orange. Wild type (WT) sequence of mS27 and the different mutation sequences are indicated below. A) Mutation in allele 1: mS27 c.64 A>G and c.75_76insG was present in one clone B) Mutation in allele 2: mS27 c.75_76insG was present in 17 clones C) Mutation in allele 3: mS27 c.76_88delCGGCAAGTGGTT was present in one clone. The HEK293T mS27$^{-/-}$ cell line was generated by Elena Lavdovskaia (AG Richter-Dennerlein) and further characterized.

Similar, TOPO® sequencing analysis of mS27$^{-/-}$ cells reveals mutations in three alleles, which results in a premature stop codon in exon 2 in all cases. This is caused by a 1bp insertion at c.75_76insG in allele 1 (Figure 13A) and allele 2 (Figure 13B) and the 13bp deletion at c.76_88delCGGCAAGTGGTT in allele 3 (Figure 13C).

Figure 14: Sequencing analysis of 19 mS40 knockout clones with TOPO® sequencing. The mS40 coding sequence consists of 776 bp. The start codon ATG is indicated by a light blue arrow and exons in grey. Substitutions are indicated in red and deletions in turquoise. Wild type (WT) sequence of mS40 and the different mutated sequences are indicated below. A) Mutation in allele 1: mS40 c.158 A>G; 182_185delGTGC was present in one clone B) Mutation in allele 2: mS40 c.182_185delGTGC was present in 11 clones C) Mutation in allele 3: mS40 c.339_346 CAGAAGA > GTCTTAG was present in 7 clones. The HEK293T mS40$^{-/-}$ cell line was generated by Elena Lavdovskaia (AG Richter-Dennerlein) and further characterized.

TOPO® sequencing analysis of mS40$^{-/-}$ cell reveals mutations in three alleles. Twelve clones show a four base pair deletion causing a frameshift with a subsequent premature stop codon in exon 1 (Figure 14A, B). One of these clones also reveals a substitution at c.158 A>G, which would replace the start codon for methionine with a valine (Figure 14A). As this mutation was detected only once, it might present a technical issue using *Taq* polymerase for TOPO cloning. Seven clones reveal a five bp deletion, which results in a frameshift causing a premature stop codon between exon 1 and 2 (Figure 14C).

4.1.2 Impact of uS7m, mS27 and mS40 ablation on the mitochondrial translation

To address the question how the loss of uS7m, mS27 or mS40 affects the mitochondrial translation, *de novo* synthesized mitochondrial-encoded proteins were analyzed. In uS7m$^{-/-}$ cells, most of the mitochondrial-encoded protein levels are strongly decreased (Figure 15A).

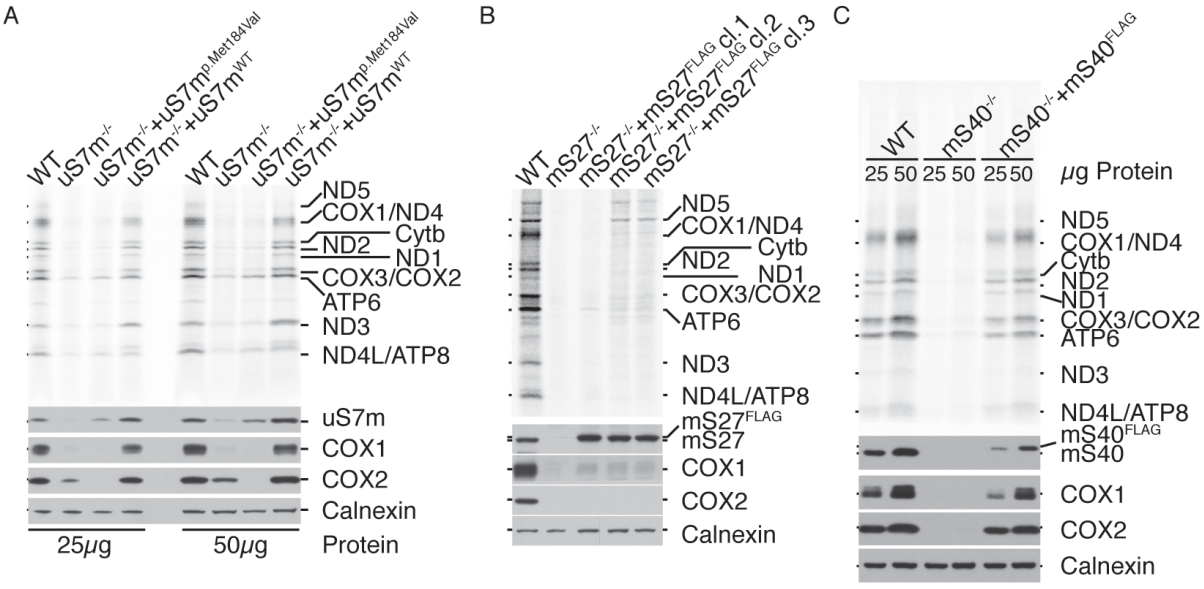

Figure 15: Loss of uS7m, mS27 and mS40 lead to a decreased mitochondrial translation. [^{35}S]-L-methionine labeling of *de novo* synthesized mitochondrial-encoded proteins in HEK293T WT, A) uS7m$^{-/-}$, uS7m$^{-/-}$ + uS7m$^{p.Met184Val}$ and uS7m rescue (uS7m$^{-/-}$ +uS7m^{WT}) cells, B) mS27$^{-/-}$ and three different mS27 rescue (mS27$^{-/-}$ + mS27^{FLAG} cl.1-3) and C) mS40$^{-/-}$ and mS40 rescue (mS40$^{-/-}$ + mS40^{FLAG}) cells was performed and radioactively labelled proteins were visualized by autoradiography. Cell extracts were also separated by SDS-PAGE and visualized by western blot. Calnexin was used as a loading control.

Especially the synthesis of the OXPHOS components ND5, ND4, ND1 (complex I), and COX1 (complex IV) are severely reduced. Interestingly, low levels of ND2, ND3 and ND4L (complex I) as well as COX3, COX2 (complex IV) are still observed in uS7m-/-. Similarly, Cytb (complex III) and ATP6, ATP8, components of complex V, are weakly detectable (Figure 15A). Detection of the uS7m protein revealed that it is weakly present in uS7m$^{-/-}$ cells, whereby TOPO® sequencing analysis showed that the resulting protein in uS7m$^{-/-}$ cells would be truncated upon translation (Figure 12). As TOPO® sequencing could detect only one mutated allele, it is possible that due to analysis limitations the other chromosomal copies of the *MRPS7* gene (locus 17q25.1) were not disclosed. However, the parental HEK293 cell line was shown to have 4 copies of chromosome 17 (Lin et al., 2014). This further suggests that the other alleles bearing mutant uS7m isoforms might be present in uS7m$^{-/-}$ cells, which results in the presence of marginal amounts of uS7m. Residual levels of the uS7m protein appears to possess a compromised stability and function since the cell line shows a strong translation defect, therefore representing a good tool to study the uS7m function within mitochondria.

To confirm that the effect observed in knockout cells is due to the loss of the uS7m and not due to an off-target effect, a rescue experiment was performed. To do so, the open reading frame encoding uS7m was inserted into the Flp-In cassette of HEK293T uS7m$^{-/-}$ cells allowing the inducible expression of uS7m. For these purposes, a non-tagged version of uS7m had to be used as a C-terminal FLAG tagged variant of uS7m is not functional. Using uS7m^{FLAG} as a bait protein for co-immunoprecipitation other MRPs were not co-purified, indicating that the FLAG tag disturbs uS7m function during ribosome assembly (Figure 16).

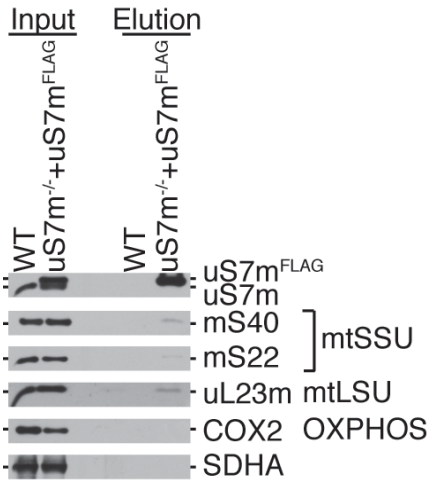

Figure 16: uS7m^{FLAG} does not assemble into mitochondrial ribosomes. Crude mitochondria (1 mg) of uS7m$^{-/-}$+uS7m^{FLAG} and wild type (WT) cells were isolated. Upon solubilization with digitonin, extracts were subjected to co-immunoprecipitation with anti-FLAG beads. Bound proteins were eluted from the anti-FLAG beads natively via FLAG-peptide and analyzed by SDS-PAGE and western blotting. Proteins belonging to the 28S mtSSU (mtSSU), the 39S mtLSU (mtLSU) and the OXPHOS subunits (OXPHOS) are indicated in brackets. SDHA was used as an experimental control. Input: 1%, Eluate: 100%.

Therefore, the untagged WT version (uS7m^{WT}) was introduced into uS7m$^{-/-}$ cells which enabled the phenotype's rescue (Figure 15A). In uS7m$^{-/-}$ + uS7m^{WT} cells, the *de novo* synthesized mtDNA-encoded protein levels were similar to WT cells. This observation confirms that the translation defect in uS7m$^{-/-}$ cells is indeed due to the loss of uS7m. western blot analysis shows furthermore that uS7m protein levels in uS7m$^{-/-}$+uS7m^{WT} cells are similar to WT cells, which is also observed for COX1 and COX2 protein levels (Figure 15A). Additionally, a cell line containing the uS7m c.550 A>G (p.Met184Val) patient mutation published by Menezes et al. (2015) was generated and analyzed upon its effect on the mitochondrial translation. Furthermore, a comparison of both uS7m$^{-/-}$ and uS7m$^{-/-}$ + uS7m$^{p.Met184Val}$ elucidates how this mutation affects the assembly pathway of the mtSSU and its sub-modules. The inducible expression of uS7m$^{p.Met184Val}$ in the uS7m$^{-/-}$ cell line is detectable by the used antibody, confirming that the cells express the uS7m patient mutation (Figure 15A). Interestingly, the expression of the uS7m$^{p.Met184Val}$ is considerably decreased compared to expression of uS7m^{WT}, although both make use of the Flp-In cassette. These results indicate that the p.Met184Val mutation leads to a destabilization of the uS7m structure, which is in agreement with the *in silico* analysis done by Menezes et al. (2015). The western blot analysis confirms further the results obtained by autoradiograph. In uS7m$^{-/-}$ cells, COX1 levels are strongly depleted, while COX2 levels are reduced by approximately

80% compared to WT. On the contrary, in uS7m$^{-/-}$ + uS7m$^{p.Met184Val}$ cells, COX1 and COX2 levels are decreased to non-detectable levels (Figure 15A). This indicates that the introduced patient mutation leads to a more severe phenotype than the depletion of uS7m.

While the mitochondrial translation was partially reduced in uS7m$^{-/-}$ and uS7m$^{-/-}$ + uS7m$^{p.Met184Val}$ cells, the loss of mS27 results in a completely abolished mitochondrial translation. None of the OXPHOS core proteins encoded by the mtDNA are detectable in the autoradiograph (Figure 15B). COX1 and COX2 protein analysis show a reduction to non-detectable levels. Furthermore, mS27 is indeed not present and therefore verifies that the introduced mutation leads to a deletion of mS27. To rescue the phenotype of mS27 ablation, a FLAG-tagged version of mS27 (mS27^{FLAG}) was introduced into mS27$^{-/-}$ cells. mS27^{FLAG} was previously used in a study by Dennerlein et al. (2010), where its functionality and ability to co-purify MRPs was confirmed. Three different mS27$^{-/-}$+mS27^{FLAG} clones were screened for this purpose (Figure 15B). The autoradiograph reveals that ATP6 levels are elevated in mS27$^{-/-}$+mS27^{FLAG} clone 1 cells in comparison to mS27$^{-/-}$ cells but are comparably weak to WT levels. In mS27$^{-/-}$ +mS27^{FLAG} clone 2 and 3 on the other hand, ND5 levels are elevated compared to mS27$^{-/-}$ cells, albeit weak in comparison to WT cells (Figure 15B). Although western blot analysis of all three clones shows higher mS27 protein levels compared to WT cells, a complete rescue of the phenotype was not possible. This is further confirmed in the western blot analysis by a weak detection of COX1 in the mS27$^{-/-}$+mS27^{FLAG} clones and the absence of detectable COX2 (Figure 15B). The inability to fully rescue the mS27 ablation phenotype might be the result of a) the strong overexpression of mS27^{FLAG} compared to endogenous mS27, b) mS27^{FLAG} can assemble in the mitochondrial ribosome, but the FLAG tag interferes with a second, yet to be identified, function or c) the observed phenotype results from an off target-effect.

Similar to mS27$^{-/-}$ the mitochondrial translation was severely affected in mS40$^{-/-}$. None *de novo* synthesized OXPHOS subunits of complex I, III, IV or V could be detected in the mS40$^{-/-}$ autoradiograph. Furthermore, using mS40$^{-/-}$ cell lysates, detection of COX1 or COX2 by using antibodies confirmed this observation, as neither was detectable. The western blot analysis confirmed further the deleterious nature of the introduced mutations in mS40$^{-/-}$ cells, which downstream leads to the absence of mS40 (Figure

15C). Rescue of the mS40$^{-/-}$ clone was done using a FLAG tagged version of mS40 (mS40^{FLAG}). This FLAG-tagged version was previously used in a study by Lavdovskaia et al. (2018), where the functionality of mS40^{FLAG} and its ability to co-purify MRPs was proven. Introduction of mS40^{FLAG} rescues the translation phenotype in mS40$^{-/-}$ (Figure 15C). *De novo* synthesized mtDNA encoded protein levels are approximately 50% lower in mS40$^{-/-}$+mS40^{FLAG} compared to WT cells. This effect is most likely due to a lower expression of mS40^{FLAG} in mS40$^{-/-}$+mS40^{FLAG} cells compared to the endogenous mS40 protein in WT cells (Figure 15C). To verify the observation, antibody detection of COX1 and COX2 showed that both proteins are expressed, albeit COX1 expression was lower compared to WT. In conclusion, the expression of mS40^{FLAG} in mS40$^{-/-}$ cells is able to rescue the phenotype. Therefore, the phenotype observed in the knockout cell line is a specific effect caused by the loss of mS40.

4.1.3 Consequences of loss of uS7m, mS27 and mS40 on mtSSU and mtLSU MRPs and assembly factors

As already shown in chapter 3.1.2, the loss of uS7m, mS27 or mS40 affect the mitochondrial translation differently. Loss of uS7m in uS7m$^{-/-}$ cells results in a partial reduction of mitochondrial translation, while ablation of mS27 or mS40 abolishes mitochondrial translation to non-detectable levels. To further elucidate how the loss of uS7m, mS27 or mS40 affects the biogenesis of the mtSSU and mtLSU, steady state analysis of different MRPs belonging to each subunit were monitored by western blotting. Furthermore, steady state protein levels of different assembly factors of the mtSSU and mtLSU were included in the analysis. According to a previous study by Bogenhagen et al. (2018), during mtSSU assembly, uS7m is present in an early sub-module with mS29 and mS35. In uS7m$^{-/-}$, protein levels of mS29 are reduced by more than 50%, while mS35 is reduced by approximately 50% compared to WT cells (Figure 17A), indicating an instability of both proteins in uS7m$^{-/-}$.

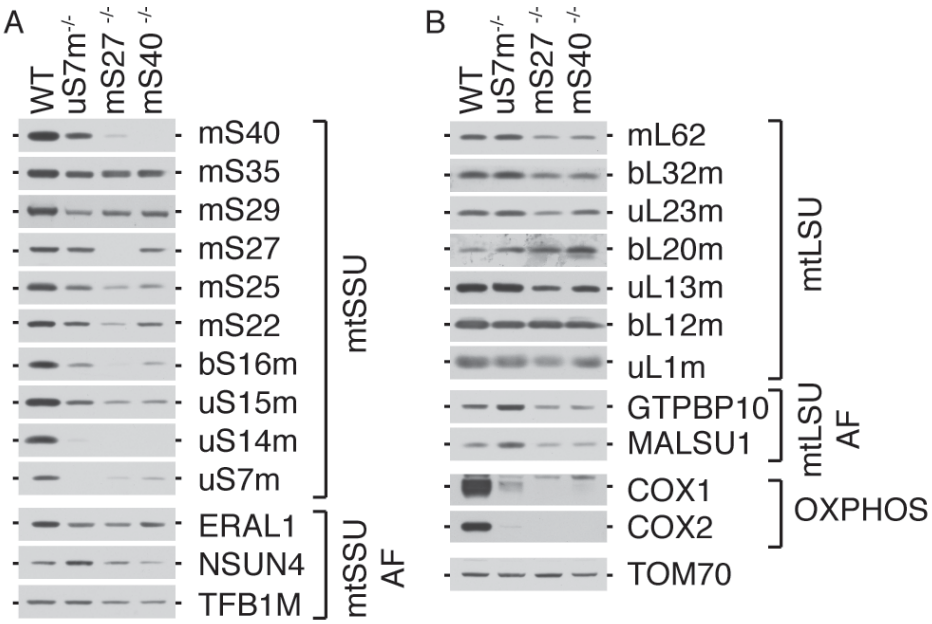

Figure 17: Steady state analysis of MRPs, assembly factors of the mtLSU and mtSSU and OXPHOS subunits. Mitochondria from HEK293T WT, uS7m$^{-/-}$, mS27$^{-/-}$ and mS40$^{-/-}$ cells were isolated and lysates analyzed by western blot. The steady state of A) the mtSSU and its assembly factors (mtSSU AF) and B) mtLSU and its assembly factors (mtLSU AF) were analyzed with the indicated antibodies. Furthermore, steady state levels of the cytochrome c oxidase OXPHOS core subunits (OXPHOS) were analyzed. TOM 70 was used as a loading control.

This suggests that mS35 and mS29 depend on the presence or function of uS7m. Similarly, the protein level of the bS16m is reduced to comparable levels to mS29 in uS7m$^{-/-}$ (Figure 17A). According to the study presented by Bogenhagen et al. (2018), bS16m assembles in a distinct early sub-module with mS22, mS27 and mS40 during mtSSU biogenesis. Interestingly, mS22 shows a reduction similar to mS29, while mS40 levels are comparable to mS35 in uS7m$^{-/-}$. Furthermore, mS27 protein levels appear unchanged in uS7m$^{-/-}$ cells (Figure 17A). This indicates that mS27 stability is independent of the loss of uS7m. In uS7m$^{-/-}$, protein levels of mS25 and uS15m are reduced by more than 50% (Figure 17A). Interestingly, uS14m protein levels are not detectable in uS7m$^{-/-}$ cells (Figure 17A). uS14m was suggested to assemble late during mtSSU biogenesis, similarly to uS15m and mS25, albeit in a different sub-module than uS15m and mS25 (Bogenhagen et al., 2018). The lack of detectable uS14m is possibly due to the overall disruption of the mtSSU assembly in the absence of uS7m, leading therefore to a fast degradation of the MRPs. Interestingly, the assembly factor of the mtSSU (mtSSU AF) ERAL1 is reduced by approximately 50% in uS7m$^{-/-}$ (Figure 17A). In contrast, NSUN4 steady state levels are increased in uS7m$^{-/-}$ while TFB1M is

unaffected (Figure 17A). Protein steady state levels of mtLSU MRPs mL62, bL32m, uL23m and bL20m, on the other hand, reveal a slight increase compared to WT cells (Figure 17B). The MRPs uL13m, bL12m and uL1m (Figure 17B) remain unchanged in uS7m-deficient cells, indicating that the mtLSU assembly is not affected by the loss of uS7m. Instead, ablation of uS7m leads to an accumulation of mtLSU complexes, which cannot join an assembled mtSSU to form the 55S ribosome. This possibility is further emphasized by analyzing the steady state protein levels of mtLSU assembly factors (mtLSU AF). Here, GTPBP10 and MALSU1 protein levels are increased in uS7m$^{-/-}$ cells similar to the elevated levels of NSUN4 (Figure 17B). Previous studies by Cámara et al. (2011) and Spåhr et al. (2012) reported that NSUN4 not only methylates the 12S mt-rRNA but also plays a role in the mtLSU biogenesis. In a complex with MTERF4, NSUN4 binds to the mtLSU, which is required for 55S ribosome formation. Inhibiting 55S monosome assembly due to the disruption of mtSSU biogenesis in uS7m$^{-/-}$ cells is thereby a potential factor that leads to an increase in NSUN4 levels.

Steady state protein levels of mS40, mS22 and bS16m, all part of the same sub-module according to Bogenhagen et al. (2018), are strongly decreased in mS27$^{-/-}$ cells. In case of mS40 and mS22, the MRPs levels are reduced by more than 90% compared to WT cells. bS16m is decreased to low levels upon loss of mS27 (Figure 17A). Interestingly, mS35, mS29 and uS7m are affected to different degrees. As already mentioned above, mS35, mS29 and uS7m are a part of one sub-module in the mtSSU assembly (Bogenhagen et al., 2018). mS35 and mS29 show a partial reduction of approximately 50% compared to WT upon loss of mS27 but appear rather stable in comparison to other MRPs of the mtSSU. uS7m on the other hand is decreased strongly (Figure 17A). As loss of mS27 potentially decreases the stability of its sub-module, mS40, mS22 and bS16m are strongly affected. In contrast, mS35, mS29 and uS7m show a decrease in their steady state levels, potentially due to the overall disruption in the mtSSU biogenesis. Analysis of mS25 and uS15m showed that both are decreased to levels similar to mS22 in mS27$^{-/-}$ cells (Figure 17A). This is possibly due to the loss of the direct interaction to the sub-module devoid of mS27. Similar to the loss of uS7m, ablation of mS27 leads to a reduction of uS14m to non-detectable levels (Figure 17A). This further supports the possibility that uS14m assembles later during mtSSU biogenesis compared to mS25 and uS15m. Analysis of mtSSU AF

revealed that upon loss of mS27, ERAL1 is decreased to similar levels as in uS7m$^{-/-}$ cells (Figure 17A). Interestingly, NSUN4 levels are not elevated in mS27$^{-/-}$ cells as in uS7m$^{-/-}$ cells. TFB1M is partially reduced in mS27$^{-/-}$ cells (Figure 17A), which might hint at the instability of the 12S mt-rRNA, the target of TFB1M. While loss of uS7m leads to a partial increase of mtLSU MRPs, in mS27$^{-/-}$ cells a partial decrease is observed. mL62, bL32m, uL23m, uL13m and uL1m are decreased upon loss of mS27. bL20m and bL12m on the other hand are unaffected (Figure 17B). Additionally, GTPBP10 and MALSU1 levels are comparable to WT (Figure 17B). These results indicate that mS27 might act earlier during mtSSU assembly in comparison to the uS7m. In turn, an early disruption of mtSSU assembly potentially affects the mtLSU assembly.

MRP levels in the same sub-module as mS40 are differently affected in mS40 deficient cells. mS22 and mS27 are reduced by approximately 50% compared to WT, whereby mS22 is not as strongly reduced in mS40$^{-/-}$ as in mS27$^{-/-}$ cells (Figure 17A). bS16m levels are reduced stronger in mS40$^{-/-}$ cells compared to uS7m$^{-/-}$ cells, but not as severe as in mS27-deficient cells (Figure 17A). In mS40-deficient cells, mS35 and mS29 show a reduction similar as in mS27$^{-/-}$, indicating that mS35 and mS29 are most likely independent of mS27 or mS40, as proposed by Bogenhagen et al. (2018). mS27 and mS40 are a part of the same sub-module and potentially act at similar time points. The presence of mS22 and bS16m in mS27$^{-/-}$ and mS40$^{-/-}$ cells indicate that the sub-module is able to form even in the absence of mS27 or mS40. (Figure 17A). The most drastic effect is observed in mS27$^{-/-}$. mS40 shows a strong reduction, which indicates that mS40 assembles downstream of mS27 (Figure 17A). Additionally, in mS40-deficient cells, mS25, uS15m and uS14m are reduced to comparable levels as in mS27$^{-/-}$ cells. These results confirm the possibility of uS14m acting at a late stage of the mtSSU assembly in comparison to the mS25 and uS15m sub-module (Figure 17A). While ERAL1 seems to be unaffected in mS40$^{-/-}$, NSUN4 and TFB1M levels are reduced in mS40$^{-/-}$ cells to similar levels as observed in mS27$^{-/-}$ cells (Figure 17A). Contrary to mS27$^{-/-}$ cells, protein levels of different mtLSU MRPs are not as strongly affected by the ablation of mS40. Upon loss of mS40, mL62 levels decrease to similar levels as observed in mS27$^{-/-}$ cells. bL32m, uL23m, bL20m, uL13m and uL1m on the other hand are not affected in mS40$^{-/-}$ cells (Figure 17B). GTPBP10 and MALSU1, on the other hand, are decreased in mS40$^{-/-}$ cells to levels comparable as in mS27$^{-/-}$ cells

(Figure 17B). This raises the question whether the disruption of the mtSSU assembly at an early stage negatively affects the mtLSU assembly. As already observed, loss of uS7m, mS27 or mS40 also leads to a loss of mitochondrial translation due to the lack of mtSSU and therefore to the inability to form the 55S monosome particle (Figure 15). Steady state protein level analysis of COX1 and COX2 emphasizes this observation due to the absence of both mitochondrial encoded cytochrome *c* oxidase subunits in mS27- and mS40-deficient cells (Figure 17B). Only in uS7m$^{-/-}$ low levels of COX1 and COX2 are still detectable.

4.1.4 Loss of uS7m, mS27 and mS40 leads to a decrease in 12S mt-rRNA, COX1 and COX2 mt-mRNA

Upon loss of uS7m, mS27 or mS40, mitochondrial translation is disrupted and steady state levels of MRPs of the mtSSU are decreased, indicating defects in the mtSSU biogenesis. As MRPs assemble together with the mtDNA-encoded 12S mt-rRNA to form a functional mtSSU, steady state RNA levels were measured by northern blotting and autoradiography.

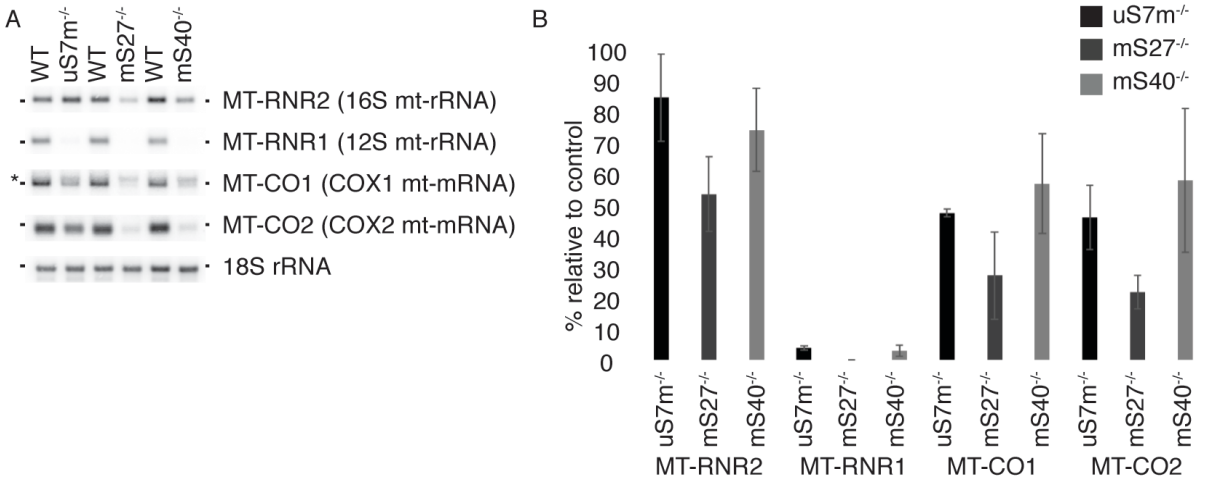

Figure 18: Loss of uS7m, mS27 or mS40 leads to loss of the 12S mt-**rRNA mtSSU core.** A) RNA was extracted from HEK293T WT, uS7m$^{-/-}$, mS27$^{-/-}$ and mS40$^{-/-}$ cell lines, separated on an agarose gel and analyzed via Northern blot. The mt-rRNA cores of the mtLSU (16S mt-rRNA), mtSSU (12S mt-rRNA) and mt-mRNA of COX1 (MT-CO1) and COX2 (MT-CO2) were radioactively labeled with [^{32}P] -γ-ATP and visualized by autoradiography. Labelling of the cytosolic ribosomal SSU 18S rRNA was used as a loading control. B) MT-RNR2, MT-RNR1, MT-CO1 and MT-CO2 were quantified using ImageJ and normalized to 18S rRNA (mean ± SEM; n = 3)

The steady state levels of the 16S mt-rRNA (*MT-RNR2*) are not affected in uS7m$^{-/-}$, while 12S mt-rRNA (*MT-RNR1*) steady state levels are decreased to non-detectable levels (Figure 18A). Quantification of the transcript levels revealed that in uS7m$^{-/-}$ the 16S mt-rRNA is decreased by approximately 10% (Figure 18B). 12S mt-rRNA levels are decreased by over 95% in uS7m$^{-/-}$ cells. mt-mRNAs encoding for COX1 (*MT-CO1*) and COX2 (*MT-CO2*) are reduced by 40% and 50% respectively compared to WT (Figure 18A, B). Thus, disruption of the mtSSU assembly by loss of uS7m leads to a decrease in mt-mRNAs. Decrease of 12S mt- rRNA is a potential result of degradation due to defects in mtSSU formation. On the other hand, 16S mt-rRNA appears stable and is in agreement with protein steady state levels of mtLSU MRPs analyzed in chapter 3.1.3. Similarly, 12S mt-rRNA is also not detectable in mS27-deficient cells. In contrast to uS7m$^{-/-}$, 16S mt-rRNA levels were reduced in mS27$^{-/-}$ by 40%. *MT-CO1* transcript levels are reduced by over 50% in mS27 and thus to a higher degree than in uS7m$^{-/-}$ cells. Furthermore, COX2 levels are reduced in mS27$^{-/-}$ cells by 80% compared to WT cells. These observations suggest that loss of mS27 not only impacts the mtSSU assembly but potentially also the mtLSU biogenesis. These results confirm the protein steady state analysis, where some mtLSU MRPs are reduced in the absence of mS27 (Figure 17B).

Similar results are observed in mS40$^{-/-}$ cells. 16S mt-rRNA levels are reduced to a higher degree upon loss of mS40 compared to uS7m$^{-/-}$ cells but to a lesser degree in comparison to a lack of mS27 (Figure 18A). Quantification analysis furthermore shows, that *MT-CO1* and *MT-CO2* levels are reduced to a similar degree in mS40$^{-/-}$ cells as observed in uS7m$^{-/-}$ cells (Figure 18B). Furthermore, 12S mt-rRNA levels are depleted to non-detectable levels as visualized in the Northern blot (Figure 18A) and seen in the quantification (Figure 18B). Different extents of 16S mt-rRNA decrease underline the possibility that upon disruption of mtSSU assembly the mtLSU is also affected.

4.1.5 Effect of loss of uS7m, mS27 and mS40 on mtSSU sub-modules

Loss of uS7m, mS27 or mS40 differentially affects the steady state protein levels of mtSSU and mtLSU MRPs as well as of the mt-RNAs. Hence, how does the ablation of uS7m, mS27 or mS40 affect mtSSU assembly and which sub-modules can still be

formed? Additionally, in this thesis, the question whether the biogenesis of the mtSSU is independent from the mtLSU is addressed. For this, mitoplasts were isolated from HEK293T WT cells, as well as uS7m$^{-/-}$, mS27$^{-/-}$ and mS40$^{-/-}$ cells and subjected to a sucrose density ultracentrifugation. Upon fractionation and precipitation of 16 fractions, the samples were analyzed by western blotting.

In uS7m$^{-/-}$ cells, the formation of the mtSSU (fraction 6 and 7) and 55S particle (fraction 11) is weakly detectable (Figure 19). However, potential sub-modules of mtSSU MRPs are still visible in the low dense fractions. Analysis of mS35 and mS29 revealed that both MRPs co-migrate in fraction two, which might reflect the early sub-module containing uS7m described by Bogenhagen et al. (2018) (Figure 19A). The absence of uS7m does not affect the sub-module assembly, resulting in the conclusion that it can be either formed independently or upstream of uS7m.

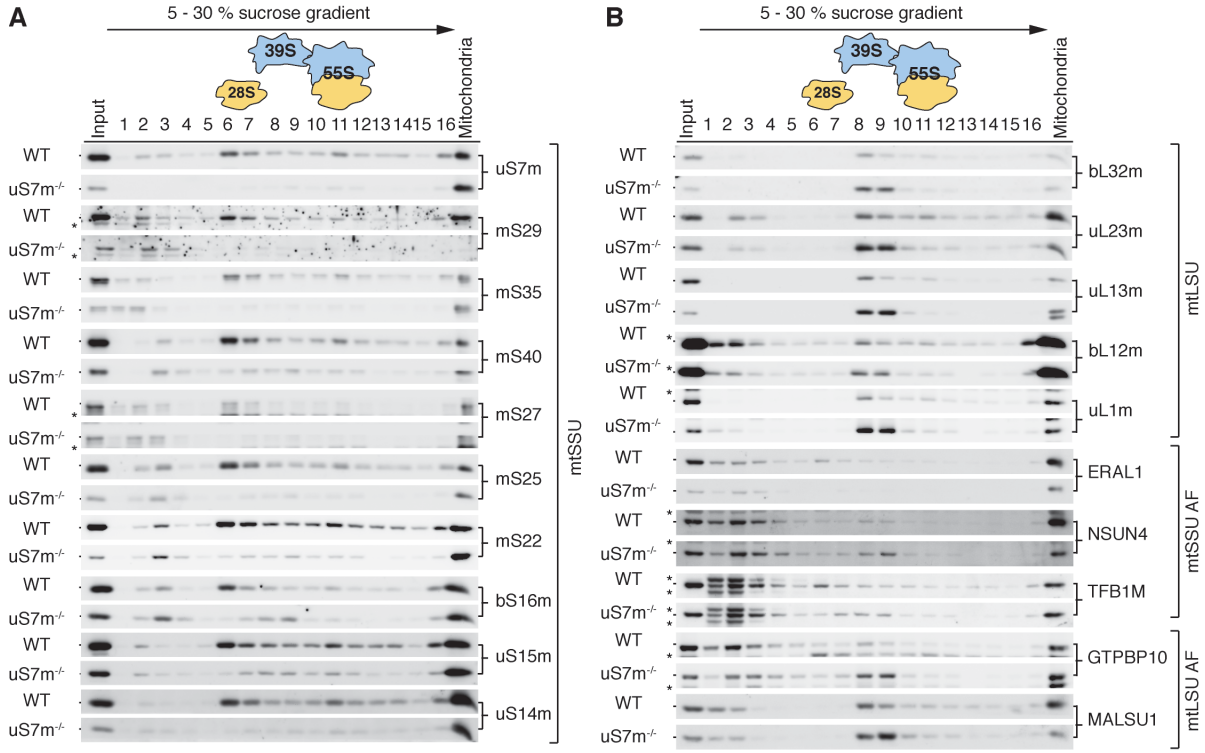

Figure 19: Ribosome complex formation in uS7m-deficient cells. Mitoplasts (0.5mg) were isolated from HEK293T WT (WT) and uS7m$^{-/-}$ cells and their lysates subjected to sucrose density ultracentrifugation. The gradients were fractionated into 16 fractions and upon precipitation analyzed via western blot. 10μg Mitochondria were used as detection control. (*) indicate unspecific signals. Input: 10%

mS40, mS27, mS22 and bS16m migrate in fractions 2, 3 and 4 in WT cells. The formation of this sub-module seems to be unaffected in uS7m$^{-/-}$ cells (Figure 19A).

Interestingly, in uS7m$^{-/-}$ cells, bS16m is also detectable in the fractions 8 and 9 corresponding to the mtLSU. In the study provided by Bogenhagen et al. (2018), bS16m was reported to form a complex with mS22. The bS16m-mS22 complex belongs to early binding proteins in the mtSSU assembly, resulting in those proteins binding to the mtSSU outer surface and away from the mtLSU interface (Bogenhagen et al., 2018). Detection of bS16m in the mtLSU fraction raises the question if, in the early stages of mtSSU biogenesis, a potential cross-talk between the mtSSU and mtLSU assembly is present, which potentially facilitates the coordination of subunits biogenesis before their joining to form the 55S. Analysis of the mS25-uS15m sub-complex show that mS25 is present in the low-density fractions 2, 3 and 4 in WT cells, the same fractions, where mS25 is predominantly present upon loss of uS7m (Figure 19a). On the other hand, uS15m is detectable in WT cells in fraction 2, where uS15m also mainly resides in uS7m$^{-/-}$ cells. Detection in the fractions 2, 3 and 4 in uS7m$^{-/-}$ are, as mentioned above, visible in mtSSU MRPs belonging to the mS40-mS27 containing sub-module. The presence of mS25 in the low-density fractions 2, 3 and 4 therefore raises the question whether mS25 takes part late in the biogenesis as proposed by Bogenhagen et al. (2018) (Figure 19A). Furthermore, uS15m is detected in the higher density fractions, indicating that uS15m, similar to bS16m, potentially plays a role in a mtSSU/mtLSU cross-talk in the mitochondrial ribosome biogenesis (Figure 19A). On the other hand, uS14m is present in the uS7m$^{-/-}$ gradient, which is in agreement with the steady state protein levels. This indicates that the assembly of uS14m strongly depends on the presence of uS7m and supports the hypothesis that uS14m assembles rather late. In fractions 8 and 9, corresponding to the mtLSU, MRPs bL32m, uL23m, uL13m, bL12m and uL1m levels are elevated in uS7m$^{-/-}$ cells compared to WT cells (Figure 19B). Thus, these data show that mtLSU particles accumulate due to defects in the mtSSU assembly. The assembly factor ERAL1 is detected in the low-density fraction 2 and 3 but not in the mtSSU fraction 6 and 7 in uS7m$^{-/-}$ cells (Figure 19B). As an RNA chaperone that protects the 12S mt-rRNA (Dennerlein et al., 2010), this result is in agreement with the Northern blot analysis, where 12S mt-rRNA is not detectable in the absence of uS7m (Figure 18A). Similarly, TFB1M is not present in the fractions corresponding to the mtSSU. Instead, TFB1M is detectable mainly in fraction 2 and 3 and in lower intensities in the higher dense fractions in uS7m$^{-/-}$ cells without a clear intensity peak in fraction 6, as observed in WT cells (Figure 19B). On the other hand,

in uS7m$^{-/-}$ cells, NSUN4 accumulated in the mtLSU fractions 8 and 9. Similarly, the mtLSU assembly factors GTPBP10 and MALSU1 accumulated in the mtLSU fractions in uS7m$^{-/-}$ (Figure 19B). This emphasizes that a strong decrease of uS7m leads to mtLSU particle accumulation due to the inability to form the 55S particle.

Analysis of mS27$^{-/-}$ reveals similar results as observed in uS7m$^{-/-}$ cells. Detection of MRPs of the uS7m containing sub-module revealed that mS35 is visibly enriched in the low-density fractions 1 and 2 (Figure 20A). Furthermore, mS29 and uS7m are present in mS27$^{-/-}$ cells in the low-density fractions 2 and 3. This emphasizes the possibility of mS35 acting early in the uS7m-containing sub-module, where mS29 and uS7m join at a later stage. Analysis of MRPs of the mS40-mS27 containing sub-module confirms the presence of this sub-module in the low-density fractions 2, 3 and 4 as shown in the detections of mS40, mS22 and bS16m (Figure 20A). Interestingly, mS25, which was supposed to be part of the same sub-module as uS15m, is predominantly present in the low-density fractions 2, 3 and 4 in mS27$^{-/-}$ cells (Figure 20A). As these results align with the observation made in uS7m$^{-/-}$ cells, this further emphasizes the possibility of mS25 being part of the mS40-mS27 containing sub-module instead of the uS15m containing sub-module.

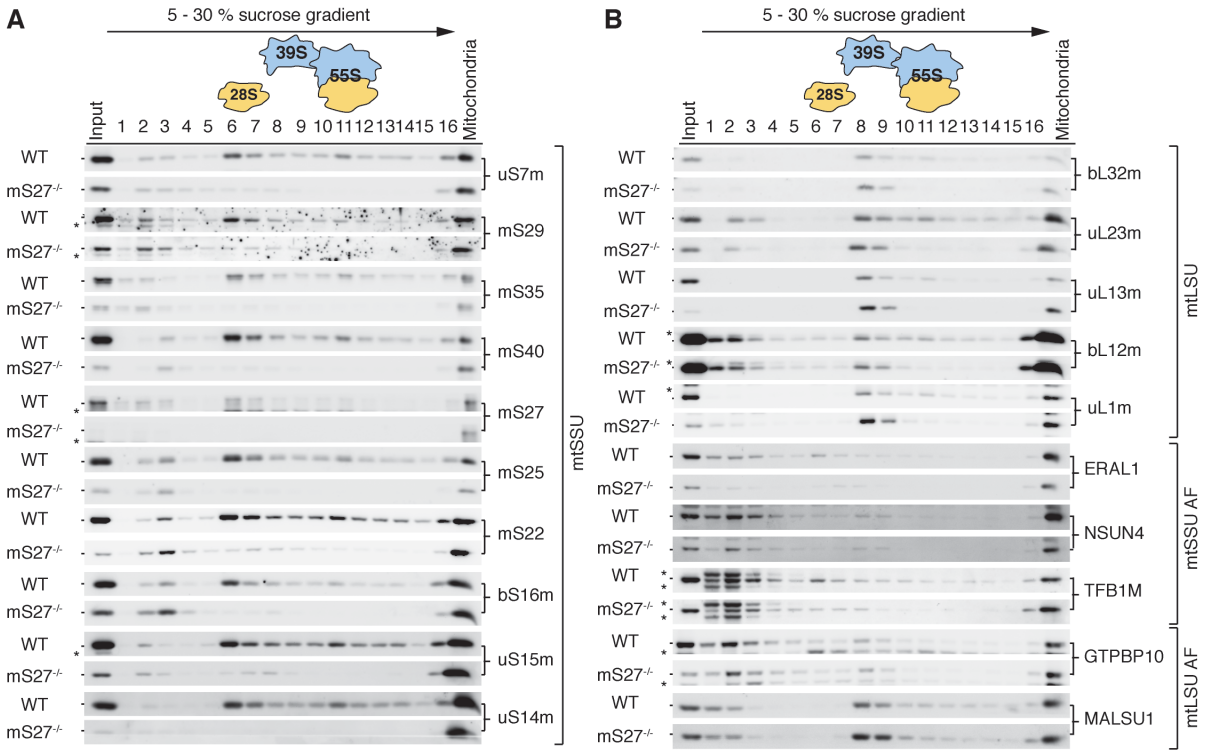

Figure 20: Ribosome complex formation in the absence of mS27. Mitoplasts (0.5mg) were isolated from HEK293T WT (WT) and mS27$^{-/-}$ cells and their lysates subjected to sucrose density ultracentrifugation. The gradients were fractionated into 16 fractions and upon precipitation analyzed via western blot. 10μg Mitochondria were used as detection control. (*) indicate unspecific signals. Input: 10%

Similarly, uS15m is visible in mS27$^{-/-}$ cells in the low-density fraction 2 and 3, and in fractions 8 and 9, however, the overall level of uS15m is strongly decreased (Figure 20B). These results hint that the late assembling uS15m sub-module is affected by the loss of mS27. Although uL13m and uL1m show a slight accumulation in the mtLSU fraction 8 in the absence of mS27 (Figure 20B), the overall protein steady state levels of uL13m, uL1m, bL32m, uL23m and bL12m reveals a decrease in mS27-deficient cells compared to WT. Therefore, these results indicate that the absence of mS27 does not stall the mtLSU assembly. As no accumulation of the late mtLSU assembly factors GTPBP10 and NSUN4 is observed in mS27-deficient cells, this result stands in contrast to the observed phenotype in uS7m$^{-/-}$. Only MALSU1 showed moderately elevated levels in the absence of mS27 (Figure 20B). Reduced 16S mt-rRNA steady state levels in mS27$^{-/-}$ cells (Figure 18) hint to an instability of the mtLSU, as uL13m, uL1m, bL32m, uL23m and bL12m are reduced in mS27-deficient cells (Figure 20A). Similarly, upon loss of mS40, MRPs of the uS7m containing sub-module is present in their respective fractions as seen in uS7m$^{-/-}$ and mS27$^{-/-}$ cells (Figure 19A and Figure 20A). mS35 is detectable in the low-density fraction 1 and 2. Similarly, mS29 is present in the low-density fractions 2 and 3, while uS7m levels are only detectable in fraction 2 and 3 (Figure 21A). Analysis of MRPs of the mS40-mS27 containing sub-module showed that in mS40$^{-/-}$ cells mS27, mS22 and bS16m are detectable in the fractions 2, 3 and 4 (Figure 21A). Although loss of mS40 leads to a decrease of mS27, mS22 and bS16m in fraction 3, the mS40-mS27 containing sub-module is able to assemble, as seen in mS27$^{-/-}$ cells. Similarly, mS25 migrates in the low-density fractions 2, 3 and 4, albeit with a weak signal in fraction 4 (Figure 21A). This emphasizes the possibility that mS25 belongs rather to the early-assembled mS40-mS27 containing sub-module instead of being recruited late together with uS15m, as reported by Bogenhagen et al. (2018).

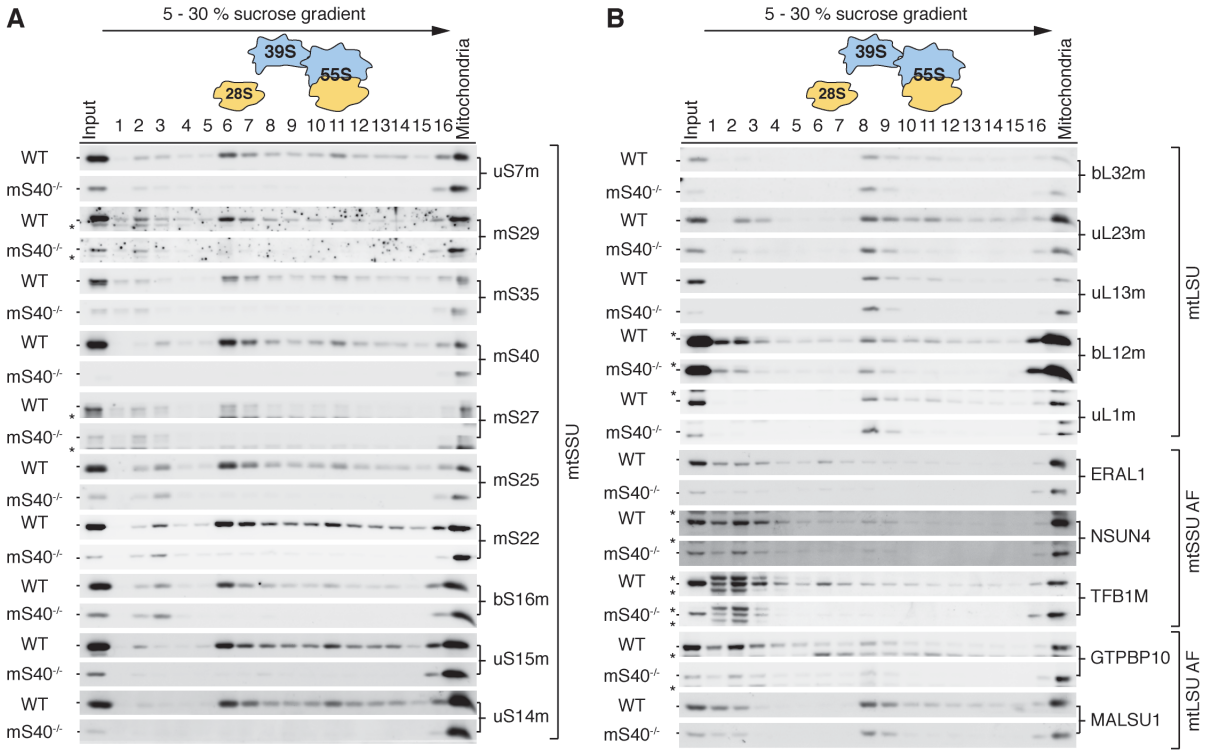

Figure 21: Ribosome complex formation in mS40-deficient cells. Mitoplasts were isolated from HEK293T WT (WT) and mS40$^{-/-}$ cells and their lysates subjected to sucrose density ultracentrifugation. The gradients were fractionated into 16 fractions and upon precipitation analyzed via western blot. 10μg Mitochondria were used as detection control. (*) indicate unspecific signals. Input: 10%

Contrary to the observation of uS15m migration in uS7m$^{-/-}$ and mS27$^{-/-}$ cells, in mS40$^{-/-}$ cells uS15m is weakly detectable, leading to the conclusion that loss of mS40 disrupts the late uS15m sub-module assembly. The mtLSU is still formed migrating in the fractions 8 and 9 and appears in mS40$^{-/-}$ cells compareable to WT (Figure 21B), indicating that the mtLSU assembly is not disrupted in the absence of mS40, although the overall protein steady state levels of mtLSU proteins are reduced (Figure 17B). Analysis of the mtSSU and mtLSU assembly factors show furthermore, that ERAL1 and TFB1M levels are reduced strongly in the absence of mS40. This observation is similar to those made in uS7m$^{-/-}$ and mS27$^{-/-}$ cells, where ERAL1 and TFB1M are also strongly decreased (Figure 19-21B). These results raise the question whether diminished levels of ERAL1 and TFB1M are a result of the 12S mt-rRNA decrease in uS7m$^{-/-}$, mS27$^{-/-}$ and mS40$^{-/-}$ cells or if the 12S mt-rRNA reduction is caused by an instability of ERAL1 and TFB1M. Contrary to uS7m$^{-/-}$ in mS40$^{-/-}$ cells an accumulation of NSUN4 in the mtLSU fractions 8 and 9 is not observed (Figure 21B). Instead, NSUN4 is strongly reduced compared to WT and showing only weak signals in the

fractions 8 and 9. As NSUN4 also facilitates the methylation of the mtSSU (Metodiev et al., 2014), it is possible that this observation correlates with the decrease of ERAL1 and TFB1M, which hints that either the strong reduction of 12S mt-rRNA leads to the instability of NSUN4 or that the instability of NSUN4 is the cause of 12S mt-rRNA reduction. In conclusion, upon early disruption of the mtSSU formation the mtLSU is also affected, while defects in later mtSSU assembly stages have a less negative impact on the mtLSU. This can also be observed upon detection of the mtLSU biogenesis factors GTPBP10 and MALSU1, which are reduced in the absence of mS40 (Figure 21B).

Comparing the individual gradients of the three knockout cell lines confirm the above-mentioned observations. As shown in the heatmap, loss of either, uS7m, mS27 or mS40 results in an accumulation of mtSSU MRPs in the low-density fractions and no mtSSU formation in the fractions 6 and 7 (Figure 22).

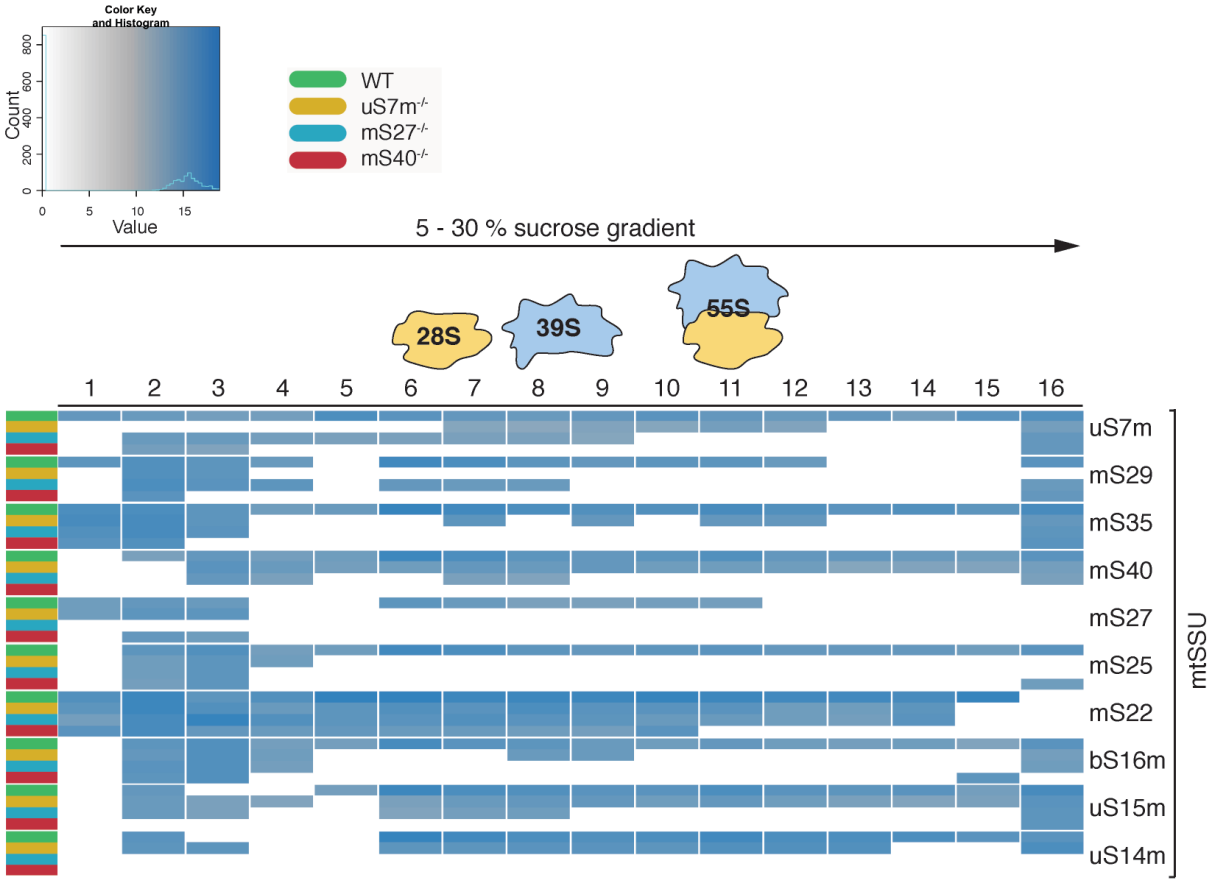

Figure 22: Comparing the ribosome assembly in HEK293T WT, uS7m-, mS27- and mS40-deficient cells by heatmap analysis. Mitoplasts were isolated from HEK293T WT (WT), uS7m$^{-/-}$, mS27$^{-/-}$ and mS40$^{-/-}$ cells and their lysates subjected to sucrose density ultracentrifugation. The gradients were fractionated into 16 fractions and analyzed via western

blot. Band intensities of the corresponding analyzed proteins of every cell line and fraction where measured using Image Quant and a heatmap generated using R studio.

Furthermore, as shown in the protein steady state analysis, mtSSU MRPs are overall reduced in the knockout cell lines compared to WT (Figure 17), which is a consequence of an impaired mtSSU biogenesis. Thereby it needs to be further elucidated whether a defective mtSSU assembly leads to degradation of mtSSU MRPs or whether the MRPs reduction is caused by a protective measure of the cell to avoid faulty mtSSU formation.

The mtLSU MRPs distribution in uS7m$^{-/-}$, mS27$^{-/-}$ and mS40$^{-/-}$ cells shows that mtLSU assembly is able to take place although the mtSSU biogenesis is disrupted (Figure 23). Compared to WT cells, in uS7m$^{-/-}$ cells, the mtLSU MRPs accumulate in the mtLSU fractions 8 and 9. A similar accumulation of mtLSU MRPs is observed in mS27-deficient cells, albeit mainly in fraction 8. In contrast, in mS40$^{-/-}$ cells, mtLSU MRPs show a weak reduction in fraction 9.

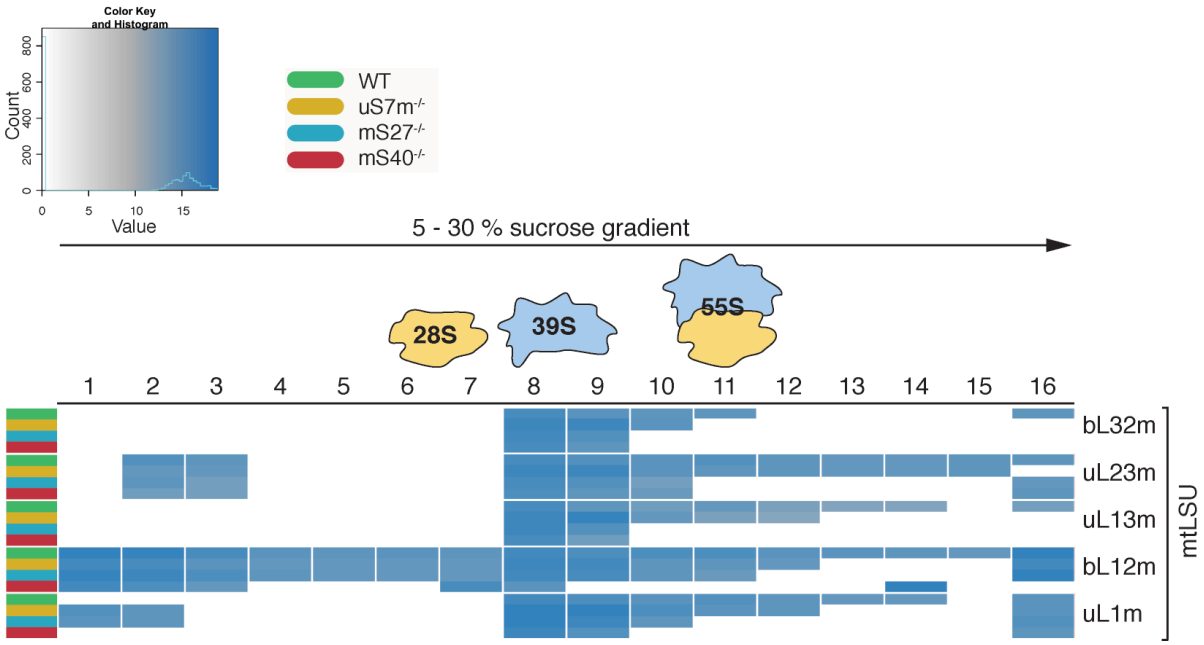

Figure 23: Absence of uS7m leads to accumulation of mtLSU MRPs. Sample preparation and heatmap generation was performed as described in Figure 22.

The absence of uS7m, mS27 or mS40 leads furthermore to a decrease of mtSSU assembly factors. In case of uS7m, NSUN4 is an exception (Figure 24). There, a clear accumulation of NSUN4 is detectable in the mtLSU fraction 8 and 9. Similarly, the mtLSU assembly factors GTPBP10 and MALSU1 accumulate strongly in uS7m$^{-/-}$ cells

(Figure 24). A similar accumulation of these biogenesis factors was observed in a recent study by Lavdovskaia et al. (2020). There, mtLSU intermediates as well as the biogenesis factors GTPBP10, MALSU1 and NSUN4 accumulate in the absence of GTPBP6 in the mtLSU fraction, which hints to a stalling of mtLSU maturation at a late stage. As a similar accumulation of the mtLSU and GTPBP10, MALSU1 and NSUN4 is observed in uS7m-deficient cells, it can be suggested that the uS7m ablation leads also to a stalling similar to the one observed in GTPBP6-deficient cells.

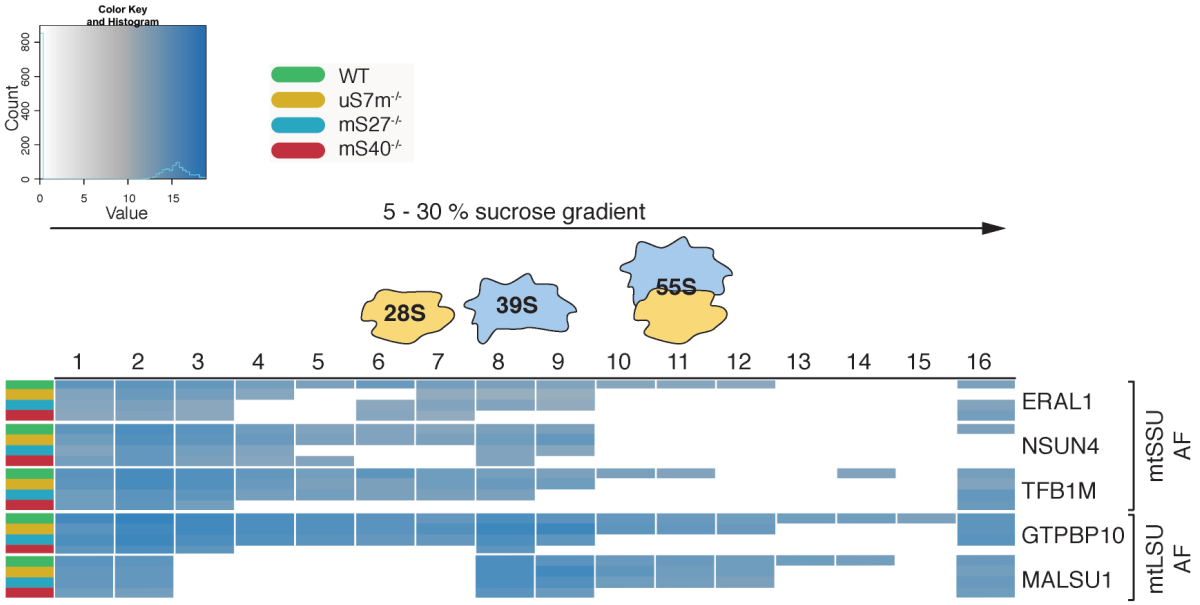

Figure 24: In uS7m$^{-/-}$ the mtLSU assembly factors (mtLSU AF) and mtSSU assembly factor (mtSSU AF) NSUN4 accumulate. Sample preparation and heatmap generation was performed as described in Figure 22.

As above mentioned in mS27- and mS40-deficient cells the mtSSU assembly factors are decreased compared to WT and no accumulation of NSUN4 in the mtLSU fractions 8 and 9 is observed as in uS7m$^{-/-}$ cells (Figure 24). In mS27$^{-/-}$ cells, monitoring GTPBP10 and MALSU1 reveals a decrease in the mtLSU fractions 8 and 9. Similarly, loss of mS40 results in a reduction of GTPBP10 and MALSU1 compared to WT, which indicates that loss of mS27 or mS40 does not accumulate late mtLSU assembly intermediates as revealed in the absence of uS7m (Figure 24).

4.1.6 The uS7m p.Met184Val patient mutation affects the mtSSU assembly

As presented in chapter 3.1.2, the loss of uS7m and the p.Met184Val patient mutation result in a partial decrease of *de novo* synthesized mitochondrial proteins. Thereby, COX2 shows a stronger reduction in uS7m$^{-/-}$+uS7m$^{p.Met184Val}$ cells compared to uS7m$^{-/-}$ cells. Upon observing these differences in the mitochondrial translation, the question arose how the mtSSU sub-modules and overall the mtSSU assembly is affected in uS7m$^{-/-}$+uS7m$^{p.Met184Val}$ cells compared to uS7m$^{-/-}$ cells. To address this question, mitoplasts of uS7m$^{-/-}$ and uS7m$^{-/-}$+uS7m$^{p.Met184Val}$ were isolated and subjected to sucrose density ultracentrifugation and individual fractions were analyzed by western blotting.

Expression of the patient mutation leads to a strong reduction of MRPs levels in mtSSU in the mtSSU fraction 6 and 7 (Figure 25A). Especially mS40, mS25, mS22 and bS16m show a drastic decrease in the low-density fractions compared to uS7m$^{-/-}$ cells. Still, detection of mS40 is possible in fraction 11 corresponding to the 55S monosome, indicating that small levels of assembled mtSSU are present in uS7m$^{-/-}$+uS7m$^{p.Met184Val}$ cells (Figure 25A). Similar to uS7m-deficient cells, expression of uS7m$^{p.Met184Val}$ leads to a decrease of uS14m to non-detectable levels, while mS35, uS15m are reduced in the low-density fractions. Interestingly, as observed by detection of mS40, mS35 and uS15m migrate in fraction 11 as well as the mutated form of uS7m. These results hint that the mutated form of uS7m assembles into the mtSSU, allowing thereby the formation of mtSSU and downstream of the 55S ribosome, although to a minor extent (Figure 25A). However, these particles might be non-functional as mitochondrial translation could not be significantly increased by expressing the mutant variant (Figure 15).

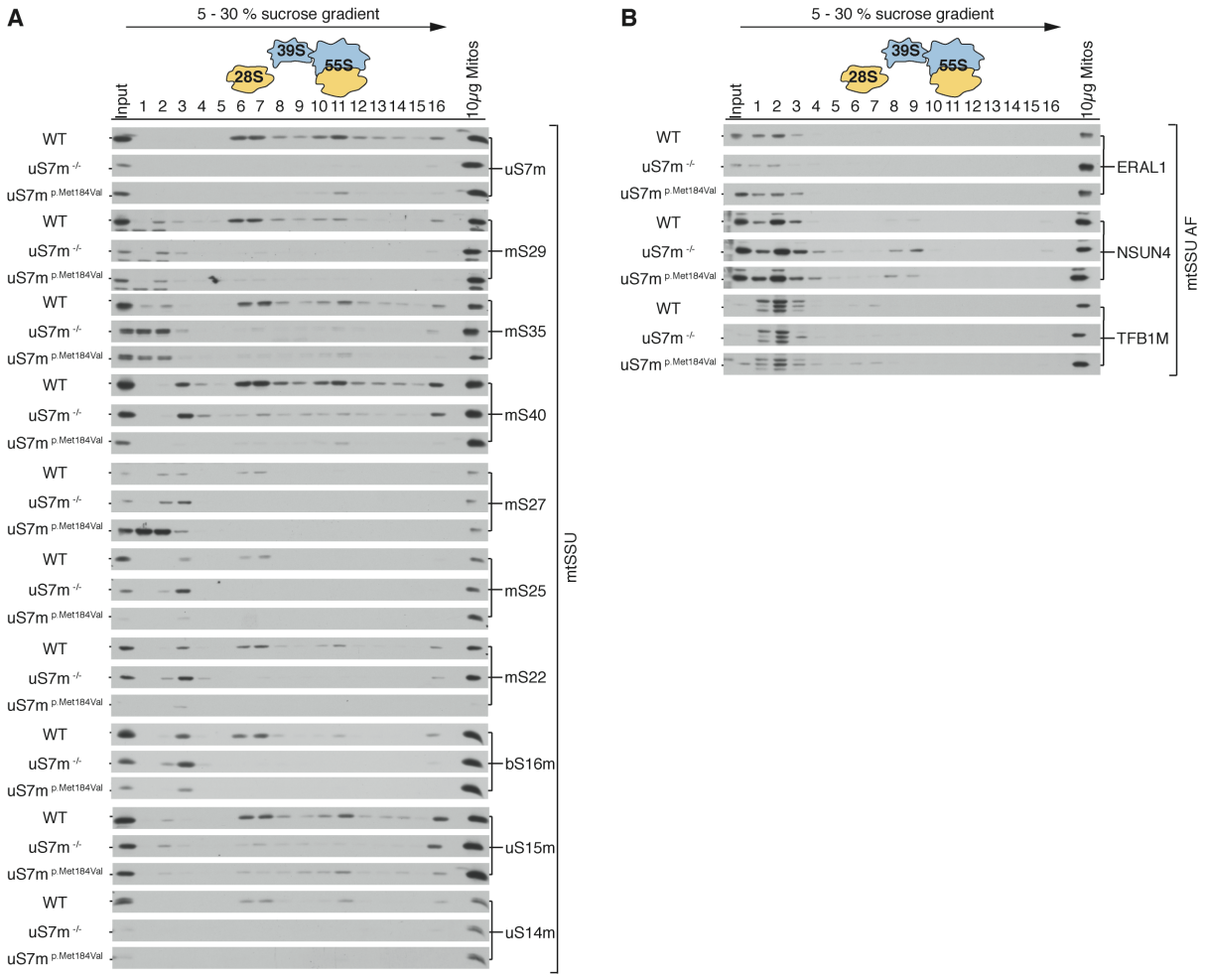

Figure 25: Comparing the ribosome assembly of uS7m$^{-/-}$ and uS7m$^{-/-}$ + uS7m$^{p.Met184Val}$ cells by sucrose density ultracentrifugation. Mitoplasts were isolated from HEK293T WT, uS7m$^{-/-}$ and uS7m$^{-/-}$+ uS7m$^{p.Met184Val}$. cells. Lysates of the mitoplasts were subjected to sucrose density ultracentrifugation. Upon fractionation of the gradient, the samples were analyzed via western blot. MRPs of the mtSSU and mtSSU assembly factors (mtSSU AF) were analyzed as indicated in brackets. Input: 10%, Fractions: 100%.

This reveals the possibility, that the patient mutation retains to a degree its structural integrity in the uS7m containing sub-module, albeit not high enough to replace the endogenous uS7m protein. Similar to uS7m$^{-/-}$ cells, mS29 migrates in the fractions 6 and 7 corresponding to the mtSSU, while mS27 strongly accumulates in the low-density fractions 1 and 2 in uS7m$^{-/-}$+uS7m$^{p.Met184Val}$ cells (Figure 25A). The large portion of free mS27 might be a result of a disrupted mtSSU formation, as the p.Met184Val mutation leads to an instability of the uS7m protein as suggested by Menezes et al. (2015) which might in turn affect negatively the mtSSU stability. Analysis of the mtSSU assembly factors revealed that upon expression of uS7m$^{p.Met184Val}$, the distribution of ERAL1 in the low-density fraction 1, 2 and 3 remained similar in HEK293T WT and uS7m$^{-/-}$+uS7m$^{p.Met184Val}$ cells (Figure 25B). Additionally, TFB1M migrates in the low-

density fractions and in the fractions 6 and 7 of uS7m$^{-/-}$+uS7m$^{p.Met184Val}$ cells, like in WT cells (Figure 25B). Interestingly, NSUN4 accumulated in the fraction 8 and 9 in uS7m$^{-/-}$+uS7m$^{p.Met184Val}$ cells, similarly to uS7m$^{-/-}$ cells, although to a minor extent (Figure 25B). Loss of uS7m leads to an increase of mtLSU MRPs in the mtLSU fraction 8 and 9 and a strong reduction of 55S particles (Figure 26A). Expression of the patient mutation also shows an increase of mtLSU MRPs in fraction 8 and reveals the formation of 55S particle in fraction 11, albeit the overall level of monosome is decreased compared to WT cells (Figure 26A). Analysis of the mtLSU assembly factors reveals similar results as observed for NSUN4 (Figure 26B). GTPBP10 accumulates in uS7m$^{-/-}$ cells predominantly in fraction 8 and 9. In comparison, in uS7m$^{-/-}$+uS7m$^{p.Met184Val}$ cells, GTPBP10 accumulates in fraction 8 but less in fraction 9 and follows more the pattern as observed in WT (Figure 26B). Similarly, MALSU1 accumulates uS7m$^{-/-}$+uS7m$^{p.Met184Val}$ cells as observed in uS7m$^{-/-}$ cells, albeit to a lesser extent (Figure 26B). These results suggest that the uS7m$^{p.Met184Val}$ mutant variant is able to assemble into the 55S ribosome, although the function of the translation machinery seems to be affected by the p.Met184Val mutation.

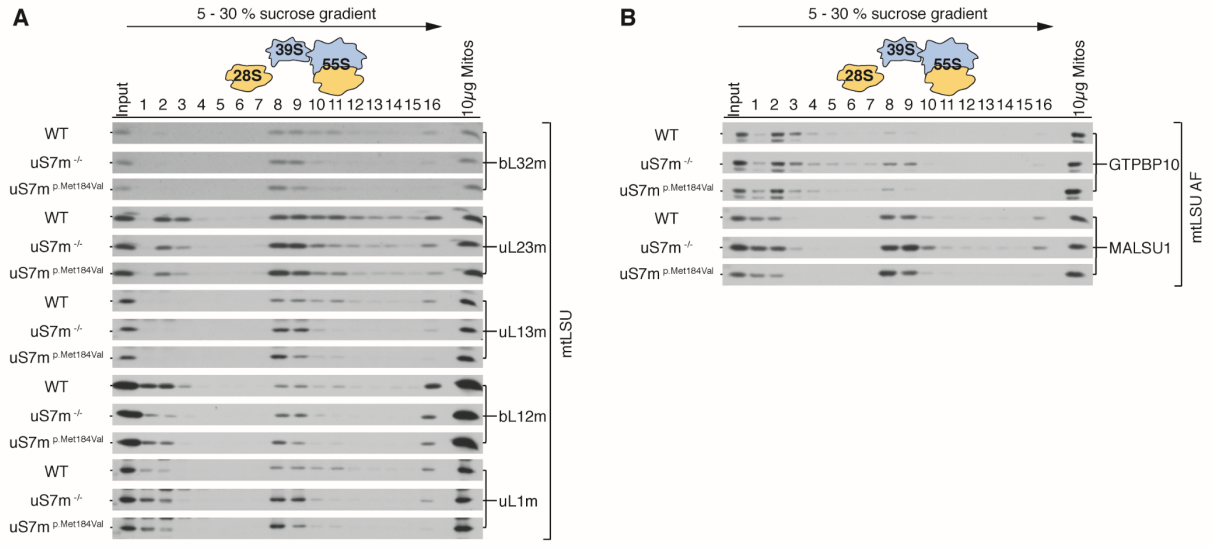

Figure 26: MRPs of the mtLSU behave similarly in uS7m-deficient and uS7m$^{p.Met184Val}$ expressing cells. Mitoplasts were isolated from HEK293T WT, uS7m$^{-/-}$ and uS7m$^{-/-}$+ uS7m$^{p.Met184Val}$ cells. Lysates of the mitoplasts were subjected to sucrose density ultracentrifugation. Upon fractionation of the gradient, the samples were analyzed by western blotting. MRPs of the mtLSU and mtLSU assembly factors (mtLSU AF) were analyzed as indicated in brackets. Input: 10%, Fractions: 100%.

Thereby, it can be concluded that the expression of the uS7m$^{p.Met184Val}$ patient mutant variant results in a severe mtSSU assembly defect similarly to the one observed in

uS7m$^{-/-}$. Only detection of mtSSU MRPs in the 55S fraction 11 indicates the formation of small amounts of mtSSU in uS7m$^{-/-}$+uS7m$^{p.Met184Val}$ cells. Thereby, the mtLSU accumulates in the mtLSU fractions 8 and 9, as only a portion forms the 55S monosome due to the low amounts of available mtSSU. As in uS7m$^{-/-}$+uS7m$^{p.Met184Val}$ cells uL23m and uL13m show weak signals in fraction 11, it can be confirmed that uS7m$^{p.Met184Val}$ is able to assembly into the 55S (Figure 26A).

4.2.1 Identification of bS16m, mS22, mS25, mS27 and mS40 protein-protein interactions

Loss of early assembled MRPs or expression of a mutation variant has severe consequences to mtSSU assembly and consequently to mitochondrial ribosomal function. The ablation of uS7m, mS27 or mS40 impairs the 28S mtSSU biogenesis as revealed by sucrose gradient ultracentrifugation while assembly intermediates that migrate in less dense fractions are still formed. The obtained results suggest that uS7m, mS29 and mS35 form the uS7m containing sub-module. Loss of uS7m leads thereby to decreased levels of mS29 and mS35, which is also observable in uS7m$^{-/-}$+uS7m$^{p.Met184Val}$ cells. Furthermore, bS16m, mS22, mS25, mS27 and mS40 form the mS40-mS27 containing sub-module. Ablation of mS40 leads to a decrease of bS16m, mS22 and mS27, while in mS27$^{-/-}$ cells, mS22 is also weakly detectable and mS40 and bS16m levels are drastically diminished. Contrary to the study of Bogenhagen et al. (2018), mS25 was suggested to be a late assembling MRP. However, in the absence of mS40, mS27 and uS7m, mS25 migrates in fraction 3, which corresponds to the mS40-mS27 containing sub-module, albeit showing reduced levels. To get further insights into the composition of these assembly intermediates stable HEK293T cell lines expressing a C-terminal FLAG-tagged variants of the MRPs bS16m, mS22, mS25, mS27 and mS40 were generated and their protein-protein interactions analyzed by co-immunoprecipitation. Analysis of bS16m^{FLAG} reveals, that aside from the FLAG-tagged version of bS16m itself, components of the mtSSU (mS40 and mS22) and the mtLSU (uL23m) are co-precipitated, indicating that bS16m^{FLAG} is functional and incorporated into the mtSSU and 55S mitochondrial ribosome (Figure 27A). Furthermore, low levels of the mtSSU assembly factors ERAL1 and TFB1M are

present, although not enriched. In contrast, NSUN4 is not detectable in bS16m^{FLAG} eluate (Figure 27A). Similarly, mtSSU MRPs mS40 and mS22 co-purify with mS25^{FLAG}, but uL23m is less enriched compared to bS16m^{FLAG} isolation (Figure 27B).

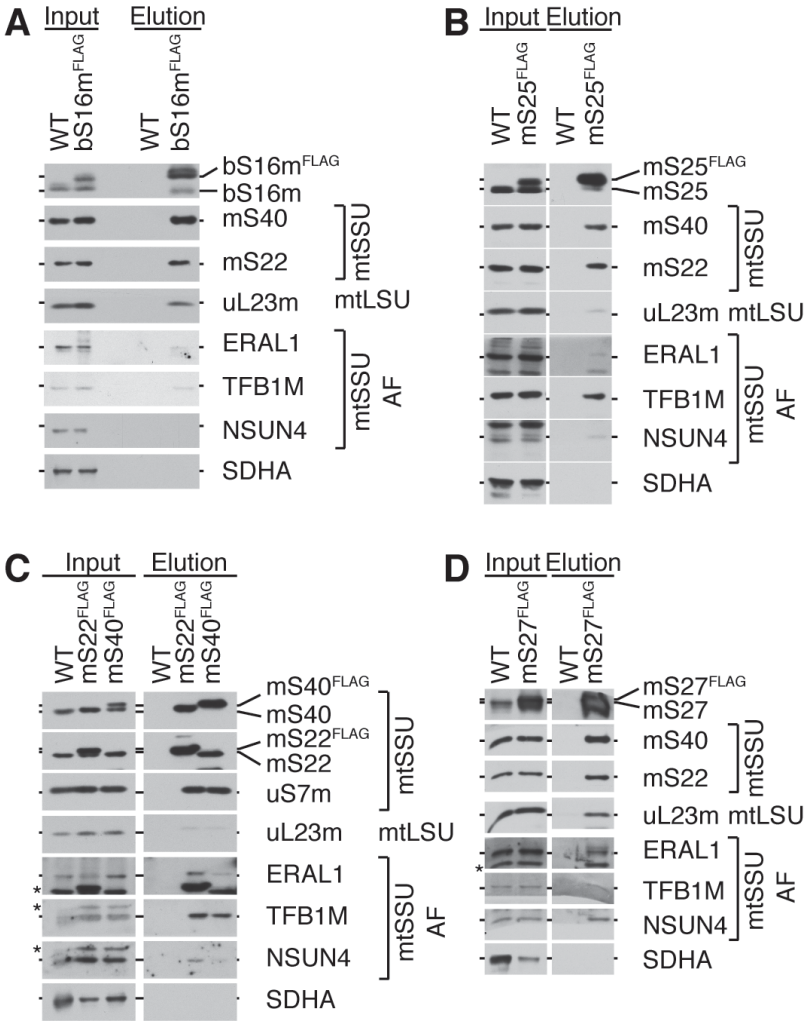

Figure 27: Co-immunoisolation of FLAG-tagged MRPs of the mtSSU. Crude mitochondria from (A) bS16m^{FLAG}, (B) mS25^{FLAG}, (C) mS22^{FLAG}, mS40^{FLAG}, (D) mS27^{FLAG} and wild type (WT) cells were isolated. Upon solubilization with digitonin, extracts were subjcted to co-immunoprecipitation. Bound proteins were eluted natively via FLAG-peptide and analyzed by SDS-PAGE and western blot ting. Proteins of the 28S mtSSU (mtSSU), the 39S mtLSU (mtLSU) and mtSSU assembly factors (mtSSU AF) are indicated in brackets. SDHA was used as a an experimental control. (*) indicate unspecific signals. Input: 1%, Eluate: 100%.

ERAL1 on the other hand is precipitated to similar levels as observed in bS16m^{FLAG} cells. Furthermore, NSUN4 is weakly detectable in mS25^{FLAG} eluates (Figure 27B). Co-immunoisolation of mS22^{FLAG} and mS40^{FLAG} cells reveals interaction with other mtSSU MRPs (mS40, mS22 and uS7m) (Figure 27C), while interaction with the mtLSU is only

feasible in low levels, similarly to the results obtained for mS25^{FLAG} cells (Figure 27B and Figure 27C). As in Lavdovskaia et al. (2018) mtLSU MRPs were co-purified to a higher degree using mS40^{FLAG}, a technical issue most likely results in low yields of mtLSU MRPs here. Detection of the mtSSU assembly factors reveals that ERAL1 is enriched in mS22^{FLAG} eluates compared to mS40^{FLAG} (Figure 27C). As reported in the study provided by Bogenhagen et al. (2018), mS22 was proposed as a secondary early binding protein without extensive RNA contacts. On the other hand, mS27 and mS29 which do have these RNA contacts were also reported to be associated with RNA chaperone ERAL1 (Dennerlein et al., 2010; Uchiumi et al., 2010). Therefore, enrichment of ERAL1 in mS22^{FLAG} is in agreement with the literature, as ERAL1 is closely associated with the mtSSU. Additionally, TFB1M is enriched in mS22^{FLAG} and mS40^{FLAG} eluates (Figure 27C), while NSUN4 is weakly detected in mS22^{FLAG} and mS40^{FLAG} eluates, albeit weakest in mS40^{FLAG}. Comparatively, mS27^{FLAG} co-immunoprecipitation with mS22, mS40 and uL23m indicate the incorporation of FLAG-tagged mS27 into the mtSSU, which forms together with the mtLSU the 55S mitochondrial ribosome (Figure 27D). These results agree with previous observations (Dennerlein et al., 2010). Additionally, mtSSU assembly factors ERAL1, TFB1M and NSUN4 are present in mS27^{FLAG} (Figure 27D).

4.2.2 mS25 is an early assembly mtSSU MRP

According to Bogenhagen et al. (2018) bS16m, mS22, mS27 and mS40 appear in an early mtSSU assembly module. uS7m was also suggested to assemble early but in a module together with mS29 and mS35. In contrast, mS25 is supposed to join the assembling mtSSU later together with uS15m. Interestingly, sucrose gradient ultracentrifugation analysis of uS7m$^{-/-}$, mS27$^{-/-}$ and mS40$^{-/-}$ reveals the migration of mS25 in the lower dense fractions 2, 3 and 4, similarly like the module containing bS16m, mS22, mS27 and mS40. The proposed late assembled MRP uS15m migrates in the low-density fraction 2. This raises the question whether mS25 assembles late with uS15m or whether it presents a rather early binding MRP joining the assembly intermediate bS16m-mS22-mS27-mS40. Furthermore, the mtSSU assembly factors ERAL1, NSUN4 and TFB1M show different interaction levels in bS16m^{FLAG}, mS22^{FLAG},

mS25^{FLAG}, mS27^{FLAG} and mS40^{FLAG} cells. This raises the question at which timepoint ERAL1, NSUN4 and TFB1M act during mtSSU assembly. To address these questions, ribosome complexes were purified by co-immunoprecipitation and separated by sucrose gradient ultracentrifugation. Obtained fractions were analyzed by western blotting or silverstaining.

Using bS16m^{FLAG} as a bait reveals the co-purification of the mtSSU and the 55S particle migrating in fraction 6/7 and 11 respectively (Figure 28A). As already observed by separating mitochondrial lysates from wild type cells via gradient centrifugation, bS16m^{FLAG} is detectable in the less dense fractions 2, 3 and 4, which is still maintained in uS7m-, mS27- and mS40-deficient cells. Also, co-purified mS22, mS25, mS27 and mS40 show a strong peak in fraction 3 presenting the early assembly intermediate (Figure 28A). This emphasizes that mS25 assembles early rather than late and belongs to the bS16m-mS22-mS27-mS40 intermediate. In contrast, uS15m is only detected in the mtSSU and 55S fractions of separated bS16m^{FLAG}-containing complexes, but not in the low-density fractions, which might agree with a proposed late assembly (Figure 28A). The mtSSU assembly factors showed that ERAL1 and TFB1M are detected predominantly in the mtSSU fraction 6 and 7 (Figure 28A).

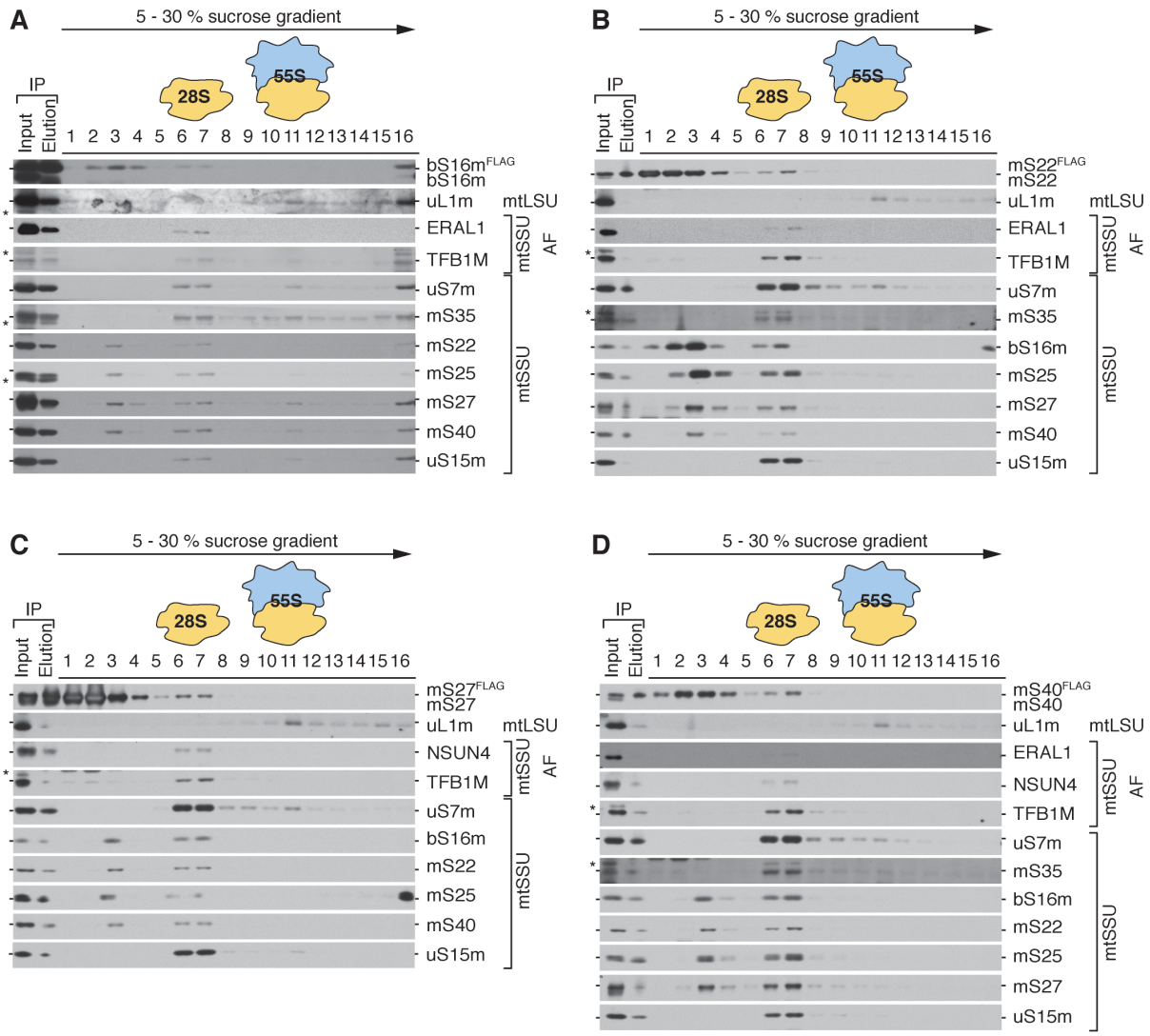

Figure 28: mS25 is part of an early assembly intermediate along with bS16m, mS22, mS27 and mS40. Eluates from the indicated immunoprecipitations bS16m^{FLAG} (A), mS22^{FLAG} (B), mS27^{FLAG} (C) and mS40^{FLAG} (D) were subjected to sucrose density ultracentrifugation and separated into 16 fractions according to their density. Fractions were analyses by SDS-PAGE and western blot. Proteins belonging to the 28S mtSSU (mtSSU), the 55S monosome (mtLSU) and mtSSU assembly factors (mtSSU AF) are indicated in brackets. (*) indicate unspecific signals. Input: 10% Eluate: 10% Fraction: 100%

Analysis of mS22^{FLAG} shows an accumulation of the MRP in the low-density fractions 1, 2, 3, 4 and 5, whereby mS22 detection in fraction 5 is the weakest (Figure 28B). As mS22^{FLAG} is overexpressed, detection of mS22 in the low-density fractions is most likely a result of free mS22 being visible in the low dense fractions. The mtLSU and mtSSU MRPs furthermore showed the possibility to co-purify the mtSSU and the 55S particle in their respective fractions 6/7 and 11. Similarly to bS16m^{FLAG}, mS22 co-purifies the early assembly intermediate containing bS16m-mS27-mS27-mS40, which mostly migrates in fraction 3 (Figure 28B), confirming previous observations that mS25

is part of the early assembled module (Figure 28A and B). Detection of the analyzed MRPs in earlier fractions might indicate the timepoint at which these MRPs are integrated in the assembly module. Interestingly, bS16m is also detectable in fraction 1 of separated mS22^{FLAG}-containing complexes, suggesting that bS16m and mS22 might interact prior to complex joining of mS27, mS25 and mS40 (Figure 28B). Similarly, as observed in bS16m^{FLAG} eluates, uS15m is not detectable besides the assembled mtSSU in fractions 6/7. These results further support the possibility of mS25 being part of the early assembled module containing bS16m-mS22-mS27-mS40, while uS15m might join later during mtSSU biogenesis. uS7m and mS35 on the other hand are only detectable in the mtSSU fraction in mS22^{FLAG}, which is in agreement with the idea that uS7m and mS35 are part of a distinct assembly intermediate.

ERAL1 and TFB1M are detectable in the mtSSU fractions 6 and 7 but not in the low-density fractions (Figure 28B). This indicates that neither ERAL1 nor TFB1M share interactions with mS22 at an early stage of the mtSSU assembly (Figure 28B).

Similar to bS16m^{FLAG} and mS22^{FLAG} analysis, using mS27^{FLAG} enabled co-purification of the mtSSU and 55S particle. Similar to mS22, mS27 is detectable in the early density fractions 1 to 5 (Figure 28C), whereby detection of mS27 in the low dense fraction is potentially a result of the overexpression, resulting in a large amount of free mS27 present in the low dense fractions. Also, under these conditions, the co-isolation of the bS16m-mS22-mS27-mS40 assembly intermediate is possible which again contains mS25 migrating mostly in fraction 3.

Consistently, uS15m is only present in fractions corresponding to the assembled mtSSU. This observation emphasizes the possibility of mS25 being a part of the intermediate containing bS16m-mS22-mS27-mS40 (Figure 28C). As uS7m is part of a distinct sub-module, it is present only in the mtSSU fractions. TFB1M and NSUN4 are only detectable in the mtSSU fraction 6/7 in mS27^{FLAG} cells, leading to the conclusion that it is unlikely that mS27 shares a direct protein-protein interaction with TFB1M or NSUN4 in the early stages of mtSSU assembly (Figure 28C).

Complex co-isolated with mS40^{FLAG} confirm previous co-immunoprecipitation analysis by the possibility of co-purifying the mtSSU and 55S particle. Consistently, the early

assembly intermediate bS16m-mS22-mS25-mS40-mS27 is present in fraction 3. mS27 and bS16m thereby migrates in the low-density fractions 2, 3 and 4, with a peak in fraction 3 (Figure 28D). Interestingly, mS22 and mS25 show signals in the fractions 3 and 4, highlighting a possibility of mS27 and mS40 interaction prior to the sub-complex formation with bS16m, mS22 and mS25. uS15m and also uS7m and mS35, both MRPs of another sub-module, only migrate in the mtSSU fractions. These observations confirm that mS25 is most likely part of the early biogenesis intermediate and does not join the mtSSU assembly late together with uS15m, as reported by Bogenhagen et al. (2018) (Figure 28D). ERAL1, TFB1M and NSUN4 revealed no further interaction with mS40 outside of the mtSSU fractions 6/7 (Figure 28D).

In summary, the separation of co-isolated ribosome complexes and assembly intermediates demonstrates that mS25 is part of the early bS16m-mS22-mS27-mS40 module and not at late assembled MRP as uS15m, as reported by Bogenhagen et al. (2018). uS7m, which was suggested to belong to a distinct earlier assembled module than the bS16m-mS22-mS25-mS27-mS40 intermediate, is only present in the mtSSU co-purified with bS16m^{FLAG}, mS22^{FLAG}, mS27^{FLAG} and mS40^{FLAG}.

As western blotting does not reveal how many protein-protein interactions are present after co-purification and sucrose gradient ultracentrifugation of mS22^{FLAG}, mS27^{FLAG} and mS40^{FLAG}, the individual fractions were also analyzed by silverstaining. This method was used to acquire an understanding if other proteins potentially interact with mS22^{FLAG}, mS27^{FLAG} or mS40^{FLAG}, especially in fractions 2 and 3, where the bS16m-mS22-mS25-mS27-mS40 intermediate is present. And indeed, silverstaining reveals that mS22^{FLAG}, mS27^{FLAG} or mS40^{FLAG} are migrating in the low dense fractions as observed in western blotting analysis (Figure 29A, B and C).

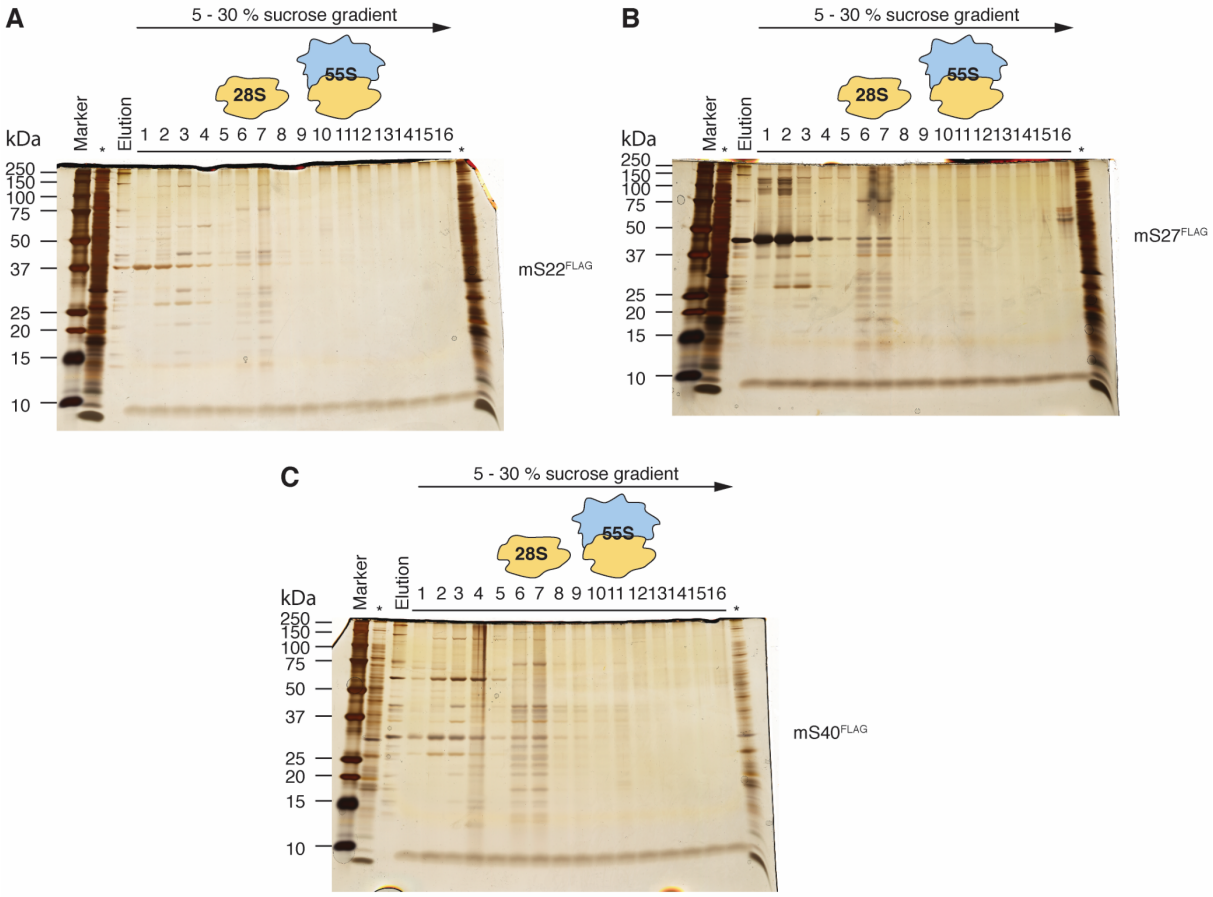

Figure 29: Initial analysis of the mS22, mS27 and mS40 interactome. Eluates from the indicated immunoprecipitations mS22^{FLAG} (A), mS27^{FLAG} (B) and mS40^{FLAG} (C) were subjected to sucrose density ultracentrifugation and separated into 16 fractions according to their density. Fractions were separated by SDS-PAGE and analyzed by silver staining. Input: 10% Eluate: 10% Fraction: 100%

Furthermore, in the bS16m-mS22-mS25-mS27-mS40 intermediate fraction 3, additional protein bands are present, and a similar result is observed in fraction 2. These results hint that other protein-protein interactions than those observed by western blotting are potentially present, which should be further analyzed to understand the full interactome of the sub-module containing bS16m, mS22, mS25, mS27 and mS40.

4.2.3 The interactome of mS40

To identify potential novel assembly factors, which might be required at early steps during mtSSU assembly, ribosome complexes were co-purified via mS40^{FLAG} and analyzed by mass spectrometry. To minimize the number of potential false positive

results, a SILAC based mass spectrometry approach was chosen. HEK293T WT and mS40^{FLAG}-expressing cells were cultured in SILAC media containing heavy or light labeled amino acids, respectively, for 10 days prior to mitochondria isolation. Equal amounts of mitochondria were mixed, lysed and subjected to FLAG-immunoprecipitation (performed by Elena Lavdovskaia, AG Richter-Dennerlein, PhD-student in GGNB program 'Molecular Biology of Cells'). Mass spectrometry analysis was done in collaboration with Prof. Dr. Henning Urlaub (MPI-BPC).

This approach confirms the co-isolation of mtSSU and 55S ribosome as e.g. uS7m, mS25, mS27, mS29, mS35, MRPs of the mtSSU and uL1m, bL13m, uL23m, mL44 and mL45, MRPs of the mtLSU are successfully co-purified with mS40^{FLAG} containing complexes. In addition, mtSSU assembly factors ERAL1, TFB1M and NSUN4 are present in the analysis. Furthermore, three potential candidates are identified, which might be involved in the ribosome biogenesis or function: 1.) 5'-nucleotidase domain-containing protein 2 (NT5DC2), 2.) the Polymerase delta-interacting protein 2 (POLDIP2) and 3.) von Willebrand factor A domain-containing protein 8 (VWA8). NT5DC2 was identified by genome-wide association studies and it was reported to be able to bind to tyrosine hydroxylase (Nakashima et al., 2019; 2020). It was suggested, that NT5DC2 may be a member of the haloacid dehalogenase-type phosphatases. NT5DC2 was additionally implicated to play a role in neuropsychiatric disorders and tumor prognoses (Chen et al., 2020; Guo et al., 2019; Jin et al., 2020; Li et al., 2020; Nakashima et al., 2020; Prados et al., 2015; van Hulzen et al., 2017). POLDIP2 (PDIP38, Mitogenin-1), is suggested to be a regulatory protein in DNA damage response and mitochondrial morphology (Arakaki et al., 2006; Tissier et al., 2010). Furthermore, POLDIP2 was detected in different cellular compartments depending on cell type and presence or absence of DNA damage; it was suggested to bind to a wide range of DNA polymerase families (Liu et al., 2003; Tissier et al., 2010). In mitochondria, POLDIP2 was reported to localize in the matrix. It was proposed that POLDIP2 plays a role in fusion and fission together with mitochondrial single-stranded DNA-binding protein (mtSSB) (Arakaki et al., 2006). Furthermore, POLDIP2 was proposed to be a transient component of the mitochondrial nucleoids (Cheng et al., 2005; Sykora et al., 2017). VWA8 is expressed in a long isoform and a shorter splice variant in mice, termed VWA8^{A} and VWA8^{B}. Structural analysis revealed a similarity to

dynein motor protein. Furthermore, Walker A and B motifs, both part of a AAA+ ATPase domain, facilitate the ATPase activity. Additionally, VWA8 was proposed to localize to the mitochondrial matrix and peroxisomes (Luo et al., 2020; 2017). VWA8 was implicated in both, neurological and oncological pathologies in humans, whereby the overall function of the protein remains to be elucidated (Anney et al., 2010; Marcucci et al., 2014; Oedegaard et al., 2010; Yuan et al., 2018). Similar to VWA8, the function of NT5DC2 and POLDIP2 in mitochondria remains unclear.

Since NT5DC2, POLDIP2 and VWA8^{B} were previously identified as mitochondrial proteins, VWA8^{B} and POLDIP2 FLAG-tagged cells were generated to identify potential ribosomal proteins as interaction partners. In an effort to verify that the FLAG-tagged versions of POLDIP2 and VWA8^{B} behave similarly to the endogenous proteins, the mitochondrial localization and protein topology of these proteins and endogenous NT5DC2 were investigated by protease protection assays. NT5DC2, POLDIP2^{FLAG} and VWA8$^{B\ FLAG}$ display resistance to externally added proteinase K in mitochondria, whereas the outer membrane protein MFN2, as well as VWA8^{A}, are degraded. Upon osmotic shock, the inter membrane space proteins become accessible to protease digestion. Under these conditions, the epitopes of NT5DC2, POLDIP2 and VWA8^{B} remain intact, suggesting that they are localized in the mitochondrial matrix, as well as the MRP mS40 (Figure 30A). In contrast, TIM23 is degraded, indicating that the epitope recognized by the antibody is exposed to the inter mitochondrial inner membrane space. These results confirm previous observations and show that NT5DC2, POLDIP2 and VWA8^{B} localize to the mitochondrial matrix.

Co-purification analysis of the complexes containing either POLDIP2^{FLAG} or VWA8$^{B\ FLAG}$ however shows that components of the mtSSU such as mS40 and mS27 could not be identified in the eluates (Figure 30B). This finding suggests either i) the C-terminal FLAG-tag inhibits the function of VWA8^{B} and POLDIP2 and therefore co-purification of other MRPs is not possible or ii) the pool of POLDIP2 and VWA8^{B} interacting with mS40 is meager or transient, resulting in the inability to detect mS40 by western blotting.

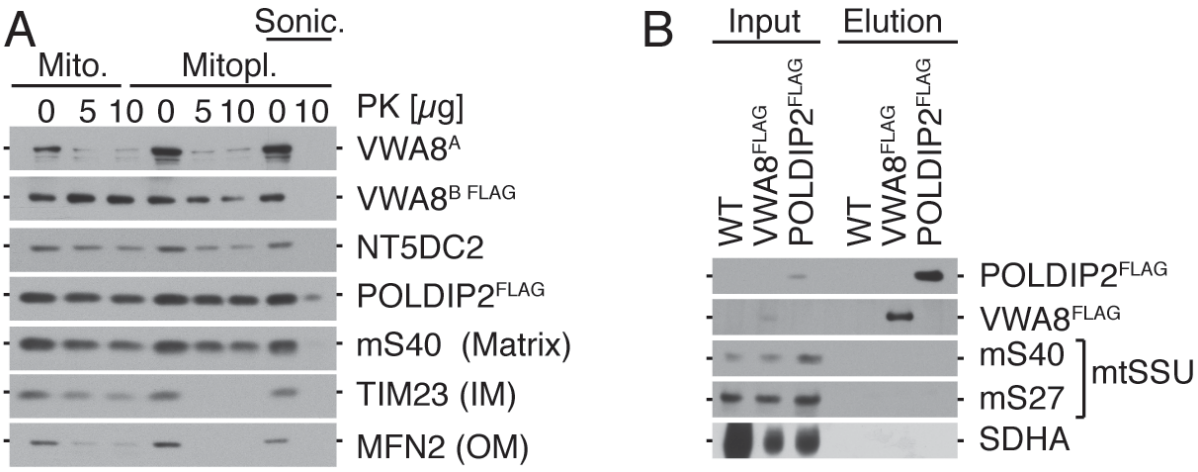

Figure 30 NT5DC2, POLDIP2 and VWA8^{B} localize in the in the mitochondrial matrix. A) Intact mitochondria (Mito.), Mitoplasts (Mito.) and sonicated mitoplasts (Sonic.) from POLDIP2^{FLAG} and VWA8$^{B\ FLAG}$ cells were treated with proteinase K (PK) as indicated. MFN2, TIM23 and mS40 were used as markers of the outer membrane (OM); inner membrane (IM) and the matrix compartments respectively. B) Crude mitochondria of POLDIP2^{FLAG} and VWA8$^{B\ FLAG}$ were isolated and upon solubilization with digitonin, subjcted to co-immunoprecipitation. Bound proteins were eluted natively via FLAG-peptide and analyzed by SDS-PAGE and western blotting. Proteins of the 28S mtSSU (mS40 and mS27) are indicated in brackets. SDHA was used as a an experimental control. (*) indicate unspecific signals. Input: 1%, Eluate: 100%.

To define the function of NT5DC2 and POLDIP2, knockout cell lines were generated by utilizing the CRISPR/Cas9 technology (Lavdovskaia et al., 2020; Ran et al., 2013). Screening of potential knockout cells lead to the use of NT5DC2$^{-/-}$ clone D2 II (Figure 31A) and POLDIP2$^{-/-}$ clones B8II and H8II (Figure 31A, B). Interestingly, the POLDIP2 knockout clones behaved similarly in culture as HEK293T WT cells, with no apparent growth defect observable. On the other hand, NT5DC2$^{-/-}$ clone D2 II appears to grow marginally slower compared to WT.

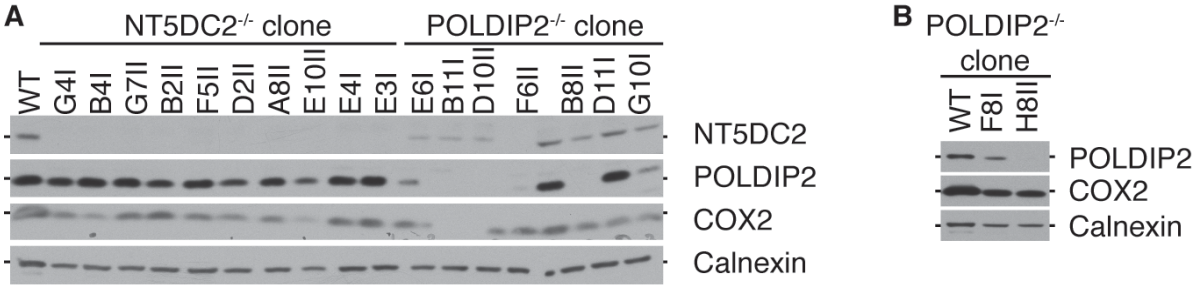

Figure 31: Screening of different CRISPR/Cas9 generated knockout clones for further characterizations. Cell lysates of different A) NT5DC2$^{-/-}$ and A/B) POLDIP2$^{-/-}$ clones were separated via SDS-PAGE and analyzed by western blotting. COX2 detection was used to determine the knockout effect. Lysates of HEK293T WT served as control. SDHA was used as a loading control. Cell lines were generated by Emely Steube (AG Richter-Dennerlein).

The confirmed mitochondrial localization of NT5DC2 and POLDIP2 and the described phenotype observed in NT5DC2- and POLDIP2-deficient cells, led to the analysis of *de novo* synthesized mitochondrial encoded proteins in NT5DC2$^{-/-}$ and POLDIP2$^{-/-}$ cells. To study the translation of mitochondrial encoded proteins, NT5DC2$^{-/-}$ cells were cultured in glucose and galactose-containing media. Glucose is being used to produce pyruvate through the anaerobic glycolytic metabolic pathway and yields 2 ATP molecules. On the other hand, using galactose as the substrate results in a slower kinetic for the glycolysis. This forces the cells to rely more on the OXPHOS machinery to produce ATP (Reitzer et al., 1979; Rossignol et al., 2004). Cells growing in galactose media are more prone to low viability rates, since they become more sensitive to mitochondrial deficiencies. Growing cells in galactose and glucose therefore serves as a method to study mitochondrial dysfunctions, whose deficiency is not clearly seen in glucose media (Aguer et al., 2011; Arroyo et al., 2016). Comparing the rate of *de novo* synthesized proteins in HEK293T WT and NT5DC2$^{-/-}$ cells reveals that the mitochondrial translation is reduced in NT5DC2-deficient cells. However, protein steady state analysis shows that core proteins of the mitochondrial cytochrome *c* oxidase remain stable (Figure 32A). On the contrary, *de novo* synthesized proteins in POLDIP2-deficient cells show that the mitochondrial translation remained unaffected, although POLDIP2 protein levels are clearly not detectable (Figure 32B).

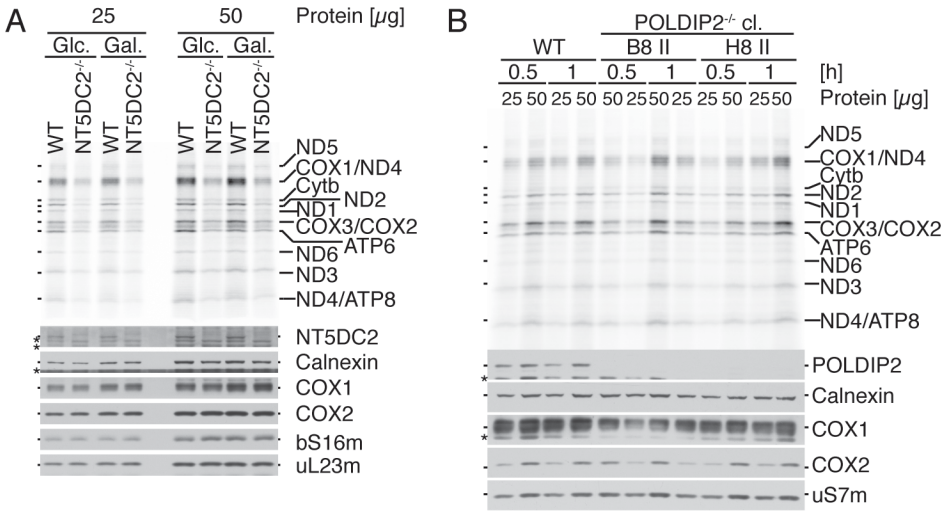

Figure 32: NT5DC2 ablation leads to reduced mtDNA encoded protein translation. [^{35}S]-L-methionine labelling of de novo synthesized mitochondrial encoded proteins was performed in A) HEK293T WT and NT5DC2$^{-/-}$ cultured in glucose (Glc) or galactose (Gal) containing media and B) POLDIP2 deficient cells. Radioactively labelled proteins were visualized by autoradiography. Cell extracts were separated by SDS-PAGE and visualized by western blot. (*) indicates unspecific signals.

4.2.4 NT5DC2 potentially interacts with the mitochondrial ribosome

NT5DC2, POLDIP2 and VWA8^{B} were detected in mS40^{FLAG} co-purified complexes by mass spectrometry. Using mtSSU-deficient cells, their potential role during mitochondrial ribosome biogenesis was investigated. The aim was thereby to understand whether they are affected by the loss of the mtSSU. First, steady state protein levels of NT5DC2, POLDIP2 and VWA8^{B} were monitored by western blotting in uS7m$^{-/-}$, mS27$^{-/-}$ and mS40$^{-/-}$ cells compared to HEK293T WT. Second, distribution of NT5DC2, POLDIP2 and VWA8^{B} were analyzed by sucrose gradient ultracentrifugation in uS7m-, mS27- and mS40-deficient cells.

Upon loss of uS7m, steady protein levels of NT5DC2, POLDIP2 and VWA8^{B} appeared similar to WT (Figure 33A). In contrast, loss of mS27 and mS40 leads to a decrease of NT5DC2 to non-detectable levels. Furthermore, POLDIP2 levels showed a decrease in mS27-deficient cells compared to WT. On the other hand, VWA8^{B} appears unaffected by the loss of mS27 (Figure 33A). This indicates, NT5DC2 is unstable upon disturbing early assembly steps of the mtSSU involving the bS16m-mS22-mS27-mS40 intermediate but remains unaffected in uS7m-deficient cells. The stability of NT5DC2 in uS7m$^{-/-}$ is most likely a result of a reduced but still present mitochondrial translation, as weak amounts of uS7m are detectable in uS7m$^{-/-}$, while in mS27- and mS40-deficient cells the mitochondrial translation is abolished. Interestingly, loss of mS40 does not affect the POLDIP2 and VWA8^{B} stability negatively (Figure 33A).

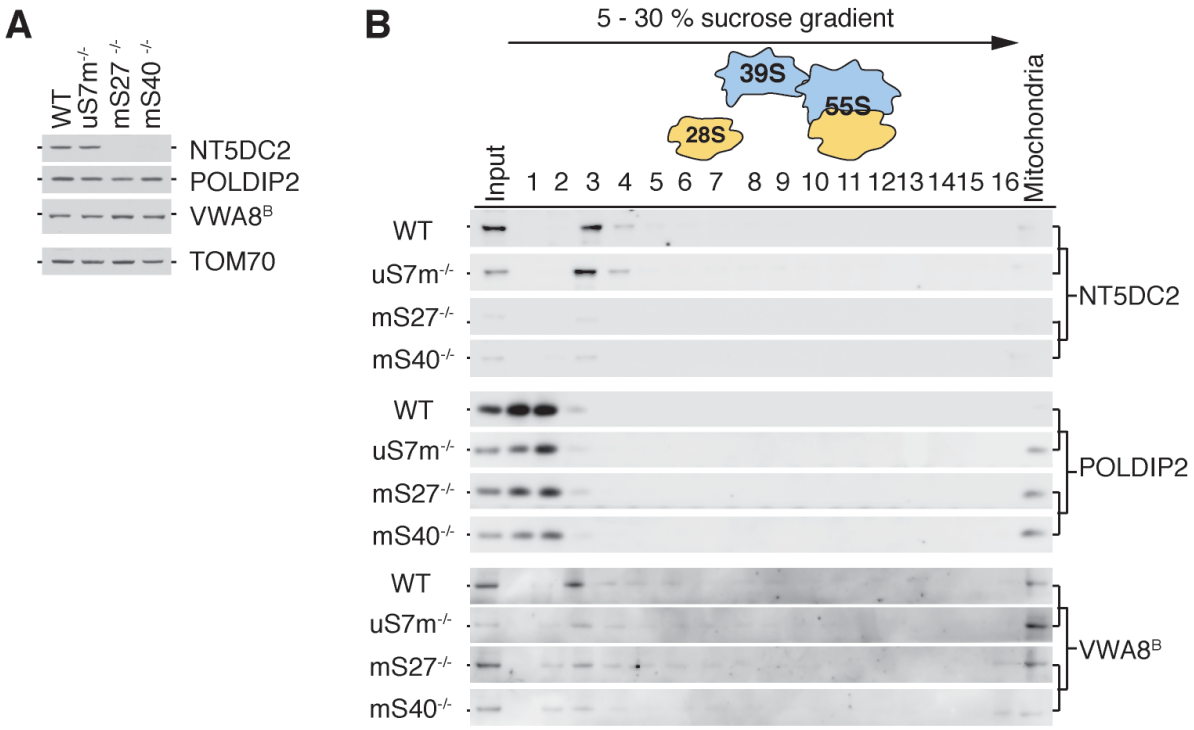

Figure 33: In mtSSU deficient cells, NT5DC2 is decreased to non-detectable levels. A) Mitochondria from HEK293T WT (WT), uS7m$^{-/-}$, mS27$^{-/-}$ and mS40$^{-/-}$ cells were isolated and their lysates (20μg) were analyzed by western blotting. The steady state protein levels of the putative assembly factors were monitored by the indicated antibodies. TOM 70 was used as a loading control. B-D) Mitoplasts were isolated from HEK293T WT, B) uS7m$^{-/-}$, C) mS27$^{-/-}$ and D) mS40$^{-/-}$ cells and their lysates subjected to sucrose density ultracentrifugation. The gradients were fractionated into 16 fractions and upon precipitation analyzed by western blot. 10μg Mitochondria were used as detection control. Input: 10% Fraction: 100%

The distribution of the putative assembly factors shows that NT5DC2 levels and migration are similar in WT and uS7m$^{-/-}$ cells. Interestingly, NT5DC2 is detectable in the fractions 3 and 4, where the bS16m-mS22-mS25-mS27-mS40 intermediate migrates consistent with the potential interaction of NT5DC2 with mS40-containing complexes, as detected by mass spectrometry (Figure 33B). On the other hand, POLDIP2 mainly migrates in the low-density fractions 1 to 3 (Figure 33B), suggesting that it potentially acts early in the mtSSU assembly. In WT cells, VWA8^{B} migrates in the low-density fractions 2 to 5 as also observed in uS7m-deficient cells (Figure 33B).

Loss of mS27 shows an overall decrease of NT5DC2 to a weakly detectable signal in fraction 3, as similarly observed in the steady state protein analysis (Figure 33B). This observation emphasizes the possibility that NT5DC2 might depend on the bS16m-mS22-mS25-mS27-mS40 intermediate. Thereby the interaction of NT5DC2 with the bS16m-mS22-mS25-mS27-mS40 intermediate is disrupted in mS27$^{-/-}$ cells as loss of

mS27 leads also to a reduction of bS16m, mS22, mS25 and mS40 levels (chapter 3.1.3). Similar to WT and uS7m-deficient cells, POLDIP2 migrates in mS27$^{-/-}$ cells in the low-density fractions 1 to 3, while VWA8^{B} is present in the fractions 2 to 5 (Figure 33B).

As observed in mS27$^{-/-}$, loss of mS40 leads to a decrease of NT5DC2 and only a weak signal present in fraction 3 (Figure 33B). This observation emphasizes that NT5DC2 depends on the bS16m-mS22-mS25-mS27-mS40 intermediate to facilitate its stability. Thereby it needs to be further elucidated whether its stability is solely depended on the bS16m-mS22-mS25-mS27-mS40 intermediate and therefore the mtSSU or on the presence of the mitochondrial ribosome. Similar to the results obtained by detection of POLDIP2 and VWA8^{B} in WT and uS7m- and mS27-deficient cells, in the absence of mS40, POLDIP2 migrates in the low dense fractions 1 to 3 and VWA8^{B} in the fractions 2 to 5. It is thereby consistent that VWA8^{B} is detectable in fraction 3 in all knockout cell lines as well as in the WT cell line, hinting that VWA8^{B} might play a role in the mtSSU biogenesis. On the contrary, as POLDIP2 remains stable in uS7m-, mS27- or mS40-deficient cells and is present in the less dense fraction 1, 2 and 3, indicating that the main portion of POLDIP2 is present in the form of a free pool. It needs therefore to be further elucidated whether POLDIP2 and VWA8^{B} aid the assembly of the mtSSU and with which direct interaction partners they facilitate their function.

In addition, the distribution of NT5DC2, POLDIP2 and VWA8^{B} in sucrose gradient fractions of uS7m$^{-/-}$+uS7m$^{p.Met184Val}$ cells was analyzed in comparison with WT and uS7m$^{-/-}$ cells.

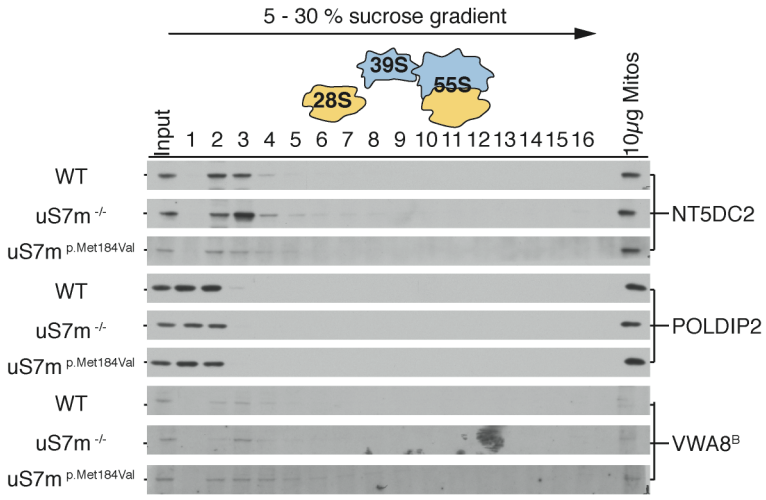

Figure 34: Expression of the patient mutation uS7m$^{p.Met184Val}$ affects NT5DC2. Mitoplasts were isolated from HEK293T WT, uS7m$^{-/-}$ and uS7m^{PM} cells. Lysates (500 μg) were subjected to sucrose density ultracentrifugation. Isolated fractions were analyzed by western blotting. Input: 10%, Fractions: 100%.

In uS7m$^{-/-}$+uS7m$^{p.Met184Val}$ cells, NT5DC2 shows a stronger decrease compared to uS7m$^{-/-}$ cells (Figure 34). Interestingly, mS40 is strongly decreased in uS7m$^{p.Met184Val}$-expressing cells (Figure 25A), which might be the reason for the reduced NT5DC2 levels. This emphasizes that mS40 or its assembly intermediate might affect NT5DC2. On the contrary, POLDIP2 and VWA8^{B} migrated in uS7m$^{-/-}$+uS7m$^{p.Met184Val}$ cells similarly as in mS27- and mS40-deficient cells, without being further affected (Figure 34). In conclusion, NT5DC2 was identified as a potential interactor of mtSSU, which depends on mS40 or its assembly intermediate, as in mS40-deficient cells, NT5DC2 is weakly detectable in the bS16m-mS22-mS25-mS27 intermediate fraction 3. Furthermore, in uS7m$^{p.Met184Val}$-expressing and mS27-deficient cells mS40 is strongly reduced, while NT5DC2 also showed a strong reduction. On the contrary, in uS7m-deficient cells, NT5DC2 was unaffected, which is most likely a result of mS40 still present to a higher degree compared to mS27-deficient cells. As these results suggest that NT5DC2 interacts with the mtSSU either with mS40 or its assembly intermediate, further investigations are required to address its direct interaction partner as well as its overall function in the mitochondrial ribosome biogenesis.

5. Discussion

CryoEM studies of the mammalian mitochondrial ribosome revealed over the years detailed structures (Amunts et al., 2015; Greber et al., 2015). They pointed out the differences from its bacterial counterpart, raising the question of how the assembly pathways potentially differ. Furthermore, key proteins taking part in the mitochondrial ribosome biogenesis could be identified over the years (Dennerlein et al., 2010; Lavdovskaia et al., 2018; 2020; Maiti et al., 2018; Metodiev et al., 2009; 2014; Rorbach et al., 2012), whereby it is suggested that yet unidentified factors play a role in the assembly pathway. Therefore, the differences between the mitochondrial and bacterial ribosome assembly and the mechanism by which the mitochondrial ribosome biogenesis is facilitated need to be further examined. As more studies reveal that mutations in MRPs encoding genes lead to diseases in humans, it becomes even more critical.

A recent study on the kinetics of mitochondrial ribosome biogenesis revealed the first model to address this question. Using SILAC and cryoEM, most MRPs could be identified in sub-modules (Bogenhagen et al., 2018). Additionally, in this model, the sub-modules and the respective MRPs could be assigned to early-, intermediate- and late-binding MRPs. However, as this study shows initial drafts of the mitochondrial ribosome assembly kinetics, it is crucial to elaborate this model further. Consequently, understanding how disease-associated MRP mutations affect the mitochondrial ribosome biogenesis may add further insight into the assembly pathway.

Therefore, this study focuses on the mtSSU assembly emphasizing how the mtSSU biogenesis is affected in the absence of the early assembling MRPs uS7m, mS27, or mS40. Thereby uS7m is in a distinct sub-module compared to mS27 and mS40, which reside in the same sub-module (Bogenhagen et al., 2018). Additionally, the effects of the patient mutation uS7m$^{p.Met184Val}$ on the mtSSU assembly is compared to the substantial reduction of uS7m. Thereby cross-connections between the mtLSU and mtSSU assembly are observed in this study and closely investigated.

5.1 The ablation of uS7m, mS27 or mS40 does not affect the assembly of their respective sub-modules

According to Bogenhagen et al. (2018), the mitochondrial ribosome biogenesis follows a modular pathway, where early-, intermediate- and late-assembling MRPs of distinct sub-modules form the mtSSU or mtLSU, which then join to form the ribosome (Bogenhagen et al., 2018). Since this study's primary focus is the mtSSU biogenesis, the early assembling sub-modules containing uS7m, mS27, or mS40 were closely analyzed. Bogenhagen et al. (2018) suggested that the early assembling MRPs bS16m and mS22 form a complex which is subsequently joined by uS5m, mS27, mS34 and mS40 to form a sub-module. Similarly, the early appearing MRPs mS35 and mS29 are joined by uS7m, mS31 and mS39 to form a distinct sub-module. It remains elusive when the sub-module joins the 12S mt-rRNA for further assembly (Figure 35A). Eventually, late assembling sub-modules, like the uS15m-containing or uS14m-containing sub-modules, appear in the mtSSU biogenesis to form the mature mtSSU.

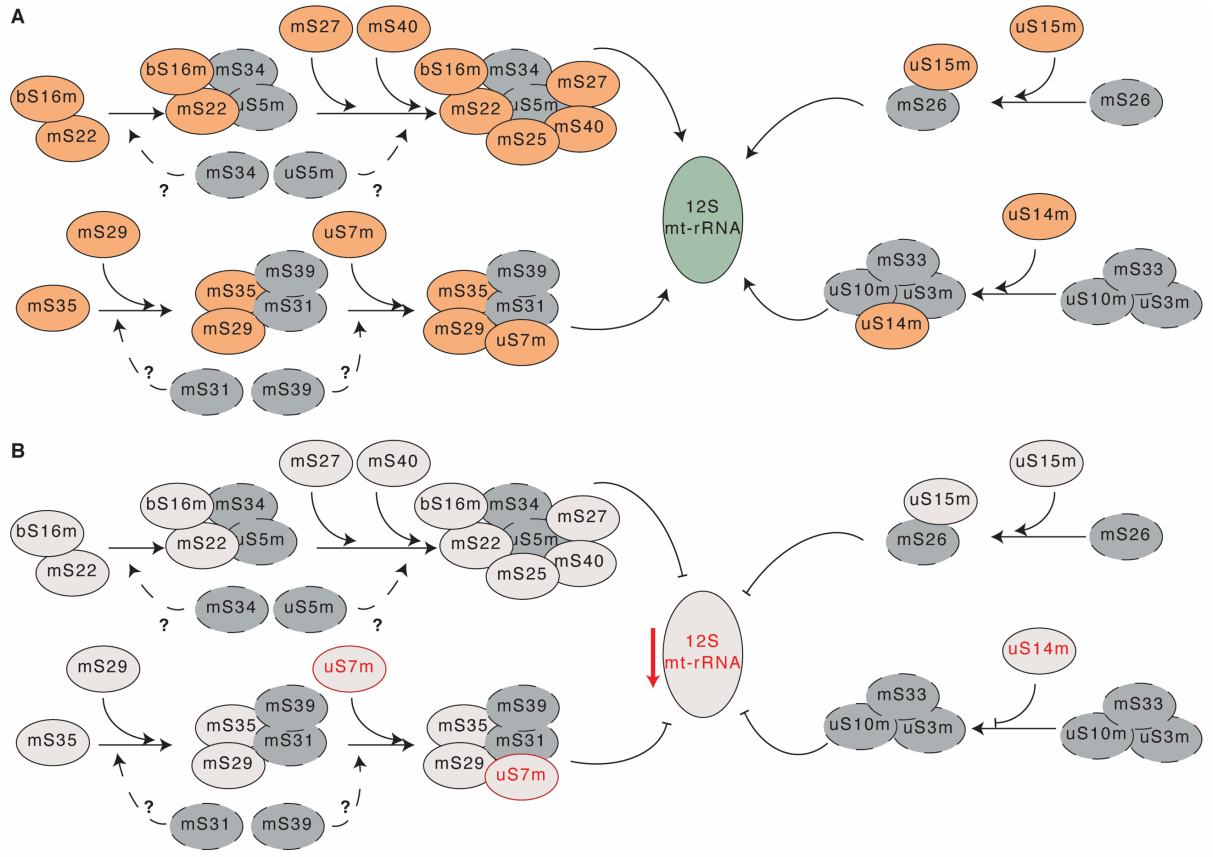

Figure 35: Ablation of uS7m does not affect its respective sub-module formation. A) mtSSU MRPs analyzed in this work (orange) assemble in their sub-modules together with other MRPs not analyzed in this study (dark grey). At a certain stage during mtSSU biogenesis

they bind to the 12S mt-rRNA and form the mtSSU with other sub-modules (here not shown). B) Drastic decrease to nearly undetectable levels (red font) of uS7m (red outline) leads to an overall decrease (grey) of mtSSU MRPs and the 12S mt-rRNA (red bold arrow). Marginal amounts of uS7m are able to be incorporated into the mtSSU, similar to the unaffected early-binding sub-module containing bS16m, mS22, mS25, mS27 and mS40 and late-binding sub-modules containing uS15m, mS25 and mS26 (red arrow). Assembly of the uS7m, mS29, mS35 as well as the aforementioned early and late sub-modules are not affected by the loss of uS7m. uS14m is decreased to undetectable levels in uS7m-deficient cells and ins therefore unable to incorporate in its respective sub-module.

In this study, depletion of uS7m does not affect the biogenesis of its respective sub-module. Instead, the analyzed MRPs mS35 and mS29 can assemble, while mature mtSSU particles are marginally detectable by western blotting (Figure 35B). This results from the uS7m ablation leading to a substantial depletion of the 12S mt-rRNA and reduction of mtSSU MRPs. Importantly, as marginally detectable levels of uS7m are still present in uS7m$^{-/-}$ cells, a small population of mature mtSSU is present (Figure 35B). This is confirmed by a mild phenotype observed by monitoring the mitochondrial translation, as OXPHOS core subunit levels are decreased but still present. This phenotype is similar to the bS16m p.Arg111* phenotype studied by Miller et al. (2004) and Haque et al. (2008). In that study, patients carrying the bS16m p.Arg111* mutation showed a drastic decrease of bS16m levels and a substantial depletion but still present mitochondrial translation (Emdadul Haque et al., 2008; Miller et al., 2004). As residual levels of uS7m are detectable in uS7m-deficient cells, it is possible that, as similarly observed by Haque et al. (2008), low levels of mature mtSSU are assembling, thus, leading to a decrease of the mitochondrial translation instead of complete depletion. Interestingly, the drastic depletion of uS7m leads to a strong diminishing of uS14m levels compared to other tested mtSSU MRPs and a strong increase of NSUN4 (Figure 35B).

In agreement with the observation in uS7m-deficient cells, depletion of either mS27 or mS40 does not inhibit the formation of their respective sub-module, indicating that sub-modules can form although a single MRP is missing. This suggests that alternative pathways for the modular assembly of the mtSSU might be present in human mitochondria, similar to the observations in bacteria (Davis et al., 2016; Mulder et al., 2010; Sykes and Williamson, 2009). Bogenhagen et al. (2018) suggested that bS16m and mS22 are early assembling MRPs of this distinct sub-module, which agrees with the data obtained in this study, as the absence of neither mS27 nor mS40 inhibits the

formation of the bS16m-mS22 intermediate (Figure 36A, B). In contrast to uS7m$^{-/-}$, in mS27- and mS40-deficient cells, mature mtSSUs are not formed. Consistently, *in vivo* labeling of mS27$^{-/-}$ and mS40$^{-/-}$ cells show the abolishing of mitochondrial translation. Additionally, RNA steady state levels reveal a drastic decrease of 12S mt-rRNA in uS7m$^{-/-}$ and mS40$^{-/-}$, whereby loss of mS27 results in undetectable 12S mt-rRNA levels. This might be a result of the 12S mt-rRNA stability being negatively affected by the ablation of uS7m, mS27 and mS40.

Interestingly, uS14m is undetectable in mS27$^{-/-}$ and mS40$^{-/-}$ cells but still present in uS7m$^{-/-}$ cells, although to reduced levels. Bogenhagen et al. (2018) suggested that uS14m acts late during mtSSU biogenesis. Thus, particularly late-binding MRPs might be strongly affected if the mtSSU assembly is disturbed at early steps (Figure 36A, B).

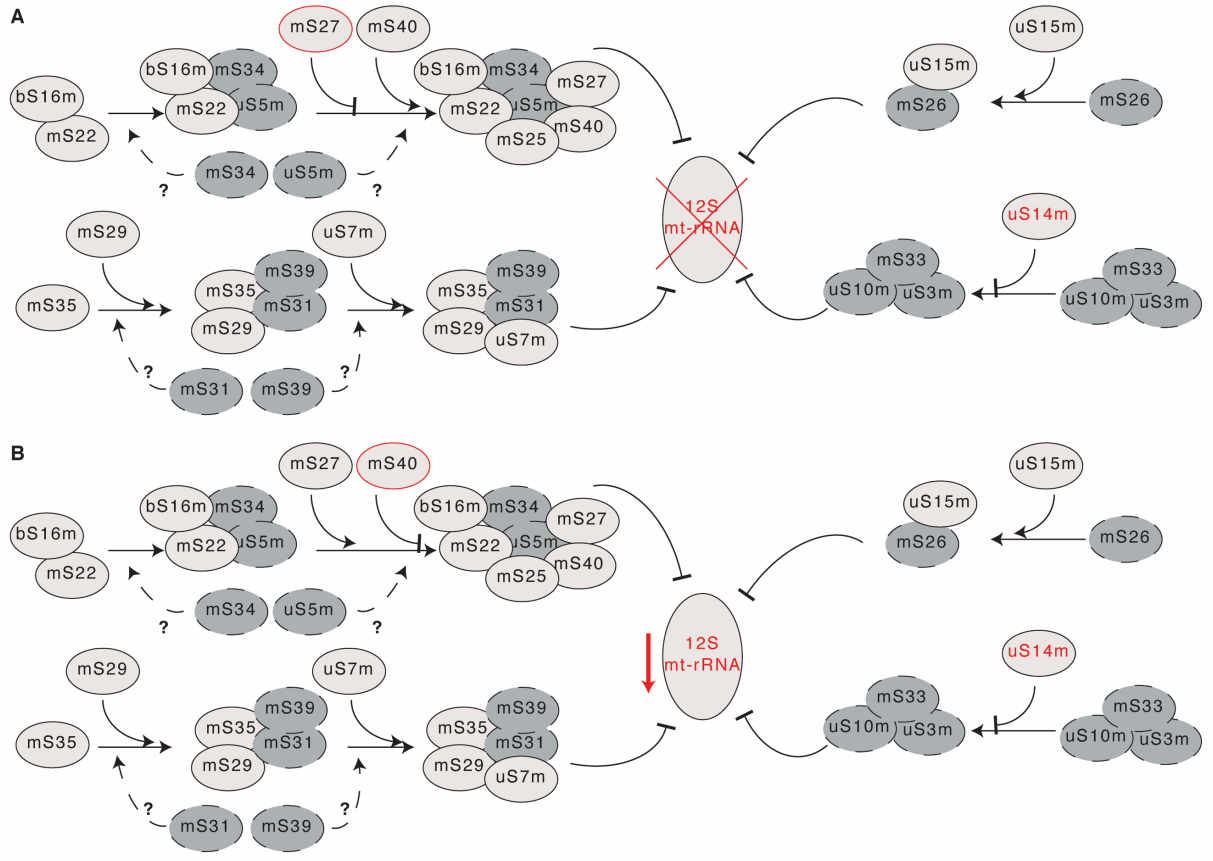

Figure 36: The absence of mS27 and mS40 impacts the mtSSU biogenesis strongly. Analyzed but reduced MRPs are in light grey and in this work not analyzed MRPs are in dark grey with dashed outlined. A) In mS27-deficient cells (red outline), the bS16m-mS22 intermediate can form and is subsequently joined by mS4. uS5m and mS34 potentially join the assembly at an unknown stage (dashed arrows and question mark). Similarly, the late-appearing uS15m containing sub-module assembles. Whether the uS14m containing sub-module can form remains to be further elucidated, as uS14m is decreased to non-detectable levels (red). 12S mt-rRNA levels are undetectable in mS27-deficient cells (red cross), leaving

no possibility for mtSSU formation. B) Ablation of mS40 (red outline) does not inhibit the formation of its respective sub-module. Loss of mS40 leads to a drastic reduction of uS14m to undetectable levels. uS15m is strongly reduced (red arrow) in the absence of mS40 but capable of assembling in its respective sub-module. 12S mt-rRNA levels are drastically depleted in mS40-deficient cells, implying that the mtSSU biogenesis is strongly inhibited.

In agreement, steady-state protein levels of uS15m are strongly decreased in mS27$^{-/-}$ and mS40$^{-/-}$ cells. A drastic decrease of uS15m as observed in mS27- and mS40-deficient cells was similarly observed by Pulman et al. (2018), where the bS1m p.Lys119Arg mutation caused the diminishing of uS15m. Aside from uS15m, early assembling MRPs remained stable (Pulman et al., 2019). As not only depletion of the early assembling MRPs mS27 and mS40 (this study) but also bS1m (Pulman et al., 2019) leads to a reduction of uS15m, it can be suggested that uS15m appears late in the mtSSU assembly as proposed by Bogenhagen et al. (2018) (Figure 36A, B). Thereby uS15m stability seems to be dependent on the presence of early-binding MRPs. Interestingly, as in mS40-deficient cells, the MRPs bS16m, mS22 and mS27 can form the sub-module, mS40 might be incorporated at a later stage or, as aforementioned, follows an alternative pathway in the absence of mS40.

In summary, as the mtSSU assembly is disrupted at an early stage in uS7m-, mS27- or mS40-deficient cells, a decrease of late-binding MRPs of the mtSSU is observed, whereby the formation of early intermediates of mtSSU biogenesis is not affected.

5.2 uS7m ablation stalls mtLSU assembly at a late stage of maturation

Although the kinetic study of Bogenhagen et al. (2018) revealed a model showing sub-module connections during the respective mtSSU and mtLSU formation, it remained unclear if a cross-dependency during the mtSSU and mtLSU assembly is present. This aspect is investigated in this study closely in uS7m-deficient cells. In this schematic overview, early and late assembling sub-modules form and joined at a particular stage the 12S mt-rRNA to complete the mature mtSSU in WT. Thereby, the mtSSU biogenesis factor NSUN4 joins in methylating the C841 of the 12S mt-rRNA, albeit it remains elusive whether NSUN4 performs the m^{5}C-methylation of C841 at the naked 12S rRNA or at a later stage where sub-modules are already bound to the 12S mt-rRNA (Figure 37) (Metodiev et al., 2014).

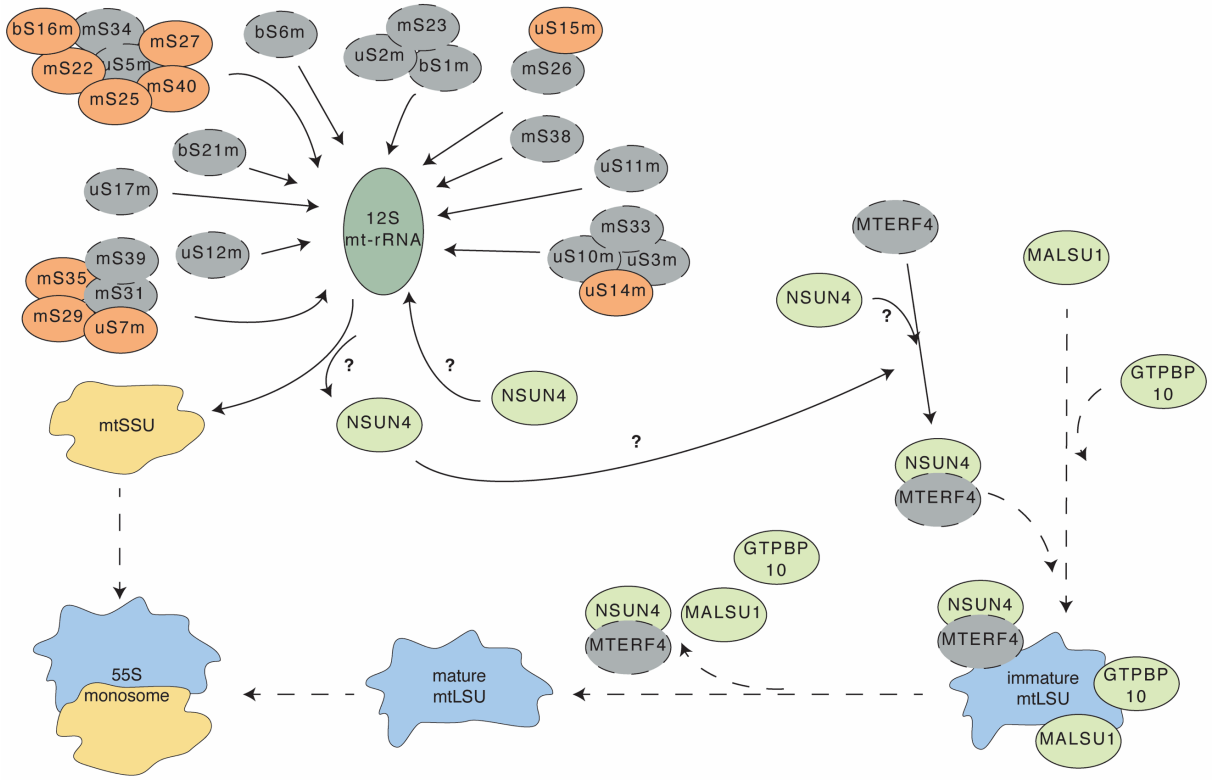

Figure 37: Schematic overview of the mtSSU and late mtLSU biogenesis. Biogenesis factors are depicted in light green, while in this study not analyzed proteins are shown in dark-grey with dashed outlined. Dashed arrows indicate several steps along the mitochondrial ribosome assembly and (?) indicate potential pathways which need to be further elucidated. The early and late assembling MRPs (orange) form their respective sub-modules assemble around the mtSSU (green). NSUN4 methylates either the naked 12S mt-rRNA or when the different sub-modules encompass the 12S mt-rRNA at a yet unknown stage together with other mtSSU biogenesis factors (here not shown). Upon release either this pool of NSUN4 or a different free pool of NSUN4, is recruited by MTERF4 and forms a complex which targets the immature mtLSU (blue) at a late stage of mtLSU biogenesis. The mtLSU biogenesis factors GTPBP10 and MALSU1 join, leading to its maturation upon release of these and other assembly factors (here not shown). The mature mtLSU is joined by the mtSSU (yellow) to form the 55S monosome.

Upon methylation of C841, NSUN4 is released from the 12S mt-rRNA by a yet unknown mechanism. Thereby it remains elusive whether NSUN4 methylates the 12S mt-rRNA first and is then recruited by MTERF4 or whether a different NSUN4 pool is recruited to form the NSUN4-MTEFR4 complex, which targets the immature mtLSU (Cámara et al., 2011; Metodiev et al., 2014). Similarly, the late mtLSU assembly factor GTPBP10, which was suggested to facilitate the mtLSU biogenesis by directly interacting with the 16S mt-rRNA (Cheng et al., 2021; Lavdovskaia et al., 2018; Maiti et al., 2018) and MALSU1 that prevents premature binding of the mtSSU by forming with L0R8F8 and mtACP the MALSU1-L0R8F8-mtACP module (Brown et al., 2017)

join the still immature mtLSU. Upon releasing these biogenesis factors, the mature mtLSU forms with the mtSSU the mitochondrial ribosome (Figure 37).

In this study, loss of uS7m leads to an increase of mtLSU MRPs, as shown in protein steady-state analysis. On the other hand, steady state RNA levels reveal a marginal decrease of the 16S mt-rRNA in uS7m-deficient cells compared to mS27 and mS40 ablation. Similarly, the mtLSU biogenesis factors GTPBP10 and MALSU1 show elevated levels in uS7m$^{-/-}$ compared to WT. As NSUN4 is a mtSSU assembly factor with a dual function (Metodiev et al., 2014), it is not surprising that also NSUN4 shows elevated levels upon loss of uS7m. Ablation of uS7m leads to a strong reduction of the 12S mt-rRNA, coupled with a drastic decrease of mature mtSSU formed (Figure 35B). This leaves NSUN4 with little to no substrate to perform its enzymatic function and potentially results in more NSUN4-MTERF4 complex formation (Figure 38). Monitoring NSUN4, GTPBP10 and MALSU1 in uS7m-deficient cells reveals the biogenesis factors migration in the mtLSU fractions, where they also accumulate (Figure 38). This result indicates that in the absence of uS7m, the mtLSU stays in its immature stage at potentially a late stage in the assembly. Only marginal mature mtLSU particles can form, as low levels of uS7m are still present in uS7m$^{-/-}$ cells and enable meager amounts of mature mtSSU to assemble.

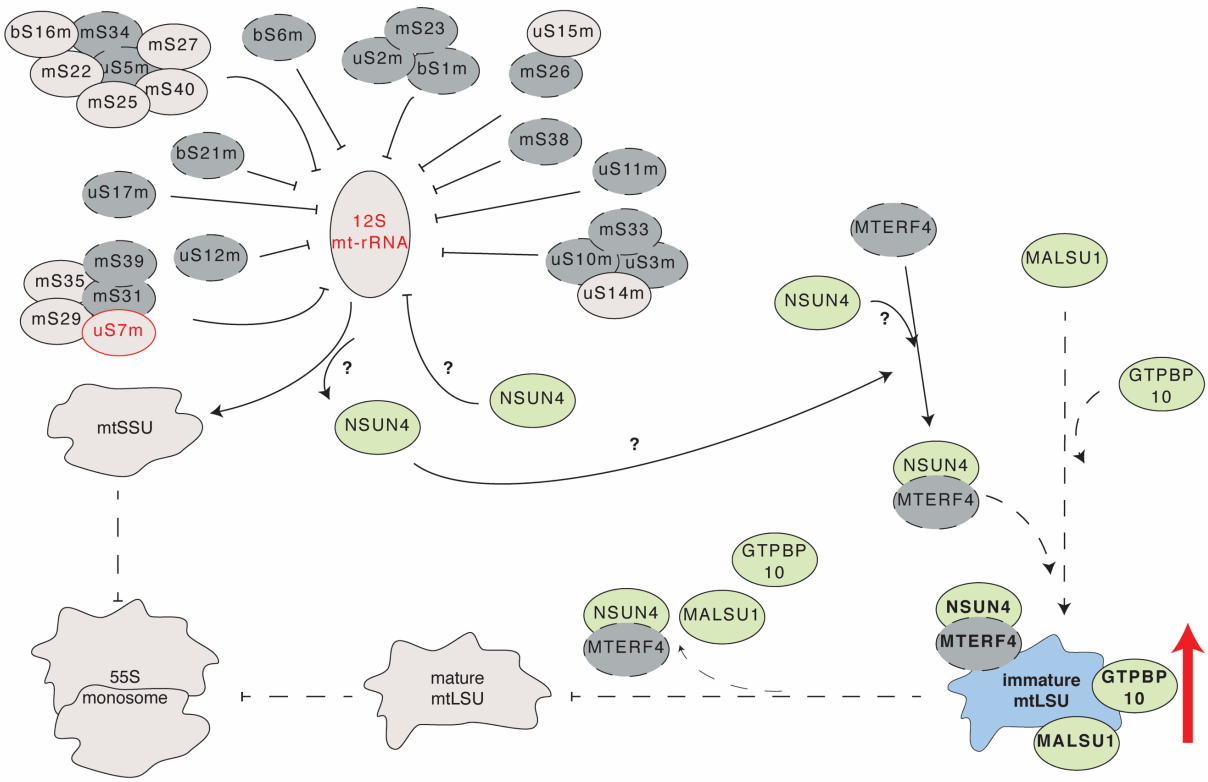

Figure 38: uS7m ablation stalls mtLSU maturation. Biogenesis factors are depicted in light green, while in this study not analyzed proteins are shown in dark-grey with dashed outlined. Dashed arrows indicate several steps along the mitochondrial ribosome assembly and (?) indicate potential pathways which need to be further elucidated. Strong diminishing of uS7m does not affect the assembly of its sub-module but leads to a drastic decrease of the 12S mt-rRNA in uS7m-deficient cells. This might result to a large pool of the biogenesis factor NSUN4, which might lead to increased formation of the NSUN4-MTERF4 and targets immature mtLSU at a late stage of the mtLSU biogenesis. Similarly, MALSU1 and GTPBP10 are enriched in the absence of uS7m and target immature mtLSU at a late biogenesis step. GTPBP10, MALSU1 and NSUN4-MTERF4 stay bound to the immature mtLSU and keep it in the immature state. As marginal levels of uS7m are still present, A small fraction of immature mtLSU can mature to form the 55S monosome, although it still inhibited. A larger amount is stalled in its maturation.

Interestingly, in a recent study by Lavdovskaia et al. (2020), a similar mtLSU intermediate was observed upon GTPBP6 ablation. There, loss of GTPBP6 leads to accumulation of immature mtLSU alongside the biogenesis factors NSUN4, MTERF4, MALSU1 and the GTPases GTPBP5, GTPBP7 and GTPBP10 (Lavdovskaia et al., 2020). Furthermore, as almost all mtLSU MRPs were detectable in GTPBP6-deficient cells, it was suggested that an almost mature mtLSU was present. This suggestion is further emphasized as the accumulation of GTPBP10, MALSU1 and NSUN4 indicates to three potential mtLSU intermediates in the late stages of mtLSU biogenesis, as proposed in a recent study by Cheng et al. (2021). There, it is suggested that MALSU1 is present throughout the late stages of the mtLSU assembly while GTPBP10 and the NSUN4-MTERF4 complex join in between to facilitate 16S mt-rRNA folding (Cheng et al., 2021). Recent studies suggest that MTERF4 is the contributor of the NSUN4-MTERF4 complex that facilitates further 16S mt-rRNA folding (Cheng et al., 2021; Cipullo et al., 2021; Hillen et al., 2021), while NSUN4 facilitates, together with GTPBP5, the PTC formation (Cipullo et al., 2021; Hillen et al., 2021). It is thereby striking that a similar mtLSU intermediate is observed by strong diminishing of uS7m or depletion of GTPBP6, as both proteins act at different stages and subunits of the mitochondrial ribosome biogenesis. Even more so, depletion of mS27 or mS40 does not show a similar immature mtLSU stage. Additionally, Maiti et al. (2020) observed a similar mtLSU intermediate in knockout analysis of the GTPase, GTPBP5. There, accumulation of GTPBP7, GTPBP10, MALSU1 and the NSUN4-MTERF4 complex was detectable. It was suggested, that accumulation of these complexes implicates to a quality control mechanism of the mitochondrial ribosome biogenesis (Maiti et al., 2020). This mechanism might be upregulated in uS7m-deficient cells, as the amount

of mature mtSSU is marginally low compared to present mtLSU. As the accumulation of the mtLSU intermediate is observed in uS7m-, GTPBP5- and GTPBP6 deficient cells, it might indicate to a cross-dependency during subunit maturation. If fully matured, the amount of mature mtLSU would significantly exceed the meager levels of mature mtSSU present in uS7m-deficient cells. As this process would be energetically inefficient, it might be possible that instead the mtLSU biogenesis is stalled to ensure that only the necessary amount of mtLSU assembles with mature mtSSU to form the mitochondrial ribosome. Therefore, it might be possible that stalling of the mtLSU biogenesis at the last steps caused by a quality control mechanism, might at the same time ensures that the chance that form functional mitochondrial ribosomes is increased.

5.3 Characterization of the uS7m p.Met184Val patient mutation reveals severe defects in the mtSSU biogenesis

A substantial decrease of uS7m in uS7m$^{-/-}$ cells leads to a disruption of the mtSSU assembly and downstream into the decline in the level of mitochondrial ribosomes and mitochondrial translation. These results are confirmed, as the mitochondrial translation is not entirely abolished and instead decreased in uS7m$^{-/-}$ cells. Expression of the uS7m$^{p.Met184Val}$ patient mutation, first described by Menezes et al. (2015), uS7m$^{-/-}$ cells leads to a less severe phenotype. Although the mitochondrial translation is decreased strongly compared to WT, mitochondrial encoded proteins are more abundant in uS7m$^{-/-}$+uS7m$^{p.Met184Val}$ cells compared to uS7m$^{-/-}$. This result agrees with the observation made by Menezes et al. (2015), since in patients' fibroblasts and liver samples complex I, III and IV activity was strongly reduced (Menezes et al., 2015). In contrast, sucrose density ultracentrifugation analysis reveals the expression of the uS7m$^{p.Met184Val}$ mutation leads to a strong decrease of mtSSU MRPs, albeit comparably stronger than in uS7m$^{-/-}$ cells. Since the inducible expression of uS7m$^{p.Met184Val}$ is weak compared to inducible expression of uS7m^{WT}, one can assume that the mutation leads to a destabilization of uS7m as proposed by Menezes et al. (2015). Of note, uS7m$^{p.Met184Val}$ and uS7m^{WT} were inserted into the same Flp-In cassette of HEK293T uS7m$^{-/-}$ cells, allowing the inducible expression of both constructs using the same promotor.

Menezes et al. (2015) observed a strong reduction of the 12S mt-rRNA while the 16S mt-rRNA remained stable in the presence of the uS7m p.Met184Val mutation. Therefore, it was suggested that the mtSSU could not form, as 12S mt-rRNA is subsequently degraded (Menezes et al., 2015). Weak amounts of the mtSSU and mitochondrial ribosome are able to form in uS7m$^{-/-}$+uS7m$^{p.Met184Val}$ cells indicate that the uS7m p.Met184Val mutation can assemble into the 55S ribosome, albeit the translation machinery is affected by the mutation. As these results agree with the monitoring of the mitochondrial translation, it is more likely that the uS7m p.Met184Val mutation retains to a certain extent the ability to assemble in the mtSSU. Additionally, mtLSU MRPs are enriched in uS7m$^{-/-}$+uS7m$^{p.Met184Val}$ cells and fewer immature mtLSU intermediates accumulate compared to uS7m$^{-/-}$. Similarly, less mtLSU late-stage assembly factors accumulate with the immature mtLSU in uS7m$^{p.Met184Val}$ expressing cells, indicating that a larger pool of mature mtSSU is able to form compared to uS7m-deficient cells. These results imply that the uS7m$^{p.Met184Val}$ patient mutation can be assembled to a minor degree into the mtSSU. Thereby, the mutation leads to the destabilization of uS7m, likely triggering a disruption in mtSSU biogenesis. As a consequence, mtSSU and 55S particles are reduced while mtLSU particles accumulate. The difference in present immature mtLSU intermediates in uS7m$^{p.Met184Val}$ expressing cells compared to uS7m-deficient cells furthermore emphasize that in the presence of marginal amounts of mature mtSSU the mtLSU biogenesis is stalled to ensure a higher chance in forming functional mitochondrial ribosome. This leads to the conclusion, that a cross-dependency during mtSSU and mtLSU might be present.

5.4 Defects during the mtSSU biogenesis affects the mtLSU formation

In contrast to the uS7m ablation, the absence of mS27 or mS40 leads to decreased mtLSU MRPs. Thereby, an immature mtLSU accumulation as in uS7m$^{-/-}$ cells (this study) or GTPBP6$^{-/-}$ cells (Lavdovskaia et al., 2020) is not observed in the absence of either mS27 or mS40. Although mtLSU MRPs are decreased in mS27$^{-/-}$ and mS40$^{-/-}$ cells, the mtLSU can assemble. Rackham et al. (2016) suggested that the mtLSU biogenesis can proceed on unprocessed 16S mt-rRNA in contrast to 12S mt-rRNA

upon transcription. This indicates that although 16S mt-rRNA levels are decreased in mS27-deficient cells, it might not inhibit the mtLSU assembly. Furthermore, Bogenhagen et al. (2018) suggested that MRPs are imported in excess into the mitochondria and are degraded when not incorporated into a sub-module or subunit. The reduced levels of mtLSU MRPs in mS27- and mS40-deficient cells support the same conclusion. The mtLSU MRP reduction in mS27$^{-/-}$ and mS40$^{-/-}$ cells is potentially the result of three factors: i) 16S mt-rRNA is reduced in both cell lines, ii) excess free mtLSU MRPs are degraded and iii) assembled mtLSU is not utilized for monosome formation. As the 16S mt-rRNA levels are reduced in mS27- and mS40-deficient cells, the pool of free mtLSU MRPs might exceed the amount of 16S mt-rRNA even more so than in WT. Since a large portion of mtLSU MRPs might be unable to assemble at the present amount of 16S mt-rRNA, the excess free mtLSU MRPs are potentially degraded, resulting in the decrease of mtLSU MRPs in mS27- and mS40-deficient cells. Furthermore, as the assembled mtLSU is not further utilized for mitochondrial ribosome formation, as no mature mtSSU is present in mS27$^{-/-}$ and mS40$^{-/-}$ cells, it might lead also to a degradation of the assembled mtLSU in the long run.

5.5 mS25 assembles early during mtSSU biogenesis

Sucrose density ultracentrifugation analysis of isolated mitoplasts of uS7m$^{-/-}$, mS27$^{-/-}$ and mS40$^{-/-}$ cells reveals that mS25 co-migrates with the bS16m-mS22-mS27-mS40 intermediate. In contrast, uS15m did not co-migrate in the same fraction, although Bogenhagen et al. (2018) suggested uS15m to be a part of a late assembly sub-module together with mS25. Furthermore, in the absence of mS40, uS15m was weakly detectable in the sucrose density ultracentrifugation analysis, indicating that the late assembled uS15m is strongly affected by the loss of mS40. However, mS25 still migrates in less dense fractions like bS16m, mS22 and mS27 in mS40-deficient cells indicating that mS25 assembles in an intermediate upstream of mS40. To confirm that mS25 is a part of the bS16m-mS22-mS27-mS40 intermediate, ribosome complexes were co-purified using FLAG-tagged variants of bS16m-mS22-mS27-mS40 intermediate and finally separated by sucrose density ultracentrifugation to define the composition of the assembly intermediate. Co-purification and co-migration of mS25

with the purified bS16m-mS22-mS27-mS40 intermediate in all cases emphasize our observation. Co-purification of uS15m and detection in the mtSSU fractions confirms that mS25 is indeed part of the early bS16m-mS22-mS27-mS40 intermediate, while uS15m is a late-binding MRP (Figure 39A). Interestingly, the bacterial homolog of bS16m, bS16 (formerly S16) was reported to assemble at an intermediate stage in the bacterial SSU, while in mammalian mitochondria, bS16m is suggested to appear early (Bogenhagen et al., 2018; Mizushima and Nomura, 1970). In bacteria, *in vitro* studies suggest that bS16 stabilizes the 16S mt-rRNA core of the SSU and can destabilize undesirable mt-rRNA interaction to suppress intermediates of the SSU, which would result in kinetic arrests (Ramaswamy and Woodson, 2009). In mammalian mitochondrial ribosomes, structural analyses by Greber et al. (2015) and Amunts et al. (2015) show that bS16m contains a zinc-binding motif similar to the three mammalian MRP homologs of bacterial bS18 (mL66, mS40 and bS18m). Thereby, more than one protein chain facilitating the coordination of a zinc ion is a rather unusual feature but is suggested to play a role in stabilizing the mitochondrial ribosome structure (Amunts et al., 2015; Greber et al., 2015). As aforementioned, bS16m contains a zinc-binding motif, which is suggested to facilitate its function by interacting with mS25 (Amunts et al., 2015; Greber et al., 2015). The potential stabilization of the mtSSU by the interaction between bS16m and mS25 would align with the observation made in this study and emphasize that mS25 is an early, not a late assembling MRP as proposed by Bogenhagen et al. (2018).

In conclusion, our results align with Bogenhagen et al. (2018) that mS35 is an early-binding MRP in mtSSU biogenesis. Furthermore, in the absence of mS27 or mS40, bS16m, mS22 and mS25 can form a complex, indicating that they appear during sub-module formation and earlier than mS27 and mS40. In agreement, Bogenhagen et al. (2018) suggested that bS16m and mS22 form an intermediate. Therefore, this sub-module assembly model starts by forming the bS16m-mS22 intermediate, which is then joined by mS25 (Figure 39A). As mS27 is present in the less dense fractions of mS40-deficient cells and vice versa, these results suggest that mS27 and mS40 might appear at similar stages after the bS16m-mS22-mS25 intermediate formation. The phenotype observed in mS27-deficient cells is more severe than the one observed in $mS40^{-/-}$ cells, leading to the conclusion that mS27 might assemble earlier in the sub-

module than mS40, whereby it remains unclear at which stages uS5m and mS34 appear in this sub-module assembly as they were not analyzed (Figure 39A).

Similarly, monitoring of mS29 and mS35 in the absence of uS7m enables a potential assembly pathway of the uS7m-mS29-mS31-mS35-mS39 sub-module. Thereby, mS35 and mS29 remain stable in uS7m-deficient cells, indicating that both can form an intermediate without uS7m and appear possibly early in the sub-module biogenesis (Figure 39B).

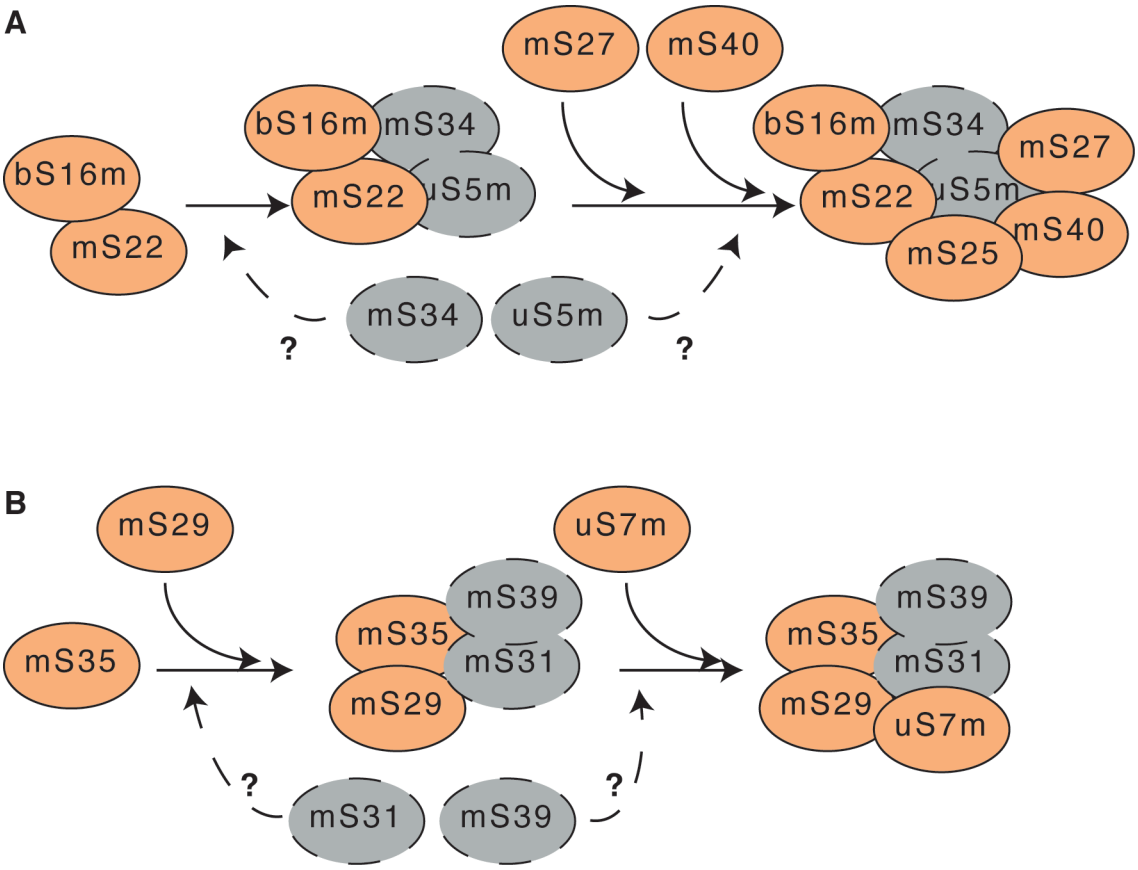

Figure 39: Assembly pathway of the uS5m-bS16m-mS22-mS25-mS27-mS34-mS40 and uS7m-mS29-mS31-mS35-mS39 sub-module. In this study, analyzed MRPs appear in orange and MRPs not analyzed are marked with dashed outlines in grey. Dashed arrows and (?) indicate unknown stages of assembly. A) The uS5m-bS16m-mS22-mS25-mS27-mS34-mS40 sub-module assembly starts with the early appearing MRPs bS16m, mS22. mS25 joins the bS16m-mS22 intermediate and is followed by mS27 and mS40. uS5m and mS34 were not analyzes, which results in an unknown stage at which they appear in this assembly line. B) mS35 potentially initiates the uS7m-mS29-mS31-mS35-mS39 sub-module formation and is joined by mS29. As mS31 and mS39 were not analyzes, it is unclear at which stage they join the assembly. uS7m appears in this assembly line after mS29-mS35 intermediate forming.

However, mS31 and mS39 were not analyzed in this study, resulting in the question of where both MRPs appear in the sub-module assembly line (Figure 39B). To obtain a

complete model for the uS5m-bS16m-mS22-mS25-mS27-mS34-mS40 and uS7m-mS29-mS31-mS35-mS39 sub-module assembly line, further analyses of the MRPs uS5m, mS34, mS31 and mS39 are needed.

5.6 mS27^{FLAG} retains its ability to integrate into the mtSSU but is possibly inhibited in its secondary function

mS27 is a PPR protein, enabling it to interact with RNA (Davies et al., 2012). The same study suggested that mS27 interacts with the 12S mt-rRNA and a small portion of 16S mt-rRNA and mt-tRNA^{Glu}. Here, we generated an mS27$^{-/-}$ cell line where the mitochondrial translation is completely abolished, and 12S mt-rRNA levels are severely reduced. Furthermore, 16S mt-rRNA levels are strongly decreased. Expressing mS27^{FLAG} in mS27$^{-/-}$ cells results in a partial rescue, although the functionality and ability to incorporate into the mtSSU was proven in the present work and a study by Dennerlein et al. (2010). This leaves room for speculation on why upon expression of mS27^{FLAG} in mS27$^{-/-}$ cells, only the mitochondrial encoded proteins ATP6 and ND5 show a weak detection. There are three possible explanations: i) mS27^{FLAG} is strongly overexpressed compared to endogenous WT levels, leading to a negative effect, which inhibits mitochondrial translation, ii) the observed phenotype in mS27$^{-/-}$ is a result of an off-target effect or iii) the FLAG tag inhibits a secondary function of mS27$^{-/-}$, which results in the translation deficiency phenotype. In this study, the same mS27^{FLAG} construct was used to analyze the mS27 interactome and also overexpressed compared to endogenous levels. However, no side effects could be observed, as MRPs of the mtSSU and mtLSU and assembly factors are co-purified. Furthermore, in the study of Dennerlein et al. (2010) and this study, mS27^{FLAG} co-purified proteins were analyzed by sucrose density ultracentrifugation. There, assembled mtSSU and mtLSU could be detected as well as 55S monosome. As mS27^{FLAG} is indeed functional and its overexpression does not affect the mitochondrial ribosome biogenesis, it appears unlikely that the phenotype observed in mS27$^{-/-}$ cannot be rescued by the expression of mS27^{FLAG}. Instead, either a secondary function of mS27 is potentially inhibited by the FLAG tag or the phenotype in mS27-deficient cells is due to an off-target effect. As a similar problem is observed in uS7m-deficient cells, where expression of uS7m^{WT}

but not uS7m^{FLAG} rescues the phenotype, it is possible that expression of endogenous mS27 could rescue the phenotype in mS27$^{-/-}$ cells. In order to test if the FLAG tag indeed inhibits mS27 secondary function, expression of the endogenous mS27 (mS27^{WT}) would need to be performed and may give answers. The absence of phenotype rescue with the expression of mS27^{WT} would be most likely due to an off-target effect caused by the guide RNA binding at a different location. To verify this conclusion, mS27-deficient cells would need to be deep sequenced.

5.7 NT5DC2, POLDIP2 and VWA8^{B} and their potential role in mitochondria

To identify novel mtSSU assembly factors, we determined the interactome of mS40^{FLAG} by mass spectrometry and obtained three possible candidates: i) 5'-nucleotidase domain-containing protein 2 (NT5DC2) ii) Polymerase delta-interacting protein 2 (POLDIP2) and iii) von Willebrand factor A domain-containing protein 8 (VWA8), which is present in two isoforms (VWA8^{A} and VWA8^{B}).

Here, knockout analysis of NT5DC2 revealed that loss of NT5DC2 leads to a reduction in mitochondrial proteins' de novo synthesis compared to WT. Interestingly, in the absence of mS27 or mS40, but not in uS7m-deficient cells, NT5DC2 levels are drastically diminished. Furthermore, in mL44- and mL45-deficient cells NT5DC2 showed similar reduced levels (unpublished data of Dr. Elisa Hanitsch, AG Richter-Dennerlein, GGNB program ‘Biomolecules’). The drastic reduction of NT5DC2 is likely a consequence of the abolished mitochondrial translation observed in all four knockouts. As NT5DC2 was suggested to be a phosphatase (Nakashima et al., 2019; 2020; Seifried et al., 2013), it is tempting to speculate whether NT5DC2 might play a role in mitochondrial translation. This scenario is possible, as in uS7m-deficient cells, the mitochondrial translation is reduced but not abolished, and NT5DC2 is not as affected as in the mS27-, mS40-, mL44-, and mL45-deficient cells.

In contrast, knockout analysis of POLDIP2 revealed no apparent defect in the mitochondrial translation, albeit POLDIP2 protein levels are not detectable. Furthermore, POLDIP2 appears not be affected in uS7m-, mS27- or mS40-deficient cells. Similarly, sucrose density ultracentrifugation analysis does not reveal a

difference in the migration pattern of POLDIP2 in the absence of uS7m, mS27, or mS40 compared to WT. These results indicate that POLDIP2 might not play a role in the mitochondrial ribosome biogenesis or translation, as the absence of uS7m, mS27 and mS40 does not affect POLDIP2 and depletion of POLDIP2 does not affect the mitochondrial translation. As POLDIP2-deficient cells only exhibit a different morphology compared to WT cells, this raises the question of which role POLDIP2 might play. Cheng et al. (2005) suggested that POLDIP2 may play a role in mtDNA metabolism in mitochondrial nucleoids by directly interacting with the mitochondrial single-strand DNA-binding protein (mtSSB) and mitochondrial transcription factor A (TFAM). Recent studies provided evidence of the mitochondrial ribosome biogenesis taking place to a certain extent in the nucleoids and RNA granules (Antonicka and Shoubridge, 2015; Bogenhagen et al., 2014). Thereby, processing of the 12S mt-rRNA 5' and 3' ends was suggested to be a requirement to initiate the mtSSU biogenesis. In contrast, the biogenesis of the mtLSU can be performed by using an unprocessed 16S mt-rRNA (Rackham et al., 2016). Therefore, it might be that POLDIP2 interaction with the mitochondrial ribosome is transient, whereby its actual function lies similar to mtSSB in the mtDNA metabolism as proposed by Cheng et al. (2005).

Similar to POLDIP2, VWA8^{B} exhibits no difference in its migration pattern in sucrose density ultracentrifugation analysis compared to WT. VWA8 was suggested to localize in mitochondria (Luo et al., 2017) and in peroxisomes (Imanaka and Kawaguchi, 2020; Niwa et al., 2018). It was suggested that VWA8 is involved in the quality control of proteins, although its overall function in peroxisomes remains elusive (Imanaka and Kawaguchi, 2020). Knockout analysis of VWA8 by Luo et al. (2019 and 2021) suggested that in the absence of VWA8, HNF4α plays a compensatory role, leading to an increase in OXPHOS activity. As VWA8^{B} is not affected by the absence of uS7m, mS27, or mS40, it remains to be further elucidated whether VWA8^{B} is involved in the mitochondrial protein quality control as suggested by Imanaka et al. (2020) or whether VWA8^{B} exhibit a different function.

Summary and conclusion

For an efficient mitochondrial translation, the mitochondrial ribosome needs to be assembled in a coordinated manner. Although the biogenesis of the bacterial ribosome was excessively studied, little is known about the mitochondrial ribosome biogenesis in humans. Similarly, only a fraction of biogenesis factors has so far been characterized. With the rise of human diseases caused by mitochondrial mutations, especially mutations affecting MRPs, it becomes more crucial to understand mitochondrial ribosome biogenesis. This work provides insight into the early assembly stages of the mtSSU and the effect of early-binding MRPs ablation in the mtLSU biogenesis and mitochondrial translation.

During this work, analysis of the early-binding MRPs uS7m, mS27 and mS40 enabled a better understanding of the mtSSU biogenesis, especially by characterizing the assembly line of the uS7m-containing and mS27-mS40-containing sub-modules. The ablation of uS7m, mS27 and mS40 were analyzed by western blotting, northern blotting, *de novo* synthesis of mitochondrial encoded proteins and sucrose gradient ultracentrifugation. The results obtained reveal a model, which suggests a potential assembly pathway of the analyzed sub-modules. Thereby, ablation of neither uS7m, mS27, nor mS40 inhibited their respective sub-modules formation. This observation implies that the formation of early assembly intermediates are not affected by the absence of either uS7m, mS27 or mS40. Furthermore, it was possible to define mS25 as an early-binding MRP in the mS27-mS40 containing sub-module, which was further confirmed by co-purification of ribosome complexes using FLAG-tagged variants of the bS16m-mS22-mS27-mS40 intermediate. Additionally, it was possible to support the possibility that uS14m and uS15m are late-binding MRPs.

Monitoring of mtLSU MRPs and biogenesis factors enabled the observation of an immature mtLSU intermediate in uS7m-deficient cells. Thereby it is suggested that the observed mtLSU intermediate plays a role at a late stage of assembly. As the accumulation of this particular intermediate was not observed in mS27- and mS40-deficient cells, it is plausible that the accumulation results from marginal amounts of mature mtSSU present in uS7m-deficient cells. Thereby, the mtLSU biogenesis is stalled at a late stage in uS7m$^{-/-}$ cells, as the amount of mature mtLSU would exceed

the meager levels of mature mtSSU. These results implicate a possible cross-dependency of the mtSSU and mtLSU during maturation, facilitating the monosome formation in a situation where either subunit biogenesis is stalled.

Additionally, in this work, the effect on the mtSSU biogenesis was analyzed by the expression of uS7m$^{p.Met184Val}$ mutation in uS7m-deficient cells. Characterization of the mutation by monitoring the mitochondrial translation and sucrose gradient ultracentrifugation revealed that the p.Met184Val mutation leads to a destabilization of uS7m protein. This results in a disrupted mtSSU biogenesis, albeit marginal amounts of functional mitochondrial ribosomes can be formed although most likely not as stable as in WT cells.

To rescue the phenotype in mS27-deficient cells, mS27^{FLAG} was introduced into mS27$^{-/-}$ cells. Expression of mS27^{FLAG} did not rescue the phenotype, although the functionality of the construct was confirmed. This leads to troubleshooting with two possibilities: i) the observed phenotype is an off-target effect mediated by the Cas9 enzyme and ii) the FLAG tag inhibits a secondary function of mS27. To discern between the two possibilities, future work should express the untagged mS27 into mS27-deficient cells. If this rescues the phenotype, then the FLAG tag indeed inhibits a secondary function of mS27, which calls for further elucidation.

Lastly, in this study, analysis of the mS40 interactome revealed three proteins that might facilitate an unknown function in mitochondria. While it was not possible to elaborate which function POLDIP2 or VWA8^{B} promote in mitochondria, the results imply that NT5DC2 might play a role in the mitochondrial translation since abolishing the translation leads to severe depletion of NT5DC2. NT5DC2 involvement is further confirmed, as monitoring of the mitochondrial translation in NT5DC2-deficient cells revealed a decrease of mitochondrial encoded proteins.

In this study, it was possible to outline a potential assembly line of the early-binding proteins uS7m, mS27 and mS40. Although the generated model is incomplete, it helps to understand part of the early mtSSU sub-module assembly, as the mitochondrial ribosome biogenesis is still poorly understood. Furthermore, a potential cross-dependency between the mtSSU and mtLSU biogenesis was observed, albeit the mechanism by which it facilitates it is unknown and needs further analysis. During this

work, NT5DC2 could be identified as a protein that plays a role in the mitochondrial translation, albeit the process by which it expedites its function needs to be elucidated.

References

Agaronyan, K., Morozov, Y.I., Anikin, M., and Temiakov, D. (2015). Mitochondrial biology. Replication-transcription switch in human mitochondria. Science *347*, 548–551.

Agirrezabala, X., and Frank, J. (2009). Elongation in translation as a dynamic interaction among the ribosome, tRNA, and elongation factors EF-G and EF-Tu. Q Rev Biophys *42*, 159–200.

Aguer, C., Gambarotta, D., Mailloux, R.J., Moffat, C., Dent, R., McPherson, R., and Harper, M.-E. (2011). Galactose Enhances Oxidative Metabolism and Reveals Mitochondrial Dysfunction in Human Primary Muscle Cells. PLoS ONE *6*, e28536–11.

Amunts, A., Brown, A., Bai, X.C., Llácer, J.L., Hussain, T., Emsley, P., Long, F., Murshudov, G., Scheres, S.H.W., and Ramakrishnan, V. (2014). Structure of the yeast mitochondrial large ribosomal subunit. Science *343*, 1485–1489.

Amunts, A., Brown, A., Toots, J., Scheres, S.H.W., and Ramakrishnan, V. (2015). Ribosome. The structure of the human mitochondrial ribosome. Science *348*, 95–98.

Anderson, S., Bankier, A.T., Barrell, B.G., de Bruijn, M.H., Coulson, A.R., Drouin, J., Eperon, I.C., Nierlich, D.P., Roe, B.A., Sanger, F., et al. (1981). Sequence and organization of the human mitochondrial genome. Nature *290*, 457–465.

Anney, R., Klei, L., Pinto, D., Regan, R., Conroy, J., Magalhaes, T.R., Correia, C., Abrahams, B.S., Sykes, N., Pagnamenta, A.T., et al. (2010). A genome-wide scan for common alleles affecting risk for autism. Human Molecular Genetics *19*, 4072–4082.

Antonicka, H., and Shoubridge, E.A. (2015). Mitochondrial RNA Granules Are Centers for Posttranscriptional RNA Processing and Ribosome Biogenesis. Cell Reports *10*, 920–932.

Antonicka, H., Choquet, K., Lin, Z.Y., Gingras, A.C., Kleinman, C.L., and Shoubridge, E.A. (2017). A pseudouridine synthase module is essential for mitochondrial protein synthesis and cell viability. EMBO Rep *18*, 28–38.

Antonicka, H., Sasarman, F., Nishimura, T., Paupe, V., and Shoubridge, E.A. (2013). The Mitochondrial RNA-Binding Protein GRSF1 Localizes to RNA Granules and Is Required for Posttranscriptional Mitochondrial Gene Expression. Cell Metabolism *17*, 386–398.

Arakaki, N., Nishihama, T., Kohda, A., Owaki, H., Kuramoto, Y., Abe, R., Kita, T., Suenaga, M., Himeda, T., Kuwajima, M., et al. (2006). Regulation of mitochondrial morphology and cell survival by Mitogenin I and mitochondrial single-stranded DNA binding protein. Biochimica Et Biophysica Acta (BBA) - General Subjects *1760*, 1364–1372.

Arroyo, J.D., Jourdain, A.A., Calvo, S.E., Ballarano, C.A., Doench, J.G., Root, D.E., and Mootha, V.K. (2016). A Genome-wide CRISPR Death Screen Identifies Genes Essential for Oxidative Phosphorylation. Cell Metabolism *24*, 875–885.

Baertling, F., Haack, T.B., Rodenburg, R.J., Schaper, J., Seibt, A., Strom, T.M., Meitinger, T., Mayatepek, E., Hadzik, B., Selcan, G., et al. (2015). MRPS22 mutation causes fatal neonatal lactic acidosis with brain and heart abnormalities. Neurogenetics *16*, 237–240.

Balsa, E., Marco, R., Perales-Clemente, E., Szklarczyk, R., Calvo, E., Landázuri, M.O., and Enríquez, J.A. (2012). NDUFA4 Is a Subunit of Complex IV of the Mammalian Electron Transport Chain. Cell Metabolism *16*, 378–386.

Bar-Yaacov, D., Frumkin, I., Yashiro, Y., Chujo, T., Ishigami, Y., Chemla, Y., Blumberg, A., Schlesinger, O., Bieri, P., Greber, B., et al. (2016). Mitochondrial 16S rRNA Is Methylated by tRNA Methyltransferase TRMT61B in All Vertebrates. PLoS Biol *14*, e1002557.

Barchiesi, A., Wasilewski, M., Chacinska, A., Tell, G., and Vascotto, C. (2015). Mitochondrial translocation of APE1 relies on the MIA pathway. Nucleic Acids Research *43*, 5451–5464.

Barkan, A., Rojas, M., Fujii, S., Yap, A., Chong, Y.S., Bond, C.S., and Small, I. (2012). A combinatorial amino acid code for RNA recognition by pentatricopeptide repeat proteins. PLoS Genet. *8*, e1002910.

Battey, J., and Clayton, D.A. (1978). The transcription map of mouse mitochondrial DNA. Cell *14*, 143–156.

Belevich, I., and Verkhovsky, M.I. (2008). Molecular Mechanism of Proton Translocation by Cytochrome cOxidase. Antioxidants & Redox Signaling *10*, 1–30.

Ben-Shem, A., Garreau de Loubresse, N., Melnikov, S., Jenner, L., Yusupova, G., and Yusupov, M. (2011). The structure of the eukaryotic ribosome at 3.0 Å resolution. Science *334*, 1524–1529.

Benz, R. (1994). Permeation of hydrophilic solutes through mitochondrial outer membranes: review on mitochondrial porins. Biochim Biophys Acta *1197*, 167–196.

Berk, A.J., and Clayton, D.A. (1974). Mechanism of mitochondrial DNA replication in mouse L-cells: asynchronous replication of strands, segregation of circular daughter molecules, aspects of topology and turnover of an initiation sequence. Journal of Molecular Biology *86*, 801–824.

Bezawork-Geleta, A., Rohlena, J., Dong, L., Pacak, K., and Neuzil, J. (2017). Mitochondrial Complex II: At the Crossroads. Trends in Biochemical Sciences *42*, 312–325.

Boczonadi, V., and Horvath, R. (2014). Mitochondria: Impaired mitochondrial translation in human disease. International Journal of Biochemistry and Cell Biology *48*, 77–84.

Boehm, E., Zaganelli, S., Maundrell, K., Jourdain, A.A., Thore, S., and Martinou, J.C. (2017). FASTKD1 and FASTKD4 have opposite effects on expression of specific mitochondrial RNAs, depending upon their endonuclease-like RAP domain. Nucleic Acids Research *45*, 6135–6146.

Bogenhagen, D.F. (2012). Mitochondrial DNA nucleoid structure. Biochim Biophys Acta *1819*, 914–920.

Bogenhagen, D.F., Martin, D.W., and Koller, A. (2014). Initial Steps in RNA Processing and Ribosome Assembly Occur at Mitochondrial DNA Nucleoids. Cell Metabolism *19*, 618–629.

Bogenhagen, D.F., Ostermeyer-Fay, A.G., Haley, J.D., and Garcia-Diaz, M. (2018). Kinetics and Mechanism of Mammalian Mitochondrial Ribosome Assembly. Cell Reports *22*, 1935–1944.

Borna, N.N., Kishita, Y., Kohda, M., Lim, S.C., Shimura, M., Wu, Y., Mogushi, K., Yatsuka, Y., Harashima, H., Hisatomi, Y., et al. (2019). Mitochondrial ribosomal protein PTCD3 mutations cause oxidative phosphorylation defects with Leigh syndrome. Neurogenetics *20*, 9–25.

Britton, R.A. (2009). Role of GTPases in bacterial ribosome assembly. Annu Rev Microbiol *63*, 155–176.

Brown, A., Amunts, A., Bai, X.C., Sugimoto, Y., Edwards, P.C., Murshudov, G., Scheres, S.H.W., and Ramakrishnan, V. (2014). Structure of the large ribosomal subunit from human mitochondria. Science *346*, 718–722.

Brown, A., Rathore, S., Kimanius, D., Aibara, S., Bai, X.C., Rorbach, J., Amunts, A., and Ramakrishnan, V. (2017). Structures of the human mitochondrial ribosome in native states of assembly. Nat Struct Mol Biol *24*, 866–869.

Bugiardini, E., Mitchell, A.L., Rosa, I.D., Horning-Do, H.-T., Pitmann, A.M., Poole, O.V., Holton, J.L., Shah, S., Woodward, C., Hargreaves, I., et al. (2019). MRPS25 mutations impair mitochondrial translation and cause encephalomyopathy. Human Molecular Genetics *28*, 2711–2719.

Bunner, A.E., Nord, S., Wikström, P.M., and Williamson, J.R. (2010). The Effect of Ribosome Assembly Cofactors on In Vitro 30S Subunit Reconstitution. Journal of Molecular Biology *398*, 1–7.

Burger, G., Gray, M.W., and Lang, B.F. (2003). Mitochondrial genomes: anything goes. Trends Genet *19*, 709–716.

Cai, Y.C., Bullard, J.M., Thompson, N.L., and Spremulli, L.L. (2000). Interaction of mammalian mitochondrial elongation factor EF-Tu with guanine nucleotides. Protein Sci *9*, 1791–1800.

Callegari, S., Cruz-Zaragoza, L.D., and Rehling, P. (2020). From TOM to the TIM23 complex – handing over of a precursor. Biological Chemistry *401*, 709–721.

Carroll, C.J., Isohanni, P., Pöyhönen, R., Euro, L., Richter, U., Brilhante, V., Götz, A., Lahtinen, T., Paetau, A., Pihko, H., et al. (2013). Whole-exome sequencing identifies a mutation in the mitochondrial ribosome protein MRPL44 to underlie mitochondrial infantile cardiomyopathy. J Med Genet *50*, 151–159.

Cámara, Y., Asin-Cayuela, J., Park, C.B., Metodiev, M.D., Shi, Y., Ruzzenente, B., Kukat, C., Habermann, B., Wibom, R., Hultenby, K., et al. (2011). MTERF4 regulates translation by targeting the methyltransferase NSUN4 to the mammalian mitochondrial ribosome. Cell Metabolism *13*, 527–539.

Cecchini, G. (2003). Function and Structure of Complex II of the Respiratory Chain. Annu. Rev. Biochem. *72*, 77–109.

Chacinska, A., Lind, M., Frazier, A.E., Dudek, J., Meisinger, C., Geissler, A., Sickmann, A., Meyer, H.E., Truscott, K.N., Guiard, B., et al. (2005). Mitochondrial Presequence Translocase: Switching between TOM Tethering and Motor Recruitment Involves Tim21 and Tim17. *120*, 817–829.

Charollais, J. (2004). CsdA, a cold-shock RNA helicase from Escherichia coli, is involved in the biogenesis of 50S ribosomal subunit. Nucleic Acids Research *32*, 2751–2759.

Chen, A., Tiosano, D., Guran, T., Baris, H.N., Bayram, Y., Mory, A., Shapiro-Kulnane, L., Hodges, C.A., Akdemir, Z.C., Turan, S., et al. (2018). Mutations in the mitochondrial ribosomal protein MRPS22 lead to primary ovarian insufficiency. Human Molecular Genetics *27*, 1913–1926.

Chen, H., Shi, Z., Guo, J., Chang, K.-J., Chen, Q., Yao, C., Haigis, M.C., and Shi, Y. (2019). The human mitochondrial 12S rRNA m 4C methyltransferase METTL15 is required for proper mitochondrial function. *75*, 241–40.

Chen, J., Cao, J., Wang, P., and He, X. (2020). NT5DC2 is a novel prognostic marker in human hepatocellular carcinoma. Oncol Lett *20*, 70.

Chen, S.S., Sperling, E., Silverman, J.M., Davis, J.H., and Williamson, J.R. (2012). Measuring the dynamics of E. coli ribosome biogenesis using pulse-labeling and quantitative mass spectrometry. Mol Biosyst *8*, 3325–3334.

Chen, Y., Zhou, G., Yu, M., He, Y., Tang, W., Lai, J., He, J., Liu, W., and Tan, D. (2005). Cloning and functional analysis of human mTERFL encoding a novel mitochondrial transcription termination factor-like protein. Biochemical and Biophysical Research Communications *337*, 1112–1118.

Cheng, J., Berninghausen, O., and Beckmann, R. (2021). A distinct assembly pathway of the human 39S late pre-mitoribosome. bioRxiv 2021.03.17.435838.

Cheng, X., Kanki, T., Fukuoh, A., Ohgaki, K., Takeya, R., Aoki, Y., Hamasaki, N., and Kang, D. (2005). PDIP38 Associates with Proteins Constituting the Mitochondrial DNA Nucleoid. The Journal of Biochemistry *138*, 673–678.

Christian, B.E., and Spremulli, L.L. (2010). Preferential Selection of the 5′-Terminal Start Codon on Leaderless mRNAs by Mammalian Mitochondrial Ribosomes. Journal of Biological Chemistry *285*, 28379–28386.

Christian, B.E., and Spremulli, L.L. (2012). Mechanism of protein biosynthesis in mammalian mitochondria. Biochim Biophys Acta *1819*, 1035–1054.

Cipullo, M., Gesé, G.V., Khawaja, A., Hällberg, B.M., and Rorbach, J. (2021). Structural basis for late maturation steps of the human mitoribosomal large subunit. bioRxiv 2021.03.15.435084.

Cipullo, M., Pearce, S.F., Lopez Sanchez, I.G., Gopalakrishna, S., Krüger, A., Schober, F., Busch, J.D., Li, X., Wredenberg, A., Atanassov, I., et al. (2020). Human GTPBP5 is involved in the late stage of mitoribosome large subunit assembly. Nucleic Acids Research *49*, 354–370.

Cogliati, S., Enriquez, J.A., and Scorrano, L. (2016). Mitochondrial Cristae: Where Beauty Meets Functionality. Trends in Biochemical Sciences *41*, 261–273.

Connolly, K., Rife, J.P., and Culver, G. (2008). Mechanistic insight into the ribosome biogenesis functions of the ancient protein KsgA. Molecular Microbiology *70*, 1062–1075.

Corliss, J.O., and Margulis, L. (1972). Origin of Eukaryotic Cells. Transactions of the American Microscopical Society.

Cowling, V.H. (2009). Regulation of mRNA cap methylation. Biochem J *425*, 295–302.

Dalla Rosa, I., Durigon, R., Pearce, S.F., Rorbach, J., Hirst, E.M.A., Vidoni, S., Reyes, A., Brea-Calvo, G., Minczuk, M., Woellhaf, M.W., et al. (2014). MPV17L2 is required for ribosome assembly in mitochondria. Nucleic Acids Research *42*, 8500–8515.

Dame, R.T., Espéli, O., Grainger, D.C., and Wiggins, P.A. (2012). Multidisciplinary perspectives on bacterial genome organization and dynamics. Molecular Microbiology *86*, 1023–1030.

Dammel, C.S., and Noller, H.F. (1995). Suppression of a cold-sensitive mutation in 16S rRNA by overexpression of a novel ribosome-binding factor, RbfA. Genes Dev *9*, 626–637.

Davies, S.M.K., Lopez Sanchez, M.I.G., Narsai, R., Shearwood, A.M.J., Razif, M.F.M., Small, I.D., Whelan, J., Rackham, O., and Filipovska, A. (2012). MRPS27 is a pentatricopeptide repeat domain protein required for the translation of mitochondrially encoded proteins. FEBS Lett *586*, 3555–3561.

Davis, J.H., Tan, Y.Z., Carragher, B., Potter, C.S., Lyumkis, D., and Williamson, J.R. (2016). Modular Assembly of the Bacterial Large Ribosomal Subunit. 1–29.

Decatur, W.A., and Fournier, M.J. (2002). rRNA modifications and ribosome function. Trends in Biochemical Sciences *27*, 344–351.

Dennerlein, S., Rozanska, A., Wydro, M., Chrzanowska-Lightowlers, Z.M.A., and Lightowlers, R.N. (2010). Human ERAL1 is a mitochondrial RNA chaperone involved in the assembly of the 28S small mitochondrial ribosomal subunit. Biochem J *430*, 551–558.

Desai, N., Brown, A., Amunts, A., and Ramakrishnan, V. (2017). The structure of the yeast mitochondrial ribosome. Science *355*, 528–531.

Desai, N., Yang, H., Chandrasekaran, V., Kazi, R., Minczuk, M., and Ramakrishnan, V. (2020). Elongational stalling activates mitoribosome-associated quality control. Science *370*, 1105–1110.

Di Nottia, M., Marchese, M., Verrigni, D., Mutti, C.D., Torraco, A., Oliva, R., Fernandez-Vizarra, E., Morani, F., Trani, G., Rizza, T., et al. (2020). A homozygous MRPL24 mutation causes a complex movement disorder and affects the mitoribosome assembly. Neurobiology of Disease *141*, 104880.

DiMauro, S., Schon, E.A., Carelli, V., and Hirano, M. (2013). The clinical maze of mitochondrial neurology. Nat Rev Neurol *9*, 429–444.

Distelmaier, F., Haack, T.B., Catarino, C.B., Gallenmüller, C., Rodenburg, R.J., Strom, T.M., Baertling, F., Meitinger, T., Mayatepek, E., Prokisch, H., et al. (2015). MRPL44 mutations cause a slowly progressive multisystem disease with childhood-onset hypertrophic cardiomyopathy. Neurogenetics *16*, 319–323.

D'Souza, A.R., Van Haute, L., Powell, C.A., Rebelo-Guiomar, P., Rorbach, J., and Minczuk, M. (2019). YbeY is required for ribosome small subunit assembly and tRNA processing in human mitochondria. *46*, 8471–46.

Eaton, S., Bartlett, K., and Pourfarzam, M. (1996). Mammalian mitochondrial beta-oxidation. Biochemical Journal *320 (Pt 2)*, 345–357.

Emdadul Haque, M., Grasso, D., Miller, C., Spremulli, L.L., and Saada, A. (2008). The effect of mutated mitochondrial ribosomal proteins S16 and S22 on the assembly of the small and large ribosomal subunits in human mitochondria. Mitoch *8*, 254–261.

Englmeier, R., Pfeffer, S., and Förster, F. (2017). Structure of the Human Mitochondrial Ribosome Studied In Situ by Cryoelectron Tomography. Structure *25*, 1574–1581.e2.

Falkenberg, M., Gaspari, M., Rantanen, A., Trifunovic, A., Larsson, N.-G., and Gustafsson, C.M. (2002). Mitochondrial transcription factors B1 and B2 activate transcription of human mtDNA. Nat Genet *31*, 289–294.

Feng, B., Mandava, C.S., Guo, Q., Wang, J., Cao, W., Li, N., Zhang, Y., Zhang, Y., Wang, Z., Wu, J., et al. (2014). Structural and functional insights into the mode of action of a universally conserved Obg GTPase. PLoS Biol *12*, e1001866.

Fernandez-Vizarra, E. (2015). Nuclear gene mutations as the cause of mitochondrial complex III deficiency. 1–11.

Ferrari, A., Del'Olio, S., and Barrientos, A. (2020). The Diseased Mitoribosome. FEBS Lett *233*, 657–38.

Fiedorczuk, K., Letts, J.A., Degliesposti, G., Kaszuba, K., Skehel, M., and Sazanov, L.A. (2016). Atomic structure of the entire mammalian mitochondrial complex I. Nature *538*, 406–410.

Formenoy, L.J., Cunningham, P.R., Nurse, K., Pleij, C.W., and Ofengand, J. (1994). Methylation of the conserved A1518-A1519 in Escherichia coli 16S ribosomal RNA by the ksgA methyltransferase is influenced by methylations around the similarly conserved U1512.G1523 base pair in the 3' terminal hairpin. Biochimie *76*, 1123–1128.

Frey, T.G., and Mannella, C.A. (2000). The internal structure of mitochondria. Trends in Biochemical Sciences *25*, 319–324.

Fung, S., Nishimura, T., Sasarman, F., and Shoubridge, E.A. (2013). The conserved interaction of C7orf30 with MRPL14 promotes biogenesis of the mitochondrial large ribosomal subunit and mitochondrial translation. MBoC *24*, 184–193.

Galmiche, L., Serre, V., Beinat, M., Assouline, Z., Lebre, A.S., Chretien, D., Nietschke, P., Benes, V., Boddaert, N., Sidi, D., et al. (2011). Exome sequencing identifies MRPL3 mutation in mitochondrial cardiomyopathy. Hum Mutat *32*, 1225–1231.

Gardeitchik, T., Mohamed, M., Ruzzenente, B., Karall, D., Guerrero-Castillo, S., Dalloyaux, D., van den Brand, M., van Kraaij, S., van Asbeck, E., Assouline, Z., et al. (2018). Bi-allelic Mutations in the Mitochondrial Ribosomal Protein MRPS2 Cause Sensorineural Hearing Loss, Hypoglycemia, and Multiple OXPHOS Complex Deficiencies. Am J Hum Genet *102*, 685–695.

Gaur, R., Grasso, D., Datta, P.P., Krishna, P.D.V., Das, G., Spencer, A., Agrawal, R.K., Spremulli, L., and Varshney, U. (2008). A single mammalian mitochondrial translation initiation factor functionally replaces two bacterial factors. Mol Cell *29*, 180–190.

Gelfand, R., and Attardi, G. (1981). Synthesis and turnover of mitochondrial ribonucleic acid in HeLa cells: the mature ribosomal and messenger ribonucleic acid species are metabolically unstable. Mcb *1*, 497–511.

Ghosal, A., Köhrer, C., Babu, V.M.P., Yamanaka, K., Davies, B.W., Jacob, A.I., Ferullo, D.J., Gruber, C.C., Vercruysse, M., and Walker, G.C. (2017). C21orf57 is a human homologue of bacterial YbeY proteins. Biochemical and Biophysical Research Communications *484*, 612–617.

Gray, M.W. (1998). Rickettsia, typhus and the mitochondrial connection. Nature *396*, 109–110.

Gray, M.W. (1983). The Bacterial Ancestry of Plastids and Mitochondria. *33*, 693–699.

Greber, B.J., and Ban, N. (2016). Structure and Function of the Mitochondrial Ribosome. Annu Rev Biochem *85*, 103–132.

Greber, B.J., Bieri, P., Leibundgut, M., Leitner, A., Aebersold, R., Boehringer, D., and Ban, N. (2015). Ribosome. The complete structure of the 55S mammalian mitochondrial ribosome. Science *348*, 303–308.

Greber, B.J., Boehringer, D., Leitner, A., Bieri, P., Voigts-hoffmann, F., Erzberger, J.P., Leibundgut, M., Aebersold, R., and Ban, N. (2014). Architecture of the large subunit of the mammalian mitochondrial ribosome. Nature *505*, 515–519.

Gualerzi, C.O., and Pon, C.L. (2015). Initiation of mRNA translation in bacteria: structural and dynamic aspects. Cell Mol Life Sci *72*, 4341–4367.

Guarani, V., McNeill, E.M., Paulo, J.A., Huttlin, E.L., Fröhlich, F., Gygi, S.P., Van Vactor, D., and Harper, J.W. (2015). QIL1 is a novel mitochondrial protein required for MICOS complex stability and cristae morphology. eLife *4*, 1–23.

Guo, S., Ran, H., Xiao, D., Huang, H., Mi, L., Wang, X., Chen, L., Li, D., Zhang, S., Han, Q., et al. (2019). NT5DC2 promotes tumorigenicity of glioma stem-like cells by upregulating fyn. Cancer Letters *454*, 98–107.

Gustafsson, C.M., Falkenberg, M., and Larsson, N.-G. (2016). Maintenance and Expression of Mammalian Mitochondrial DNA. Annu Rev Biochem *85*, 133–160.

Hage, El, A., Sbaï, M., and Alix, J.H. (2001). The chaperonin GroEL and other heat-shock proteins, besides DnaK, participate in ribosome biogenesis in Escherichia coli. Mol Gen Genet *264*, 796–808.

Hammarsund, M., Wilson, W., Corcoran, M., Merup, M., Einhorn, S., Grandér, D., and Sangfelt, O. (2001). Identification and characterization of two novel human mitochondrial elongation factor genes, hEFG2 and hEFG1, phylogenetically conserved through evolution. Hum Genet *109*, 542–550.

Harner, M., rner, C.K.O., Walther, D., Mokranjac, D., Kaesmacher, J., Welsch, U., Griffith, J., Mann, M., Reggiori, F., and Neupert, W. (2011). The mitochondrial contact site complex, a determinant of mitochondrial architecture. The EMBO Journal *30*, 4356–4370.

Haute, L.V., Hendrick, A.G., D'Souza, A.R., Powell, C.A., Rebelo-Guiomar, P., Harbour, M.E., Ding, S., Fearnley, I.M., Andrews, B., and Minczuk, M. (2019). METTL15 introduces N4-methylcytidine into human mitochondrial 12S rRNA and is required for mitoribosome biogenesis. Nucleic Acids Research *47*, 10267–10281.

Hällberg, B.M., and Larsson, N.-G. (2014). Making proteins in the powerhouse. Cell Metabolism *20*, 226–240.

He, J., Cooper, H.M., Reyes, A., Di Re, M., Kazak, L., Wood, S.R., Mao, C.C., Fearnley, I.M., Walker, J.E., and Holt, I.J. (2012). Human C4orf14 interacts with the mitochondrial nucleoid and is involved in the biogenesis of the small mitochondrial ribosomal subunit. Nucleic Acids Research *40*, 6097–6108.

He, J., Ford, H.C., Carroll, J., Douglas, C., Gonzales, E., Ding, S., Fearnley, I.M., and Walker, J.E. (2018). Assembly of the membrane domain of ATP synthase in human mitochondria. Proc Natl Acad Sci USA *115*, 2988.

Herold, M., and Nierhaus, K.H. (1987). Incorporation of six additional proteins to complete the assembly map of the 50 S subunit from Escherichia coli ribosomes. Journal of Biological Chemistry *262*, 8826–8833.

Hillen, H.S., Lavdovskaia, E., Nadler, F., Hanitsch, E., Linden, A., Bohnsack, K.E., Urlaub, H., and Richter-Dennerlein, R. (2021). Structural basis of GTPase-mediated mitochondrial ribosome biogenesis and recycling. bioRxiv 2021.03.17.435767.

Hillen, H.S., Temiakov, D., and Cramer, P. (2018). Structural basis of mitochondrial transcription. Nat Struct Mol Biol *25*, 754–765.

Holzmann, J., Frank, P., Löffler, E., Bennett, K.L., Gerner, C., and Rossmanith, W. (2008). RNase P without RNA: identification and functional reconstitution of the human mitochondrial tRNA processing enzyme. Cell *135*, 462–474.

Hou, Y.M. (2010). CCA addition to tRNA: implications for tRNA quality control. IUBMB Life *62*, 251–260.

Imanaka, T., and Kawaguchi, K. (2020). A novel dynein-type AAA+ protein with peroxisomal targeting signal type 2. The Journal of Biochemistry *167*, 429–432.

Iost, I., and Jain, C. (2019). A DEAD-box protein regulates ribosome assembly through control of ribosomal protein synthesis. Nucleic Acids Research *47*, 8193–8206.

Iost, I., Bizebard, T., and Dreyfus, M. (2013). Functions of DEAD-box proteins in bacteria: Current knowledge and pending questions. BBA - Gene Regulatory Mechanisms *1829*, 866–877.

Jackson, C.B., Huemer, M., Bolognini, R., Martin, F., Szinnai, G., Donner, B.C., Richter, U., Battersby, B.J., Nuoffer, J.M., Suomalainen, A., et al. (2019). A variant in MRPS14 (uS14m) causes perinatal hypertrophic cardiomyopathy with neonatal lactic acidosis, growth retardation, dysmorphic features and neurological involvement. Human Molecular Genetics *28*, 639–649.

Jain, C. (2008). The E. coli RhlE RNA helicase regulates the function of related RNA helicases during ribosome assembly. Rna *14*, 381–389.

Jin, X., Liu, X., Zhang, Z., and Xu, L. (2020). NT5DC2 suppression restrains progression towards metastasis of non-small-cell lung cancer through regulation p53 signaling. Biochemical and Biophysical Research Communications 1–8.

Jones, C.N., Wilkinson, K.A., Hung, K.T., Weeks, K.M., and Spremulli, L.L. (2008). Lack of secondary structure characterizes the 5' ends of mammalian mitochondrial mRNAs. Rna *14*, 862–871.

Jones, P.G., Mitta, M., Kim, Y., Jiang, W., and Inouye, M. (1996). Cold shock induces a major ribosomal-associated protein that unwinds double-stranded RNA in Escherichia coli. Proceedings of the National Academy of Sciences *93*, 76–80.

Jourdain, A.A., Boehm, E., Maundrell, K., and Martinou, J.C. (2016). Mitochondrial RNA granules: Compartmentalizing mitochondrial gene expression. J Cell Biol *212*, 611–614.

Jourdain, A.A., Koppen, M., Wydro, M., Rodley, C.D., Lightowlers, R.N., Chrzanowska-Lightowlers, Z.M., and Martinou, J.C. (2013). GRSF1 regulates RNA processing in mitochondrial RNA granules. Cell Metabolism *17*, 399–410.

Kang, Y., Fielden, L.F., and Stojanovski, D. (2017). Mitochondrial protein transport in health and disease. Seminars in Cell and Developmental Biology 1–34.

Karbstein, K. (2007). Role of GTPases in ribosome assembly. Biopolymers *87*, 1–11.

Khawaja, A., Itoh, Y., Remes, C., Spåhr, H., Yukhnovets, O., Höfig, H., Amunts, A., and Rorbach, J. (2020). Distinct pre-initiation steps in human mitochondrial translation. Nature Communications 1–10.

Kim, H.J., and Barrientos, A. (2018). MTG1 couples mitoribosome large subunit assembly with intersubunit bridge formation. Nucleic Acids Research *46*, 8435–8453.

Kobayashi, G., Moriya, S., and Wada, C. (2001). Deficiency of essential GTP-binding protein ObgE in Escherichia coli inhibits chromosome partition. Molecular Microbiology *41*, 1037–1051.

Koc, E.C., and Spremulli, L.L. (2002). Identification of mammalian mitochondrial translational initiation factor 3 and examination of its role in initiation complex formation with natural mRNAs. Journal of Biological Chemistry *277*, 35541–35549.

Koch, M., Clementi, N., Rusca, N., Vögele, P., Erlacher, M., and Polacek, N. (2015). The integrity of the G2421-C2395 base pair in the ribosomal E-site is crucial for protein synthesis. RNA Biology *12*, 70–81.

Kohda, M., Tokuzawa, Y., Kishita, Y., Nyuzuki, H., Moriyama, Y., Mizuno, Y., Hirata, T., Yatsuka, Y., Yamashita-Sugahara, Y., Nakachi, Y., et al. (2016). A Comprehensive Genomic Analysis Reveals the Genetic Landscape of Mitochondrial Respiratory Chain Complex Deficiencies. PLoS Genet. *12*, e1005679.

Kolanczyk, M., Pech, M., Zemojtel, T., Yamamoto, H., Mikula, I., Calvaruso, M.-A., van den Brand, M., Richter, R., Fischer, B., Ritz, A., et al. (2011). NOA1 is an essential GTPase required for mitochondrial protein synthesis. MBoC *22*, 1–11.

Koopman, W.J.H., Distelmaier, F., Smeitink, J.A.M., and Willems, P.H.G.M. (2013). OXPHOS mutations and neurodegeneration. The EMBO Journal *32*, 9–29.

Korepanov, A.P., Korobeinikova, A.V., Shestakov, S.A., Garber, M.B., and Gongadze, G.M. (2012). Protein L5 is crucial for in vivo assembly of the bacterial 50S ribosomal subunit central protuberance. Nucleic Acids Research *40*, 9153–9159.

Koripella, R.K., Deep, A., Agrawal, E.K., Keshavan, P., Banavali, N.K., and Agrawal, R.K. (2020a). Structures of the human mitochondrial ribosome recycling complexes reveal distinct mechanisms of recycling and antibiotic resistance. bioRxiv 2020.12.20.423689.

Koripella, R.K., Sharma, M.R., Bhargava, K., Datta, P.P., Kaushal, P.S., Keshavan, P., Spremulli, L.L., Banavali, N.K., and Agrawal, R.K. (2020b). Structures of the human mitochondrial ribosome bound to EF-G1 reveal distinct features of mitochondrial translation elongation. Nature Communications 1–11.

Korkmaz, G., Holm, M., Wiens, T., and Sanyal, S. (2014). Comprehensive analysis of stop codon usage in bacteria and its correlation with release factor abundance. J Biol Chem *289*, 30334–30342.

Kukat, C., and Larsson, N.-G. (2013). mtDNA makes a U-turn for the mitochondrial nucleoid. Trends Cell Biol *23*, 457–463.

Kummer, E., Leibundgut, M., Rackham, O., Lee, R.G., Boehringer, D., Filipovska, A., and Ban, N. (2018). Unique features of mammalian mitochondrial translation initiation revealed by cryo-EM. Nature 1–23.

Kurland, C.G., and Andersson, S.G. (2000). Origin and evolution of the mitochondrial proteome. Microbiol Mol Biol Rev *64*, 786–820.

Kılıç, M., Oğuz, K.-K., Kılıç, E., Yüksel, D., Demirci, H., Sağıroğlu, M.Ş., Yücel-Yılmaz, D., and Özgül, R.K. (2017). A patient with mitochondrial disorder due to a novel mutation in MRPS22. Metab Brain Dis *32*, 1389–1393.

Larburu, N., Montellese, C., O'Donohue, M.-F., Kutay, U., Gleizes, P.-E., and Plisson-Chastang, C. (2016). Structure of a human pre-40S particle points to a role for RACK1 in the final steps of 18S rRNA processing. Nucleic Acids Research *44*, 8465–8478.

Lake, N.J., Webb, B.D., Stroud, D.A., Richman, T.R., Ruzzenente, B., Compton, A.G., Mountford, H.S., Pulman, J., Zangarelli, C., Rio, M., et al. (2017). Biallelic Mutations in MRPS34 Lead to Instability of the Small Mitoribosomal Subunit and Leigh Syndrome. The American Journal of Human Genetics *101*, 239–254.

Lavdovskaia, E., Denks, K., Nadler, F., Steube, E., Linden, A., Urlaub, H., Rodnina, M.V., and Richter-Dennerlein, R. (2020). Dual function of GTPBP6 in biogenesis and recycling of human mitochondrial ribosomes. Nucleic Acids Research *48*, 12929–12942.

Lavdovskaia, E., Kolander, E., Steube, E., Mai, M.M.Q., Urlaub, H., and Richter-Dennerlein, R. (2018). The human Obg protein GTPBP10 is involved in mitoribosomal biogenesis. Nucleic Acids Research *46*, 8471–8482.

Lee, K.W., and Bogenhagen, D.F. (2014). Assignment of 2'-O-methyltransferases to modification sites on the mammalian mitochondrial large subunit 16 S ribosomal RNA (rRNA). J Biol Chem *289*, 24936–24942.

Li, K.-S., Zhu, X.-D., Liu, H.-D., Zhang, S.-Z., Li, X.-L., Xiao, N., Liu, X.-F., Bin Xu, Lei, M., Zhang, Y.-Y., et al. (2020). NT5DC2 promotes tumor cell proliferation by stabilizing EGFR in hepatocellular carcinoma. Cell Death and Disease 1–15.

Li, X., Sun, Q., Jiang, C., Yang, K., Hung, L.-W., Zhang, J., and Sacchettini, J.C. (2015). Structure of Ribosomal Silencing Factor Bound to Mycobacterium tuberculosis Ribosome. Structure *23*, 1858–1865.

Lin, Y.-C., Boone, M., Meuris, L., Lemmens, I., Van Roy, N., Soete, A., Reumers, J., Moisse, M., Plaisance, S., Drmanac, R., et al. (2014). Genome dynamics of the human embryonic kidney 293 lineage in response to cell biology manipulations. Nature Communications *5*, 4767–12.

Lindahl, L. (1973). Two new ribosomal precursor particles in E. coli. Nat New Biol *243*, 170–172.

Lindahl, L. (1975). Intermediates and time kinetics of the in vivo assembly of Escherichia coli ribosomes. Journal of Molecular Biology *92*, 15–37.

Ling, M., Merante, F., Chen, H.S., Duff, C., Duncan, A.M., and Robinson, B.H. (1997). The human mitochondrial elongation factor tu (EF-Tu) gene: cDNA sequence, genomic localization, genomic structure, and identification of a pseudogene. Gene *197*, 325–336.

Liu, L., Rodriguez-Belmonte, E.M., Mazloum, N., Bin Xie, and Lee, M.Y.W.T. (2003). Identification of a Novel Protein, PDIP38, That Interacts with the p50 Subunit of DNA Polymerase ÃŽÂ´ and Proliferating Cell Nuclear Antigen*. Journal of Biological Chemistry *278*, 10041–10047.

Lorenzi, I., Oeljeklaus, S., Ronsör, C., Bareth, B., Warscheid, B., Rehling, P., and Dennerlein, S. (2016). Ribosome-Associated Mba1 Escorts Cox2 from Insertion Machinery to Maturing Assembly Intermediates. Mcb *36*, 2782–2793.

Luo, M., Ma, W., Sand, Z., Finlayson, J., Wang, T., Brinton, R.D., Willis, W.T., and Mandarino, L.J. (2020). Von Willebrand factor A domain-containing protein 8 (VWA8) localizes to the matrix side of the inner mitochondrial membrane. Biochemical and Biophysical Research Communications *521*, 158–163.

Luo, M., Mengos, A.E., Ma, W., Finlayson, J., Bustos, R.Z., Xiao Zhu, Y., Shi, C.X., Stubblefield, T.M., Willis, W.T., and Mandarino, L.J. (2017). Characterization of the novel protein KIAA0564 (Von Willebrand Domain-containing Protein 8). Biochemical and Biophysical Research Communications *487*, 545–551.

Maiti, P., Antonicka, H., Gingras, A.C., Shoubridge, E.A., and Barrientos, A. (2020). Human GTPBP5 (MTG2) fuels mitoribosome large subunit maturation by facilitating 16S rRNA methylation. Nucleic Acids Research *48*, 7924–7943.

Maiti, P., Kim, H.J., Tu, Y.T., and Barrientos, A. (2018). Human GTPBP10 is required for mitoribosome maturation. Nucleic Acids Research *46*, 11423–11437.

Maki, J.A., Schnobrich, D.J., and Culver, G.M. (2002). The DnaK chaperone system facilitates 30S ribosomal subunit assembly. Mol Cell *10*, 129–138.

Malarkey, C.S., and Churchill, M.E.A. (2012). The high mobility group box: the ultimate utility player of a cell. Trends in Biochemical Sciences *37*, 553–562.

Marcucci, G., Yan, P., Maharry, K., Frankhouser, D., Nicolet, D., Metzeler, K.H., Kohlschmidt, J., Mrózek, K., Wu, Y.-Z., Bucci, D., et al. (2014). Epigenetics Meets Genetics in Acute Myeloid Leukemia: Clinical Impact of a Novel Seven-Gene Score. Jco *32*, 548–556.

Martijn, J., Vosseberg, J., Guy, L., Offre, P., and Ettema, T.J.G. (2018). Deep mitochondrial origin outside the sampled alphaproteobacteria. Nature *557*, 101–105.

Meisinger, C., Sickmann, A., and Pfanner, N. (2008). The mitochondrial proteome: from inventory to function. Cell *134*, 22–24.

Menezes, M.J., Guo, Y., Zhang, J., Riley, L.G., Cooper, S.T., Thorburn, D.R., Li, J., Dong, D., Li, Z., Glessner, J., et al. (2015). Mutation in mitochondrial ribosomal protein S7 (MRPS7) causes congenital sensorineural deafness, progressive hepatic and renal failure and lactic acidemia. Human Molecular Genetics *24*, 2297–2307.

Metodiev, M.D., Lesko, N., Park, C.B., Cámara, Y., Shi, Y., Wibom, R., Hultenby, K., Gustafsson, C.M., and Larsson, N.-G. (2009). Methylation of 12S rRNA is necessary for in vivo stability of the small subunit of the mammalian mitochondrial ribosome. Cell Metabolism *9*, 386–397.

Metodiev, M.D., Spåhr, H., Loguercio Polosa, P., Meharg, C., Becker, C., Altmueller, J., Habermann, B., Larsson, N.-G., and Ruzzenente, B. (2014). NSUN4 is a dual function mitochondrial protein required for both methylation of 12S rRNA and coordination of mitoribosomal assembly. PLoS Genet. *10*, e1004110.

Miller, C., Saada, A., Shaul, N., Shabtai, N., Ben-Shalom, E., Shaag, A., Hershkovitz, E., and Elpeleg, O. (2004). Defective mitochondrial translation caused by a ribosomal protein (MRPS16) mutation. Ann Neurol *56*, 734–738.

Mizushima, S., and Nomura, M. (1970). Assembly mapping of 30S ribosomal proteins from E. coli. Nature *226*, 1214.

Montoya, J., Ojala, D., and Attardi, G. (1981). Distinctive features of the 5'-terminal sequences of the human mitochondrial mRNAs. Nature *290*, 465–470.

Mulder, A.M., Yoshioka, C., Beck, A.H., Bunner, A.E., Milligan, R.A., Potter, C.S., Carragher, B., and Williamson, J.R. (2010). Visualizing ribosome biogenesis: parallel assembly pathways for the 30S subunit. Science *330*, 673–677.

Nakashima, A., Yamaguchi, H., Kodani, Y., Kaneko, Y.S., Kawata, M., Nagasaki, H., Nagatsu, T., and Ota, A. (2019). Identification by nano-LC-MS/MS of NT5DC2 as a

protein binding to tyrosine hydroxylase: Down-regulation of NT5DC2 by siRNA increases catecholamine synthesis in PC12D cells. Biochemical and Biophysical Research Communications *516*, 1060–1065.

Nakashima, A., Yamaguchi, H., Kondo, M., Furumura, T., Kodani, Y., Kaneko, Y.S., Kawata, M., Nagasaki, H., Nagatsu, T., and Ota, A. (2020). NT5DC2 affects the phosphorylation of tyrosine hydroxylase regulating its catalytic activity. Journal of Neural Transmission *127*, 1631–1640.

Nass, M.M. (1966). The circularity of mitochondrial DNA. Proceedings of the National Academy of Sciences *56*, 1215–1222.

Nierhaus, K.H., Bordasch, K., and Homann, H.E. (1973). Ribosomal proteins. 43. In vivo assembly of Escherichia coli ribosomal proteins. Journal of Molecular Biology *74*, 587–597.

Nierlich, D.P. (1982). Fragmentary 5S rRNA gene in the human mitochondrial genome. Mcb *2*, 207–209.

Niwa, H., Miyauchi-Nanri, Y., Okumoto, K., Mukai, S., Noi, K., Ogura, T., and Fujiki, Y. (2018). A newly isolated Pex7-binding, atypical PTS2 protein P7BP2 is a novel dynein-type AAA+ protein. The Journal of Biochemistry *164*, 437–447.

Nowotny, V., and Nierhaus, K.H. (1988). Assembly of the 30S subunit from Escherichia coli ribosomes occurs via two assembly domains which are initiated by S4 and S7. Biochemistry *27*, 7051–7055.

O'Brien, R.L., and Brierley, G. (1965). Compartmentation of heart mitochondria. I. Permeability characteristics of isolated beef heart mitochondria. Journal of Biological Chemistry *240*, 4527–4531.

Oedegaard, K.J., Greenwood, T.A., Johansson, S., Jacobsen, K.K., Halmoy, A., Fasmer, O.B., Akiskal, H.S., The Bipolar Genome Study (BiGS), Haavik, J., and Kelsoe, J.R. (2010). A genome-wide association study of bipolar disorder and comorbid migraine. Genes, Brain and Behavior *9*, 673–680.

Ojala, D., Montoya, J., and Attardi, G. (1981). tRNA punctuation model of RNA processing in human mitochondria. Nature *290*, 470–474.

Ott, M., Prestele, M., Bauerschmitt, H., Funes, S., Bonnefoy, N., and Herrmann, J.M. (2006). Mba1, a membrane-associated ribosome receptor in mitochondria. The EMBO Journal *25*, 1603–1610.

Pandey, A., Pain, J., Ghosh, A.K., Dancis, A., and Pain, D. (2015). Fe-S Cluster Biogenesis in Isolated Mammalian Mitochondria. Journal of Biological Chemistry *290*, 640–657.

Park, C.B., Asin-Cayuela, J., Cámara, Y., Shi, Y., Pellegrini, M., Gaspari, M., Wibom, R., Hultenby, K., Erdjument-Bromage, H., Tempst, P., et al. (2007). MTERF3 Is a Negative Regulator of Mammalian mtDNA Transcription. Cell *130*, 273–285.

Pearce, S.F., Rebelo-Guiomar, P., D'Souza, A.R., Powell, C.A., Van Haute, L., and Minczuk, M. (2017). Regulation of Mammalian Mitochondrial Gene Expression: Recent Advances. Trends in Biochemical Sciences *42*, 625–639.

Popow, J., Alleaume, A.M., Curk, T., Schwarzl, T., Sauer, S., and Hentze, M.W. (2015). FASTKD2 is an RNA-binding protein required for mitochondrial RNA processing and translation. Rna *21*, 1873–1884.

Posse, V., Shahzad, S., Falkenberg, M., Hällberg, B.M., and Gustafsson, C.M. (2015). TEFM is a potent stimulator of mitochondrial transcription elongation in vitro. Nucleic Acids Research *43*, 2615–2624.

Powell, C.A., and Minczuk, M. (2020). TRMT2B is responsible for both tRNA and rRNA m5U-methylation in human mitochondria. RNA Biology *00*, 1–12.

Prados, J., Stenz, L., Courtet, P., Prada, P., Nicastro, R., Adouan, W., Guillaume, S., Olié, E., Aubry, J.M., Dayer, A., et al. (2015). Borderline personality disorder and childhood maltreatment: a genome-wide methylation analysis. Genes, Brain and Behavior *14*, 177–188.

Preuss, M., Leonhard, K., Hell, K., Stuart, R.A., Neupert, W., and Herrmann, J.M. (2001). Mba1, a novel component of the mitochondrial protein export machinery of the yeast Saccharomyces cerevisiae. Journal of Cell Biology *153*, 1085–1096.

Pulman, J., Ruzzenente, B., Bianchi, L., Rio, M., Boddaert, N., Munnich, A., Rötig, A., and Metodiev, M.D. (2019). Mutations in the MRPS28 gene encoding the small mitoribosomal subunit protein bS1m in a patient with intrauterine growth retardation, craniofacial dysmorphism and multisystemic involvement. Human Molecular Genetics *28*, 1445–1462.

Rabl, R., Soubannier, V., Scholz, R., Vogel, F., Mendl, N., Vasiljev-Neumeyer, A., Körner, C., Jagasia, R., Keil, T., Baumeister, W., et al. (2009). Formation of cristae and crista junctions in mitochondria depends on antagonism between Fcj1 and Su e/g. Journal of Cell Biology *185*, 1047–1063.

Rackham, O., Busch, J.D., Matic, S., Siira, S.J., Kuznetsova, I., Atanassov, I., Ermer, J.A., Shearwood, A.M.J., Richman, T.R., Stewart, J.B., et al. (2016). Hierarchical RNA Processing Is Required for Mitochondrial Ribosome Assembly. Cell Reports *16*, 1874–1890.

Ramaswamy, P., and Woodson, S.A. (2009). S16 throws a conformational switch during assembly of 30S 5' domain. Nat Struct Mol Biol *16*, 438–445.

Ran, F.A., Hsu, P.D., Wright, J., Agarwala, V., Scott, D.A., and Zhang, F. (2013). Genome engineering using the CRISPR-Cas9 system. Nat Protoc *8*, 2281–2308.

Refaii, Al, A., and Alix, J.-H. (2009). Ribosome biogenesis is temperature-dependent and delayed in Escherichia colilacking the chaperones DnaK or DnaJ. Molecular Microbiology *71*, 748–762.

Reinhard, L., Sridhara, S., and Hällberg, B.M. (2017). The MRPP1/MRPP2 complex is a tRNA-maturation platform in human mitochondria. Nucleic Acids Research *45*, 12469–12480.

Reitzer, L.J., Wice, B.M., and Kennell, D. (1979). Evidence that glutamine, not sugar, is the major energy source for cultured HeLa cells. Journal of Biological Chemistry *254*, 2669–2676.

Reyes, A., Favia, P., Vidoni, S., Petruzzella, V., and Zeviani, M. (2020). RCC1L (WBSCR16) isoforms coordinate mitochondrial ribosome assembly through their interaction with GTPases. PLoS Genet. *16*, e1008923.

Richter, R., Pajak, A., Dennerlein, S., Rozanska, A., Lightowlers, R.N., and Chrzanowska-Lightowlers, Z.M.A. (2010a). Translation termination in human mitochondrial ribosomes. Biochem Soc Trans *38*, 1523–1526.

Richter, R., Rorbach, J., Pajak, A., Smith, P.M., Wessels, H.J., Huynen, M.A., Smeitink, J.A., Lightowlers, R.N., and Chrzanowska-Lightowlers, Z.M. (2010b). A functional peptidyl-tRNA hydrolase, ICT1, has been recruited into the human mitochondrial ribosome. The EMBO Journal *29*, 1116–1125.

Ringel, R., Sologub, M., Morozov, Y.I., Litonin, D., Cramer, P., and Temiakov, D. (2011). Structure of human mitochondrial RNA polymerase. Nature *478*, 269–273.

Rizzuto, R., De Stefani, D., Raffaello, A., and Mammucari, C. (2012). Mitochondria as sensors and regulators of calcium signalling. Nat Rev Mol Cell Biol *13*, 566–578.

Robert, F., and Brakier-Gingras, L. (2001). Ribosomal protein S7 from Escherichia coli uses the same determinants to bind 16S ribosomal RNA and its messenger RNA. Nucleic Acids Research *29*, 677–682.

Roberti, M., Bruni, F., Loguercio Polosa, P., Manzari, C., Gadaleta, M.N., and Cantatore, P. (2006). MTERF3, the most conserved member of the mTERF-family, is a modular factor involved in mitochondrial protein synthesis. Biochim Biophys Acta *1757*, 1199–1206.

Rorbach, J., Boesch, P., Gammage, P.A., Nicholls, T.J.J., Pearce, S.F., Patel, D., Hauser, A., Perocchi, F., and Minczuk, M. (2014). MRM2 and MRM3 are involved in biogenesis of the large subunit of the mitochondrial ribosome. MBoC *25*, 2542–2555.

Rorbach, J., Gammage, P.A., and Minczuk, M. (2012). C7orf30 is necessary for biogenesis of the large subunit of the mitochondrial ribosome. Nucleic Acids Research *40*, 4097–4109.

Rossignol, R., Gilkerson, R., Aggeler, R., Yamagata, K., Remington, S.J., and Capaldi, R.A. (2004). Energy substrate modulates mitochondrial structure and oxidative capacity in cancer cells. Cancer Res *64*, 985–993.

Rozanska, A., Richter-Dennerlein, R., Rorbach, J., Gao, F., Lewis, R.J., Chrzanowska-Lightowlers, Z.M., and Lightowlers, R.N. (2017). The human RNA-

binding protein RBFA promotes the maturation of the mitochondrial ribosome. Biochem J *474*, 2145–2158.

Saada, A., Shaag, A., Arnon, S., Dolfin, T., Miller, C., Fuchs-Telem, D., Lombes, A., and Elpeleg, O. (2007). Antenatal mitochondrial disease caused by mitochondrial ribosomal protein (MRPS22) mutation. J Med Genet *44*, 784–786.

Saraste, M. (1999). Oxidative phosphorylation at the fin de siècle. Science *283*, 1488–1493.

Satoh, M., and Kuroiwa, T. (1991). Organization of multiple nucleoids and DNA molecules in mitochondria of a human cell. Experimental Cell Research *196*, 137–140.

Schaechter, M., and Group, V.F.H. (2001). Escherichia coli and Salmonella 2000: the view from here. Microbiol Mol Biol Rev *65*, 119–130.

Schägger, H. (2006). Tricine–SDS-PAGE. Nat Protoc *1*, 16–22.

Schwartzbach, C.J., and Spremulli, L.L. (1989). Bovine mitochondrial protein synthesis elongation factors. Identification and initial characterization of an elongation factor Tu-elongation factor Ts complex. Journal of Biological Chemistry *264*, 19125–19131.

Seifried, A., Schultz, J., and Gohla, A. (2013). Human HAD phosphatases: structure, mechanism, and roles in health and disease. Febs J *280*, 549–571.

Serre, V., Rozanska, A., Beinat, M., Chretien, D., Boddaert, N., Munnich, A., Rötig, A., and Chrzanowska-Lightowlers, Z.M. (2013). Mutations in mitochondrial ribosomal protein MRPL12 leads to growth retardation, neurological deterioration and mitochondrial translation deficiency. Biochim Biophys Acta *1832*, 1304–1312.

Shajani, Z., Sykes, M.T., and Williamson, J.R. (2011). Assembly of bacterial ribosomes. Annu Rev Biochem *80*, 501–526.

Sharma, I.M., and Woodson, S.A. (2019). RbfA and IF3 couple ribosome biogenesis and translation initiation to increase stress tolerance. Nucleic Acids Research *20*, 116–14.

Sharma, L.K., Lu, J., and Bai, Y. (2009). Mitochondrial respiratory complex I: structure, function and implication in human diseases. Curr Med Chem *16*, 1266–1277.

Sharma, M.R., Barat, C., Wilson, D.N., Booth, T.M., Kawazoe, M., Hori-Takemoto, C., Shirouzu, M., Yokoyama, S., Fucini, P., and Agrawal, R.K. (2005). Interaction of Era with the 30S ribosomal subunit implications for 30S subunit assembly. Mol Cell *18*, 319–329.

Sharma, M.R., Koc, E.C., Datta, P.P., Booth, T.M., Spremulli, L.L., and Agrawal, R.K. (2003). Structure of the mammalian mitochondrial ribosome reveals an expanded functional role for its component proteins. Cell *115*, 97–108.

Shi, Y., Posse, V., Zhu, X., Hyvärinen, A.K., Jacobs, H.T., Falkenberg, M., and Gustafsson, C.M. (2016). Mitochondrial transcription termination factor 1 directs polar replication fork pausing. Nucleic Acids Research *44*, 5732–5742.

Signes, A., and Fernandez-Vizarra, E. (2018). Assembly of mammalian oxidative phosphorylation complexes I–V and supercomplexes. Essays in Biochemistry *62*, 255–270.

Smits, P., Saada, A., Wortmann, S.B., Heister, A.J., Brink, M., Pfundt, R., Miller, C., Haas, D., Hantschmann, R., Rodenburg, R.J.T., et al. (2011). Mutation in mitochondrial ribosomal protein MRPS22 leads to Cornelia de Lange-like phenotype, brain abnormalities and hypertrophic cardiomyopathy. Eur J Hum Genet *19*, 394–399.

Smits, P., Smeitink, J., and van den Heuvel, L. (2010). Mitochondrial Translation and Beyond: Processes Implicated in Combined Oxidative Phosphorylation Deficiencies. Journal of Biomedicine and Biotechnology *2010*, 1–24.

Soleimanpour-Lichaei, H.R., Kühl, I., Gaisne, M., Passos, J.F., Wydro, M., Rorbach, J., Temperley, R., Bonnefoy, N., Tate, W., Lightowlers, R., et al. (2007). mtRF1a is a human mitochondrial translation release factor decoding the major termination codons UAA and UAG. Mol Cell *27*, 745–757.

Spåhr, H., Habermann, B., Gustafsson, C.M., Larsson, N.-G., and Hällberg, B.M. (2012). Structure of the human MTERF4-NSUN4 protein complex that regulates mitochondrial ribosome biogenesis. Proc Natl Acad Sci U S A *109*, 15253–15258.

Stoldt, S., Wenzel, D., Kehrein, K., Riedel, D., Ott, M., and Jakobs, S. (2018). Spatial orchestration of mitochondrial translation and OXPHOS complex assembly. Nat Cell Biol *20*, 528–534.

Strauss, M., Hofhaus, G., Schröder, R.R., and Kühlbrandt, W. (2008). Dimer ribbons of ATP synthase shape the inner mitochondrial membrane. The EMBO Journal *27*, 1154–1160.

Summer, S., Smirnova, A., Gabriele, A., Toth, U., Fasemore, A.M., Förstner, K.U., Kuhn, L., Chicher, J., Hammann, P., Mitulović, G., et al. (2020). YBEY is an essential biogenesis factor for mitochondrial ribosomes. Nucleic Acids Research *48*, 9762–9786.

Suzuki, T., Terasaki, M., Takemoto-Hori, C., Hanada, T., Ueda, T., Wada, A., and Watanabe, K. (2001). Proteomic analysis of the mammalian mitochondrial ribosome. Identification of protein components in the 28 S small subunit. Journal of Biological Chemistry *276*, 33181–33195.

Sykes, M.T., and Williamson, J.R. (2009). A Complex Assembly Landscape for the 30S Ribosomal Subunit. Annu. Rev. Biophys. *38*, 197–215.

Sykora, P., Kanno, S., Akbari, M., Kulikowicz, T., Baptiste, B.A., Leandro, G.S., Lu, H., Tian, J., May, A., Becker, K.A., et al. (2017). DNA Polymerase Beta Participates in Mitochondrial DNA Repair. Mcb *37*, 1475–20.

Tait, S.W.G., and Green, D.R. (2012). Mitochondria and cell signalling. J Cell Sci *125*, 807–815.

Temperley, R.J., Wydro, M., Lightowlers, R.N., and Chrzanowska-Lightowlers, Z.M. (2010). Human mitochondrial mRNAs—like members of all families, similar but different. BBA - Bioenergetics *1797*, 1081–1085.

Terzioglu, M., Ruzzenente, B., Harmel, J., Mourier, A., Jemt, E., López, M.D., Kukat, C., Stewart, J.B., Wibom, R., Meharg, C., et al. (2013). MTERF1 binds mtDNA to prevent transcriptional interference at the light-strand promoter but is dispensable for rRNA gene transcription regulation. Cell Metabolism *17*, 618–626.

Timmis, J.N., Ayliffe, M.A., Huang, C.Y., and Martin, W. (2004). Endosymbiotic gene transfer: organelle genomes forge eukaryotic chromosomes. Nat Rev Genet *5*, 123–135.

Tiranti, V., Savoia, A., Forti, F., D'Apolito, M.F., Centra, M., Rocchi, M., and Zeviani, M. (1997). Identification of the gene encoding the human mitochondrial RNA polymerase (h-mtRPOL) by cyberscreening of the Expressed Sequence Tags database. Human Molecular Genetics *6*, 615–625.

Tissier, A., Janel-Bintz, R., Coulon, S., Klaile, E., Kannouche, P., Fuchs, R.P., and Cordonnier, A.M. (2010). Crosstalk between replicative and translesional DNA polymerases: PDIP38 interacts directly with Poleta. DNA Repair (Amst) *9*, 922–928.

Traub, P., and Nomura, M. (1968). Structure and function of E. coli ribosomes. V. Reconstitution of functionally active 30S ribosomal particles from RNA and proteins. Proceedings of the National Academy of Sciences *59*, 777–784.

Trubetskoy, D., Proux, F., Allemand, F., Dreyfus, M., and Iost, I. (2009). SrmB, a DEAD-box helicase involved in Escherichia coli ribosome assembly, is specifically targeted to 23S rRNA in vivo. Nucleic Acids Research *37*, 6540–6549.

Tu, C., Zhou, X., Tropea, J.E., Austin, B.P., Waugh, D.S., Court, D.L., and Ji, X. (2009). Structure of ERA in complex with the 3′ end of 16S rRNA: Implications for ribosome biogenesis. Proc Natl Acad Sci USA *106*, 14843.

Tu, Y.T., and Barrientos, A. (2015). The Human Mitochondrial DEAD-Box Protein DDX28 Resides in RNA Granules and Functions in Mitoribosome Assembly. Cell Reports *10*, 854–864.

Uchiumi, T., Ohgaki, K., Yagi, M., Aoki, Y., Sakai, A., Matsumoto, S., and Kang, D. (2010). ERAL1 is associated with mitochondrial ribosome and elimination of ERAL1 leads to mitochondrial dysfunction and growth retardation. Nucleic Acids Research *38*, 5554–5568.

Uicker, W.C., Schaefer, L., and Britton, R.A. (2006). The essential GTPase RbgA (YlqF) is required for 50S ribosome assembly in Bacillus subtilis. Molecular Microbiology *59*, 528–540.

Vafai, S.B., and Mootha, V.K. (2012). Mitochondrial disorders as windows into an ancient organelle. Nature *491*, 374–383.

Van Der Bliek, A.M., Sedensky, M.M., and Morgan, P.G. (2017). Cell Biology of the Mitochondrion. Genetics *207*, 843–871.

van Hulzen, K.J.E., Scholz, C.J., Franke, B., Ripke, S., Klein, M., McQuillin, A., Sonuga-Barke, E.J., Kelsoe, J.R., Landén, M., Andreassen, O.A., et al. (2017). Genetic Overlap Between Attention-Deficit/Hyperactivity Disorder and Bipolar Disorder: Evidence From Genome-wide Association Study Meta-analysis. Biological Psychiatry *82*, 634–641.

Wei, Y., Zhang, H., Gao, Z.-Q., Wang, W.-J., Shtykova, E.V., Xu, J.-H., Liu, Q.-S., and Dong, Y.-H. (2012). Crystal and solution structures of methyltransferase RsmH provide basis for methylation of C1402 in 16S rRNA. J Struct Biol *179*, 29–40.

Wiedemann, N., and Pfanner, N. (2017). Mitochondrial Machineries for Protein Import and Assembly. Annu. Rev. Biochem. *86*, 685–714.

Williamson, J.R. (2003). After the ribosome structures: how are the subunits assembled? Rna *9*, 165–167.

Williamson, J.R. (2005). Assembly of the 30S ribosomal subunit. Q Rev Biophys *38*, 397–403.

Wredenberg, A., Lagouge, M., Bratic, A., Metodiev, M.D., Spåhr, H., Mourier, A., Freyer, C., Ruzzenente, B., Tain, L., Grönke, S., et al. (2013). MTERF3 regulates mitochondrial ribosome biogenesis in invertebrates and mammals. PLoS Genet. *9*, e1003178.

Xia, B., Ke, H., Shinde, U., and Inouye, M. (2003). The Role of RbfA in 16S rRNA Processing and Cell Growth at Low Temperature in Escherichia coli. Journal of Molecular Biology *332*, 575–584.

Yuan, F., Wang, W., and Cheng, H. (2018). Co-expression network analysis of gene expression profiles of HER2+ breast cancer-associated brain metastasis. Oncol Lett 1–12.

Zaganelli, S., Rebelo-Guiomar, P., Maundrell, K., Rozanska, A., Pierredon, S., Powell, C.A., Jourdain, A.A., Hulo, N., Lightowlers, R.N., Chrzanowska-Lightowlers, Z.M., et al. (2017). The Pseudouridine Synthase RPUSD4 Is an Essential Component of Mitochondrial RNA Granules. Journal of Biological Chemistry *292*, 4519–4532.

Zengel, J.M., and Lindahl, L. (1994). Diverse mechanisms for regulating ribosomal protein synthesis in Escherichia coli. Prog Nucleic Acid Res Mol Biol *47*, 331–370.

Zong, S., Wu, M., Gu, J., Liu, T., Guo, R., and Yang, M. (2018). Structure of the intact 14-subunit human cytochrome c oxidase. Cell Research 1–9.

Acknowledgments

First and foremost, I would like to thank Dr. Ricarda Richter-Dennerlein for the opportunity to do my PhD in her lab and for giving me the possibility to work on this interesting project. I would like to express my gratitude for her supervision and guidance throughout these past years.

Next, I owe many thanks to the member of my thesis advisory committee, Prof. Dr. Markus T. Bohnsack and Prof. Dr. Dörthe M. Katschinski for their constructive criticism, and helpful discussions during the meetings.

I would like to thank also my current and former lab members for creating a stimulating environment and exciting moments. I am especially thankful for Elena Lavdovskaia for all the discussions, advices and help in Lab, which helped me advance in my projects.

I also like to express my gratitude to Dr. Nicolás Lemus Diaz and Dr. Anita Krisko for teaching me how to use R-studio and providing me with the possibility to visualize my generated data in different ways as well as for all the phrases, which were exchanged.

I also thank the former and present lab members of Prof. Dr. Peter Rehling's group and Dr. Nuno Raimundo's group for guiding and helping me during my PhD. I extent thereby my thanks to Dr. Arpita Chowdhury, Dr. Sylvie Callegari and Dr. Isotta Lorenzi. I am especially thankful for Dr. Cong Wang with whom I had also the opportunity to get to know the all the delicacies of the lab and Göttingen.

I thank the GGNB and the Molecular Medicine program for their commitment to higher education.

I extent my gratitude to my friends for all the support at any time and any possible way.

Lastly, I thank my family and my partner for always supporting, guiding and helping to become who I am today.